

**DEVELOPMENT OF METAL-AFFINITY PARTITIONING OF  
HEPATITIS B CORE ANTIGEN FROM UNCLARIFIED BACTERIA  
FEEDSTOCK**

By  
**Kok Chung Wei**

**A dissertation submitted to the Department of Biomedical Science  
Faculty of Science  
Universiti Tunku Abdul Rahman  
in partial fulfillment of the requirements for the degree of  
Master of Science**

**Dec 2018**

## **ABSTRACT**

### **DEVELOPMENT OF METAL-AFFINITY PARTITIONING OF HEPATITIS B CORE ANTIGEN FROM UNCLARIFIED BACTERIA FEEDSTOCK**

**Kok Chung Wei**

Hepatitis B core antigen (HBcAg) is one of the most frequently studied viral-like-particle (VLP) for the display of foreign epitopes and has a great potential in the development of diagnostic reagent and vaccine for hepatitis B infection. Various researches have been reported to purify HBcAg such as sucrose gradient ultracentrifugation and chromatography. However, these conventional methods are tedious, time consuming, and expensive to use due to multiple purification steps. Furthermore, the yield obtained was reported to be very low. As a result, different methods have been investigated to improve the yield and purity of HBcAg. Therefore, aqueous two-phase system (ATPS), which consists of two types of polymers or polymer with a type of salt, can be sought as an alternative method for HBcAg recovery. In this study, immobilised metal affinity partitioning (IMAP) was incorporated in ATPS to improve the overall recovery of his-tagged HBcAg from unclarified *Escherichia coli* (*E. coli*) feedstock. Modified polymer involved in IMAP was synthesised prior to ATPS purification of his-tagged HBcAg. The effects of activation duration, epichlorohydrin concentration, boron trifluoride

ethyletherate (BFEE) concentration, sodium hydroxide (NaOH) concentration, iminodiacetic acid concentration and type of metal ions were evaluated for the optimal production of modified PEG. Sodium dodecyl sulphate polyacrylamide gel electrophoresis (SDS-PAGE), the Bradford assay and densitometric analysis were used to analyse and quantify the samples obtained from ATPS. Parameters such as the mode for phase inversion and separation, molecular weight (MW) of PEG, phase-forming salts, tie-line length (TLL), phase volume ratio ( $V_R$ ), neutral salt addition, system pH and biomass concentration on the partitioning of his-tagged HBcAg were evaluated in this study. The antigenicity and the morphology of the purified HBcAg were analysed using enzyme-linked immunosorbent assay (ELISA) and transmission electron microscope (TEM), respectively. Based on the phase diagram, PEG 6000-IDA-Cu(II)- Na<sub>2</sub>SO<sub>4</sub> system was an ideal system to use in ATPS. However, when the unclarified homogenate was added to the system, it was shown that PEG 2000-IDA-Cu(II)-KPB was the optimal system to use as it partitioned the highest amount of his-tagged HBcAg to the PEG rich top phase. The optimal recovery of his-tagged HBcAg was achieved using PEG 2000-IDA-Cu(II)-KPB system with phase inversion by using a vortex mixer for 5 mins, phase separation by centrifugation for 3 mins at 2000 xg, TLL 3 and a phase volume ratio of 2.3, pH 8, without NaCl addition and loaded with 5 % (w/v) unclarified homogenate. The purity of HBcAg obtained was about 94 % with a purification factor of 3.0 and a recovery yield of approximately 91 %. Based on the ELISA results, the antigenicity of the ATPS purified his-tagged HBcAg was still preserved and it was comparable to the his-tagged HBcAg purified using sucrose-gradient ultracentrifugation. When the purified his-tagged

HBcAg were viewed using TEM, they were still able to form icosahedral particles with a diameter of about 28 to 32 nm. Therefore, this study showed that IMAP incorporated in ATPS is an efficient method to recover his-tagged HBcAg from unclarified *E. coli* homogenate.

## **ACKNOWLEDGEMENTS**

I wish to express my gratitude to Dr. Michelle Ng Yeen Tan and Dr. Ong Siew Teng and sincere thanks to their continuous supports of my research, and for their patience, motivation and immense knowledge.

I greatly appreciate all the lab officers and my labmates for helping me when I need help. Besides, I must express my gratitude to my parents for providing me with unfailing support and encouragement throughout the process of researching and writing the dissertation.

Last but not least, I would like to thank UTAR Research Fund (IPSR/RMC/UTARRF/2012-C2/M07) for providing the financial funding for this project.

## DECLARATION

I, **KOK CHUNG WEI** hereby declare that the dissertation is based on my original work except for quotations and citations which have been duly acknowledged. I also declare that it has not been previously or concurrently submitted for any other degree at UTAR or other institutions.

---

(KOK CHUNG WEI)

Date:

**FACULTY OF SCIENCE**  
**UNIVERSITI TUNKU ABDUL RAHMAN**

**Date:** \_\_\_\_\_

**PERMISSION SHEET**

It is hereby certified that **KOK CHUNG WEI (ID No: 13 ADM 08506)** has completed this dissertation entitled “**DEVELOPMENT OF METAL-AFFINITY PARTITIONING OF HEPATITIS B CORE ANTIGEN FROM UNCLARIFIED BACTERIA FEEDSTOCK**” supervised by Dr. Michelle Ng Yeen Tan from the Department of Biomedical Science, Faculty of Science, and DR. Ong Siew Teng from the Department of Chemical Science, Faculty of Science.

I understand that the University will upload softcopy of my thesis/dissertation in pdf format into UTAR Institutional Repository, which may be made accessible to UTAR community and public.

Yours truly,

\_\_\_\_\_  
(KOK CHUNG WEI)

## APPROVAL SHEET

This dissertation entitled “**DEVELOPMENT OF METAL-AFFINITY PARTITIONING OF HEPATITIS B CORE ANTIGEN FROM UNCLARIFIED BACTERIA FEEDSTOCK**” was prepared by KOK CHUNG WEI and submitted as partial fulfillment of the requirements for the degree of Master of Science at Universiti Tunku Abdul Rahman.

Approved by:

---

(Dr. Michelle Ng Yeen Tan)

Date:.....

Supervisor

Department of Biomedical Science

Faculty of Science

Universiti Tunku Abdul Rahman

---

(Dr. Ong Siew Teng)

Date:.....

Co-Supervisor

Department of Chemical Science

Faculty of Science

Universiti Tunku Abdul Rahman

	<b>Page</b>
<b>ABSTRACT</b>	<b>ii</b>
<b>ACKNOWLEDGEMENTS</b>	<b>v</b>
<b>DECLARATION</b>	<b>vi</b>
<b>PERMISSION SHEET</b>	<b>vii</b>
<b>APPROVAL SHEET</b>	<b>viii</b>
<b>LIST OF TABLES</b>	<b>xiii</b>
<b>LIST OF FIGURES</b>	<b>xv</b>
<b>LIST OF ABBREVIATIONS</b>	<b>xvii</b>
<b>CHAPTER</b>	
<b>1.0 INTRODUCTION</b>	<b>1</b>
<b>2.0 LITERATURE REVIEW</b>	<b>6</b>
2.1 Hepatitis B virus infections	6
2.1.1 HBV route of transmission and symptoms	6
2.1.2 Diagnosis and treatments for HBV infection	8
2.1.3 Prevention for HBV infection	11
2.2 Hepatitis B virus (HBV)	12
2.2.1 Structure of HBV	12
2.2.2 Hepatitis B core antigen (HBcAg)	15
2.2.3 Expression and production of HBcAg	17
2.2.4 N-terminally his-tagged HBcAg	18
2.2.5 Conventional method for HBcAg extraction and purification	19
2.3 Aqueous two phase system (ATPS)	21
2.3.1 Advantages of ATPS	22
2.3.2 Phase diagram	24
2.3.3 Factor that affected the partitioning of bio-molecules in ATPS	26
2.4 Metal affinity partitioning	28
2.4.1 Immobilized metal affinity partitioning (IMAP) in ATPS	30
2.4.2 Recent finding of IMAP in ATPS	32
<b>3.0 MATERIALS AND METHODS</b>	<b>35</b>
3.1 Materials	35
3.1.1 WB-HBcAg <i>Escherichia coli</i> cells	35
3.1.2 Chemicals and stock solutions	35
3.2 Methods	
3.2.1 Methodology overview	37
3.2.2 Synthesis of PEG-IDA-metal	39
3.2.2.1 Preparation of PEG-epoxide	39
3.2.2.2 Quantification of oxirane ring concentration in epoxidated PEG	39
3.2.2.3 Preparation of PEG-IDA	40
3.2.2.4 Coupling of metal ions onto PEG-IDA	40
3.2.2.5 Quantification of total metal ion chelated onto PEG-IDA	40

3.2.3	Construction of phase diagram	
3.2.3.1	Binodal curves	
3.2.3.2	Generation of standard curves	41
3.2.3.3	Tie-lines (TL)	43
3.2.4	Cultivation of <i>E. coli</i> cells	43
3.2.5	Preparation of unclarified <i>E. coli</i> feedstock for ATPS	46
3.2.6	Preparation of ATPS	47
3.2.7	Removal of PEG and salt from samples	47
3.2.8	Methods scouting for his-tagged HBcAg recovery	48
3.2.8.1	Phase inversion	49
3.2.8.2	Phase separation mode	49
3.2.8.3	Tie-line length (TLL)	49
3.2.8.4	Phase volume ratio	50
3.2.8.5	System pH	51
3.2.8.6	Biomass concentration	52
3.2.8.7	Additional of neutral salt	53
3.2.9	Conventional purification method for his-tagged HBcAg recovery	54
3.2.10	Quantitative analysis of ATPS-purified his-tagged HBcAg	55
3.2.10.1	Tricine-sodium dodecyl sulphate-polyacrylamide gel electrophoresis (Tricine-SDS-PAGE) analysis	57
3.2.10.2	The Bradford assay	
3.2.10.3	Densitometric analysis	59
3.2.11	Qualitative analysis of ATPS-purified his-tagged HBcAg	59
3.2.11.1	Enzyme-linked immunosorbent assay (ELISA)	60
3.2.11.2	Transmission electron microscope (TEM)	60
3.2.12	Calculations	61
<b>4.0</b>	<b>RESULTS</b>	<b>63</b>
4.1	Preparation of PEG-epoxide	63
4.1.1	Activation duration	63
4.1.2	Boron trifluoride ethyetherate (BFEE) concentration	65
4.1.3	Epichlorohydrin concentration	66
4.1.4	Sodium hydroxide (NaOH) concentration	67
4.2	Preparation of PEG-IDA and PEG-IDA-metal ions	69
4.2.1	Iminodiacetic acid (IDA) concentration	69
4.2.2	Types of metal ions	70
4.3	Construction of phase diagram	
4.3.1	Binodal curve	71
4.3.2	Standard curves for tie-lines generation	75
4.3.2.1	Standard curve for salt conductivity	75
4.3.2.2	Standard curves for refractive index of PEG	77
4.3.2.3	Standard curves for refractive index of phase forming salts	79
4.3.3	Generation of tie-lines	81
4.3.3.1	Tie-line length (TLL) and slope of tie-line length (STL)	82
4.4	Optimization of his-tagged HBcAg partitioning	85

4.4.1	Effect of phase inversion on his-tagged HBcAg partitioning	85
4.4.2	Phase separation mode	86
4.5	Methods scouting for his-tagged HBcAg recovery in IMAP-ATPS	88
4.5.1	Different PEG-IDA-Cu(II)-salt systems	
4.5.2	Tie-line length (TLL)	88
4.5.3	Phase volume ratio	92
4.5.4	Additional of NaCl	95
4.5.5	System pH	96
4.5.6	Biomass concentration	98
4.5.7	Optimized conditions for ATPS	99
4.6	Antigenicity of purified his-tagged HBcAg	101
4.7	Transmission electron microscope (TEM) on purified his-tagged HBcAg	104
		105
<b>5.0</b>	<b>DISCUSSION</b>	<b>107</b>
5.1	Preparation of PEG-epoxide, PEG-IDA, PEG-IDA-metal ions and the partitioning of metal affinity ligands in ATPS	107
5.2	Binodal curve	
5.2.1	Effect of different types of salts on bimodal curves	115
5.2.2	Effect of polymer MW on bimodal curves	115
5.3	Tie-line, TLL and STL	118
5.4	Phase inversion and phase separation on his-tagged HBcAg recovery	119
5.4.1	Phase inversion mode	121
5.4.2	Phase separation mode	121
5.5	Methods scouting for his-tagged HBcAg recovery in IMAP-ATPS	122
5.5.1	Tie-line length	125
5.5.2	Phase volume ratio	125
5.5.3	Additional of neutral salt	127
5.5.4	System pH	128
5.5.5	Biomass concentration	131
5.5.6	Optimized conditions for ATPS	134
5.6	Antigenicity and morphology of purified his-tagged HBcAg	136
		138
<b>6.0</b>	<b>CONCLUSION</b>	<b>140</b>
	<b>REFERENCES</b>	<b>143</b>
	<b>APPENDIX</b>	<b>156</b>

## LIST OF TABLES

<b>Table</b>		<b>Page</b>
2.1	Serological and virology markers for HBV.	10
2.2	Products extracted and purified with different types of ATPS.	23
2.3	Bio-separation methods based on affinity partitioning.	30
3.1	Source of chemicals and media used in the study.	36
3.2	The system composition of 5g system which consists of modified PEG with various salts [(NH <sub>4</sub> ) <sub>2</sub> SO <sub>4</sub> , Na <sub>2</sub> SO <sub>4</sub> , and KPB] at 23°C, pH 7.0.	42
3.3	Details of phase compositions for each PEG-salt system.	44
3.4	Phase compositions for TLL optimization.	51
3.5	Phase compositions of PEG 4000-IDA-Cu(II)-KPB system in the optimization of phase volume ratio.	52
3.6	Phase compositions of PEG 4000-IDA-Cu(II)-KPB in the optimization of system pH.	53
3.7	Preparation of stock solution of unclarified feedstock in optimization of biomass concentration.	54
3.8	Phase compositions of PEG 4000-IDA-Cu(II)-KPB system in the optimization of NaCl addition.	55
4.1	Effect of activation duration on oxirane ring production.	64
4.2	Effect of BFEE concentration on oxirane ring production.	66
4.3	Effect of epichlorohydrin concentration on oxirane ring production.	67
4.4	Effect of NaOH concentration on oxirane ring production.	68
4.5	Varies tie-line and their corresponding TLL and STL.	83

4.6	Effects of different modes of phase inversion on purity, purification factor, and recovery yield of his-tagged HBcAg from unclarified feedstock using 14% (w/w) PEG 6000-IDA-IDA-Cu(II) and 7.9% (w/w) Na <sub>2</sub> SO <sub>4</sub> system.	85
4.7	Effects of different phase separation methods on the purity, purification factor, and recovery yield of his-tagged HBcAg from unclarified <i>E. coli</i> feedstock using 14% (w/w) PEG 6000-IDA-Cu(II) and 7.9% (w/w) Na <sub>2</sub> SO <sub>4</sub> system.	87
4.8	Purity, purification factor, and recovery yield of his-tagged HBcAg using different PEG-IDACu(II)-salt systems.	89
4.9	Effect of different TLL in PEG 2000-IDA-Cu(II)-Na <sub>2</sub> SO <sub>4</sub> , PEG 2000-IDA-Cu(II)-KPB, and PEG 4000-IDA-Cu(II)-KPB systems on purity, purification factor, and recovery yield of his-tagged HBcAg.	93
4.10	Effects of phase volume ratio of TLL 3 in PEG 2000-IDA-Cu(II)-KPB system system on the partitioning of his-tagged HBcAg.	95
4.11	Effects of addition of different concentrations of NaCl on the partitioning of his-tagged HBcAg using 24.5% (w/w) PEG 2000-IDA-Cu(II) and 12% (w/w) KPB system.	97
4.12	Effect of system pH on the partitioning of his-tagged HBcAg using 24.5% (w/w) PEG 2000-IDA-Cu(II) and 12% (w/w) KPB system.	99
4.13	Effect of biomass concentrations on the partitioning of his-tagged HBcAg using 24.5% (w/w) PEG 2000-IDA-Cu(II) and 12% (w/w) KPB system.	100
4.14	Comparison between ATPS and sucrose gradient ultracentrifugation.	103

## LIST OF FIGURES

Figure		Page
2.1	The virion and genomic structural features	14
3.1	General overview of the methodology.	38
4.1	Effect of IDA concentration on the total copper ions detected in the final product.	69
4.2	Concentration of metal ions bound to PEG-IDA.	71
4.3	Binodal curves of different phase-forming salts with PEG 2000-IDA-Cu (II).	72
4.4	Binodal curves of different phase-forming salts with PEG 4000-IDA-Cu (II).	73
4.5	Binodal curves of different phase-forming salts with PEG 6000-IDA-Cu (II).	73
4.6	Binodal curves of different PEG-IDA-Cu (II) against $\text{Na}_2\text{SO}_4$ .	74
4.7	Standard curve for conductivity measurement (mS/cm) of $(\text{NH}_4)_2\text{SO}_4$ (w/w).	75
4.8	Standard curve for conductivity measurement (mS/cm) of $\text{Na}_2\text{SO}_4$ (% (w/w)).	76
4.9	Standard curve for conductivity measurement (mS/cm) of KPB(% (w/w)).	76
4.10	Standard curve for the refractive index of PEG 2000-IDA-Cu(II)(% (w/w)).	77
4.11	Standard curve for the refractive index of PEG 4000-IDA-Cu(II)(% (w/w)).	78
4.12	Standard curve for the refractive index of PEG 6000-IDA-Cu(II)(% (w/w)).	78
4.13	Standard curve for refractive index of $(\text{NH}_4)_2\text{SO}_4$ (% (w/w)).	79
4.14	A standard curve for refractive index of $\text{Na}_2\text{SO}_4$ (% (w/w)).	80

4.15	A standard curve for refractive index of KPB (% (w/w)).	80
4.16	A phase diagram for PEG 6000-IDA-Cu(II)-Na <sub>2</sub> SO <sub>4</sub> system.	82
4.17	SDS-PAGE gel of HBcAg recovered before and after optimizations on system parameters using PEG 2000-IDA-Cu(II)-KPB system.	102
4.18	Antigenicity determination of ATPS and sucrose gradient ultracentrifuge purified his-tagged HBcAg via ELISA.	104
4.19	Transmission electron micrograph of ATPS purified his-tagged HBcAg particles.	105
4.20	Transmission electron micrograph of sucrose gradient ultracentrifuge purified his-tagged HBcAg particles.	106

## LIST OF ABBREVIATIONS

AAS	Atomic absorption spectrophotometer
APC	Antigen presenting cell
ATPS	Aqueous two phase system
BFEE	Boron trifluoride diethyl etherate
BSA	Bovine serum albumin
cccDNA	Closed circular DNA
CMV	Human cytomegalovirus
CLEIA	Chemiluminescent enzyme immunoassay
DNA	Deoxyribonucleic acid
EDTA	Ethylenediaminetetraacetic acid tetrasodium
ELISA	Enzyme-linked immunosorbent assay
EOPO	Ethylene-oxide propylene oxide
GFPuv	Green fluorescent protein
HBcAg	Hepatitis B core antigen
HBcrAg	Hepatitis B core-related antigen
HBeAg	Hepatitis B e antigen
HBIG	Hepatitis B immunoglobulin
HBsAg	Hepatitis B surface antigen
HBV	Hepatitis B virus
HEPES	4-(2-hydroxyethyl)-1-piperazineethanesulfonic acid
HPLC	High performance liquid chromatography
IDA	Iminodiacetic acid
IgG	Immunoglobulin G

IgM	Immunoglobulin M
IMA-EBAC	Immobilized metal affinity-expanded bed adsorption chromatography
IMAP	Immobilized metal affinity partitioning
IPTG	Isopropyl- $\beta$ -D-thiogalactopyranoside
KPB	Potassium phosphate buffer
LDH	Lactate dehydrogenase
MA-ILC	Immobilized liposome partitioning chromatography
MWCO	Molecular weight cut off
NaOH	Sodium hydroxide
ORF	Open reading frame
PEG	Polyethylene glycol
SDS	Sodium dodecyl sulphate
SDS-PAGE	Sodium dodecyl sulphate-polyacrylamide gel electrophoresis
TED	Tris (carboxymethyl)ethylene-diamine
TEM	Transmission electron microscope
TEMED	Tetramethylethylenediamine
TLL	Tie-line length
TREN	Tris (2-amino-ethyl)amine
VLP	Viral like particle
WHO	World Health Organization

## **CHAPTER 1**

### **INTRODUCTION**

Hepatitis B infection remains as one of the world major health issue that is caused by hepatitis B virus (HBV). It is a serious lethal infection that causes severe chronic state of hepatitis, cirrhosis and hepatocarcinoma (WHO, 2017). HBV infection has caused 887,000 fatalities in 2015 despite the advanced development in biopharmaceutical industry around the world. World Health Organization (WHO) has estimated the number of people who are still living with HBV which is about 257 millions. It is ranked as the top 20 causes for human mortality (Lim, et al., 2017).

HBV can be transmitted through exposure to infected blood, percutaneous and sexual intercourse with average of 80 days of incubation period (Long, et al., 2012; Wyllie, et al., 2006). There are usually without any symptoms during acute HBV infection phase but some might develop into acute illnesses such as darkening of urine, lethargy, yellow eyes and skin, vomiting, disgust and abdominal pain (Long, et al., 2012). On the other hand, chronic infections will cause fatigue and right upper quadrant discomfort, with high risk in developing into cirrhosis and liver cancer, especially people deficiency in immunity (Liang, 2009; Stevens, et al., 2017).

A series of serological markers are available to diagnose and monitor patient with HBV infection such as the hepatitis B surface antigen (HBsAg), hepatitis B e antigen (HBeAg), hepatitis B core antigen (HBcAg), anti-hepatitis B surface antigen antibody (anti-HBs), anti-hepatitis B e antigen antibody (anti-HBe), anti-hepatitis core antigen antibody (anti-HBcAg) and the viral DNA (Lim, et al., 2017). Furthermore, the HBV vaccine remains as the main prevention method for HBV infection, which has proven to be immunogenic, effective and safe to prevent the virus replication and eradicate the viruses with minimum side effect (Sun and Li, 2017).

HBV is categorized as a virus in *Hepadnaviridae* family and group VII with a double stranded DNA. The entire virion is surrounded by an envelope and replicates by reverse transcription (Dandri and Petersen, 2017; Sanada, et al., 2017). The inner nucleocapsid is an icosahedral capsid of 27 nm in diameter, which consists of a HBcAg, a viral genome and a virally encoded polymerase (Block, et al., 2009; Liang, 2009). HBcAg is one of the most frequently studied viral like particle (VLP) for the display of foreign epitopes such as the foot and mouth disease virus (*Picornaviridae*) (Clarke, et al., 1987), hantavirus (Ulrich, et al., 1999) and human cytomegalovirus (CMV) (Tarar, et al., 1996). Therefore, it has a favourable potential in the diagnosis and vaccine development for HBV infection.

HBcAg has the potential in the development vaccine as VLP vaccine carrier moieties (Whitacre, et al., 2010) and to be used in diagnosis kit or

reagents for antibody detection against human HBcAg (anti-HBcAg) (Deng, et al., 2008). Therefore, there has been a rapid growing of interest to invent a more effective and low cost method for HBcAg purification. HBcAg remains as one of the best developed chimeric vaccine carrier moieties until today due to its advantageous characteristics such as the ability to self assemble into capsid like particle, high immunogenicity and can be genetically fused with foreign epitopes without losing the native properties of HBcAg (Whitacre, et al., 2010).

Many studies have been carried out to purify HBcAg from both *Escherichia coli* (*E.coli*) (prokaryotic) and yeast (eukaryotic) expression systems (Chen, et al., 2005). However, the conventional method of purification such as chromatography and ammonium sulphate precipitation require multiple steps of operation, which could lead to excessive product loss and high processing time that resulted in high production cost (Tou, et al., 2014). Consequently, these methods are unfavourable for protein purification in large scale production. Therefore, it is crucial to have an efficient and cost effective recovery and purification method such as aqueous two phase system (ATPS) to ensure a better and efficient protein recovery, especially for large scale downstream processing.

ATPS is a type of simple and versatile liquid-liquid fractionation purification technique that is employed to recover various biological products as well as to overcome the difficulties that are encountered in the conventional

purification methods. ATPS usually forms two immiscible phases either from a type of polymer and a salt, a polymer and a polymer or an ionic liquid and a salt (Chen, et al., 2017). ATPS has vast applications in biomolecules extraction and purification. It can be operated in mild conditions, contains high water content, which enhances the diffusion rate for some solutes, maintains products biological activity and prevents the denaturation risk for labile products. (Fan, et al., 2017). Furthermore, ATPS can also be used to handle highly concentrated feedstock, hence it is suitable for large scale downstream processing (Wang, et al., 2016).

Despite its advantages in protein purification, one of the main disadvantages for ATPS is the low selectivity for protein partitioning (Silva and Franco, 2000). Therefore, it needs to be further explored to improve its ability for selective purification. In this study, immobilized metal affinity partitioning (IMAP) has been incorporated with ATPS to increase the efficiency of ATPS. In this study, three types of modified PEG have been synthesized such as PEG 2000-IDA-Cu(II), PEG 4000-IDA-Cu(II) and PEG 6000-IDA-Cu(II) and all were subjected into the ATPS (polymer/salt phase) to recover HBcAg directly from unclarified bacteria feedstock. Binodal curves, tie-lines and phase diagrams were constructed for all three polymers involved against three types of salts. All these were not reported by any paper previously.

Therefore, the emphases of this study were;

- i) To develop and optimize the synthesis of PEG-IDA of various molecular weight (MW) using epichlorohydrin activation method
- ii) To construct phase diagrams for PEG-IDA-metal with different types of salts
- iii) To investigate the effects of different types of metal ions, metal ligand concentration, pH, salt concentration, biomass concentration, phase volume ratio in ATPS on the yield and purity of his-tagged HBcAg
- iv) To determine the antigenicity and morphology of the purified his-tagged HBcAg

## **CHAPTER 2**

### **LITERATURE REVIEW**

#### **2.1 Hepatitis B virus infections**

HBV has been caused a major global health problem such as hepatitis B infection, which ranked as the top 20 causes of human mortality (Lim, et al., 2017). HBV could cause both acute and chronic liver diseases that is life threatening and could cause death due to liver cirrhosis and cancer (Nosratabadi, et al., 2017). The severity of hepatitis infection is usually age dependent, whereby infants are often linked with chronic infection (Karvonen, 2017). Moreover, it was estimated that the number of people who are still living with HBV is about 257 millions (WHO, 2017). Hepatitis B infection has caused about 887 thousands deaths in 2015, which were mostly due to severe cirrhosis and liver cancer (WHO, 2017) and 50% of all cases recorded were contributed by chronic HBV infection (Sun and Li, 2017).

##### **2.1.1 HBV route of transmission and symptoms**

Hepatitis B virus able to survive outside the human body and can be in inactive form for at least 7 days (Long, et al., 2012). However, unvaccinated people can be infected by HBV if the viruses enter their body within this period (WHO, 2017). The incubation period for HBV is usually ranging from 28 to 180 days, with average of 80 days (Wyllies, et al., 2016). The transmission

modes for HBV are often through percutaneous and sexual intercourse (Long, et al., 2012). Furthermore, it can also spread through mucosal contact with infectious body fluids and blood; medical, surgical and dental unhygienic procedures, tattooing, razors and reused objects or tools that have been contaminated with infected blood; as well as through the reuse of needles and syringes among infected people (Block, et al., 2008; Wyllie, et al., 2016). Although HBV does not cross the placenta, the viremic mothers usually infect their infants with HBV during birth (Baron, 1996). HBV can also be found in human breast milk but HBV transmission through breast feeding has not been shown to increase (Long, et al., 2012).

During the acute phase of HBV infection, most of the infected people do not develop or experience any symptoms and most of the perinatal infections will remain asymptomatic (Wyllie, et al., 2016). However, some people with acute infection may encounter some symptoms like abdominal discomfort, abnormal urine colour and fatigue that last for days and weeks (Long, et al., 2012). Patients with acute infection usually recovered and only approximately 1% of this patient has risk to develop into acute liver failure and it may lead to death (Liang, 2009).

On the other hand, symptoms for chronic infection initially can be no symptoms, or develop some nonspecific symptoms such as weariness and right upper abdominal sickness (Liang, 2009). Chronic HBV infection could later develop into more severe health problem such as liver cirrhosis and cancer,

especially in those patients who have low immunity such as Down Syndrome and dialysis patients, and newborn infants (Stevens, et al., 2017). Eventually, it may lead to more significant symptoms such as jaundice, ascites, gastrointestinal bleeding, peripheral oedema, encephalopathy and splenomegaly (Liang, 2009).

### **2.1.2 Diagnosis and treatments for HBV infection**

There are serological markers available to diagnose and monitor people with HBV infection. These markers are hepatitis B surface antigen (HBsAg), hepatitis B e antigen (HBeAg), hepatitis B core antigen (HBcAg), anti-hepatitis B surface antigen antibody (anti-HBs), anti-hepatitis B e antigen antibody (anti-HBe), anti-hepatitis core antigen antibody (anti-HBcAg) and the viral DNA (Lim, et al., 2017). Patient in an acute or chronic stage of HBV infection can be identified with these markers.

The presence of HBsAg and immunoglobulin M (IgM) antibody against HBcAg indicates patient is in acute stage of hepatitis B infection. Initially, they are usually detected with the presence of HBeAg (Baron, 1996). HBeAg is an indicator for high levels of HBV replication, whereby the patient's blood and body fluids are highly infectious (Liang, 2009). Apart from that, when blood test indicates that hepatitis B surface antigen (HBsAg) has decreased with elevated level of hepatitis antibody (anti-HBs), it shows that the acute infection in healthy adults is in the recovery phase (Stevens, et al., 2017).

In contrast, chronic HBV infection is characterized by the persistent existence of HBsAg in the patient blood sample for at least half years with or without present of HBeAg (Block, et al., 2008; Wyllie, et al., 2016). The persistent existence of HBsAg is the important marker for risk of developing life threatening disease later in life such as liver cancer and cirrhosis. On the other hand, low level of HBsAg can reflect an inactive carrier state as well as strong host immune control against HBV infection (Herman and Chan, 2017). Series of details diagnoses of various clinical forms of HBV infection are tabulated in Table 2.1.

Histological test on liver tissue is crucial to evaluate fibrosis stage for HBV infected children (Wyllie, et al., 2016). The patients with acute hepatitis and those expected with good prognosis are not subjected to this test. However, in cases when the outcome is unknown, this test may become crucial to determine the diagnosis and the expected prognosis (Wyllie, et al., 2016). Besides that, a recently widely used marker known as hepatitis B core-related antigen (HBcrAg) has been utilised for the diagnosis on the severity of HBV infection (Zhang, et al., 2016). HBcrAg makeup of HBeAg, HBcAg and 22-kD precore protein (p22cr) and it has been used as a marker to detect the transcriptional activity of covalently closed circular DNA (cccDNA) in the liver cells. It has been shown to have a significant relationship with HBV DNA loads in the serum (Zhang, et al., 2016). Therefore, HBcrAg had been used to develop enzyme immunoassay kit and a chemiluminescent enzyme immunoassay (CLEIA) for the detection of serum HBcrAg (Kimura, et al., 2002).

**Table 2.1: Serological and virology markers for HBV infection (Baron, 1996; Herman and Chan, 2017; Liang, 2009).**

<b>Markers</b>	<b>Diagnosis</b>
HBsAg	Acute and chronic infection
HBsAg and HBeAg	Incubation period
HBeAg	Highly infectious HBV with high level of replication; used as treatment response marker
Viral DNA	HBV replication; used as treatment response marker
IgM	Acute and chronic HBV infection
IgG	Chronic HBV infection; stage of recovering
Anti-hepatitis B surface antigen antibody	Stage of recovering; marker for vaccination
Anti-hepatitis B e antigen antibody	Low infectivity of HBV with low HBV replication; used as treatment response marker
IgG and anti-hepatitis B surface antigen antibody	Stage of recovering; history of HBV infection
IgG and HBsAg	Chronic infection
IgG or anti-hepatitis B surface antigen antibody and viral DNA	HBV latency

So far, there is no specific treatment for acute HBV infection. Thus, the treatment is usually aimed to maintain patient in comfort phase by taking sufficient nutrition and intake plenty of water to replace the fluid lost from vomiting and diarrhoea (WHO, 2017). On the other hand, the progression of cirrhosis and liver cancer for chronic HBV infection can be slow down by the medicines such as the oral antiviral agents, which aim to prolong the survival term (Herman and Chan, 2017). Drugs such as tenofovir or entecavir are

efficient in suppressing the HBV. Furthermore, these drugs also rarely lead to drug resistance issues as compared to other drugs (Herman and Chan, 2017). The antiviral nucleotides and interferon are also effective in controlling the viral replication but they are not able to fully get rid of HBV from the infected host due to the virus mutation and drug resistance ability (Sun and Li, 2017). Therefore, treatment involved for HBV infection usually does not cure this infection but it mainly focuses on the suppression of replication for HBV. As a result, treatment for HBV infection must be continued for a life time to prevent viral relapse (Herman and Chan, 2017). Therefore, a regular check-up and diagnosis are necessary.

### **2.1.3 Prevention for HBV infection**

Hepatitis B vaccine is the mainstay for HBV infection prevention because it is immunogenic, safe and effective in controlling the virus replication as well as in the eradication of the viruses. Furthermore, their side effects are insignificant (Sun and Li, 2017). WHO (2017) has recommended that newborn infants should inject with hepatitis B vaccination as soon as within 24 hours after birth. The protective efficacy may be higher than 90% if the vaccine is taken together with hepatitis B immunoglobulin (HBIG) (Baron, 1996).

In 2015, the prevalence of HBV infection in less than five years old child was as low as 1.3%, compared to about 4.7% before the vaccination era (WHO, 2017). The HBV vaccination can produce HBV antibody above the

protective levels in more than 95% of people globally (WHO, 2017). The protection provided by the vaccine lasts for at least 20 year or till death. Children and adolescents less than 18 years old without vaccinated previously need to be vaccinated, especially for those living in countries with low and intermediate endemicity. Similarly, people who are at high risk of getting HBV infection such as from blood transfusion, dialysis, patients with prolonged treatment as well as patients with immunodeficiency or suffering from malignant diseases should be vaccinated (Baron, 1996).

## **2.2 Hepatitis B virus (HBV)**

### **2.2.1 Structure of HBV**

Hepatitis B virus is a double-stranded DNA virus of the *hepadnaviridae* family under the group VII of viruses, with small particle size between 42 to 47 nm. Moreover, the entire virion is covered by an envelope and it replicates by reverse transcription (Dandri and Petersen, 2017; Sanada, et al., 2017). It also comprises of an icosahedral capsid of 27 nm in diameter, composed of HBcAg, polymerase and the viral DNA (Block, et al., 2009; Liang, 2009). The viral genome is about 3.2 kilobase (kb) pair with partially double-stranded circular DNA. The HBV polymerase is bound to the 5' end of the negative strand of the genome (Block, et al., 2008).

The capsid of HBV acts as a protector, which prevents foreign particles from destroying the DNA. Furthermore, the capsid is also surrounded by an outer envelope known as HBsAg, which embedded in membranous lipid

derived from the host cells during the budding process from endoplasmic reticulum (Wyllie, et al., 2016). HBsAg protein is produced in excess by infected hepatocytes and is secreted into serum in the form of 22 nm small particles with filamentous and spherical particles (Block, et al., 2008; Liang, 2009; Long, et al., 2012). HBsAg categorized into small (S), medium (M) and large (L), which differentiating into S, preS2 and preS1 domains accordance to their polypeptide length and size as shown in Figure 2.1. On the other hand, the other antigen known as HBeAg is an antigenic determinant that is closely related to the capsid of HBV and it circulates as soluble protein in serum (Long, et al., 2012).

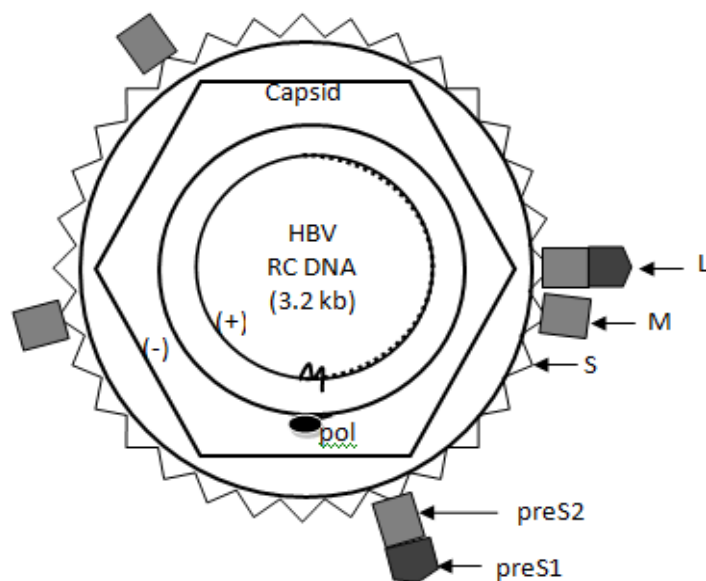


**Figure 2.1: The virion and genomic structural features**

HBsAg is the surface antigen for HBV and it is categorized into small (S), medium (M) and large (L), which consists S, preS1 and preS2 domain. The polymerase consists of 800 amino acids represented by pol and it is covalently bound to the 5' end of the negative strand of the HBV genome, which is about 3.2 kb in size.

The HBV genome encodes a total of four open reading frames (ORFs) such as the S, C, P and X. The surface enveloped protein HBsAg is encoded by S ORF; C ORF has the precore and core regions with both encode for the viral nucleocapsid HBeAg and HBcAg, respectively, depending on which region the translation is initiated. P ORF encodes the viral large protein about 800 amino acids, which known as polymerase (pol) and X ORF encodes a 16.5 kDa protein (HBxAg) that play an important role in viral signalling transduction, transcriptional activation, DNA damage repairing and inhibition of protein degradation (Baron, 1996; Liang, 2009).

### **2.2.2 Hepatitis B core antigen (HBcAg)**

Hepatitis B core antigen (HBcAg) is a 28 nm structural protein and non-secreted antigen, which acts as an indicator for the replication of the HBV that can be found on the surface of the nucleocapsid (Yu, et al., 2013). HBcAg is an important component of the nucleocapsid layer, which mediates the interaction with the viral DNA and polymerase (Chen, et al., 2004; Hatton, et al., 1992). HBcAg is assembled intracytoplasmically and it shares a similar 1-149 amino acid sequences with HBeAg, despite their remarkable difference in physical and antigenic properties (Birnbaum and Nassal, 1990). Moreover, HBcAg possesses an additional 34 residues at C-terminal but lacks the 10 residues at N-terminal of HBeAg (Milich, et al., 1990; Schodel, et al., 1993). HBeAg and HBcAg are differentiate with their primary antigen presenting cells (APC) such as the T helper (Th)-cell, which trigger specific and strong antibody production via T-cell independent for HBcAg and T-cell dependent

for both HBcAg and HBeAg pathways (Chen, et al., 2004; Millich, et al., 1990; Schodel, et al., 1993).

HBcAg consist of two domains, first, the N-terminal assembly domain (1-149 residues) and second is the basic C-terminal with 36 of arginine rich residues (Hatton, et al., 1992). The end of C-terminal of the protein contains arginine clusters, which appear to be involved in nucleotide packaging (Kenney, et al., 1995). Besides, HBcAg is structured by a single polypeptide chain with a MW of 20 kDa (Wynne, et al., 1999). On the other hand, HBcAg can be expressed in bacteria and it is able to self assemble into a icosahedral shells of two morphologies and sizes such as  $T=3$  and  $T=4$  capsids, which consist of 180 or 240 HBcAg subunits, respectively (Crowther, et al., 1994; Wynne, et al., 1999; Zlotnick, et al., 1996).

The HBV nucleocapsid contains a simple C-terminal sequence, which is very rich in arginine residues that are believed to play an important role in the interaction with the viral nucleic acid and function to encapsidate the HBV RNA pregenome (Kenney, et al., 1995). Therefore, removal of arginine rich C-terminal sequences by truncation at residue 149 causes high bacterial expression, and produce high yield of  $T=4$  capsid. It also proved that deletion of this region does not change the morphology of the particle (Wynne, et al., 1999; Zlotnick, et al., 1996).

HBcAg is widely studied motivated by its fundamental biological importance as well as due to its medical significance. HBcAg is able to form particles with protruding spikes even when a foreign peptide sequence is fused into the HBcAg coding region (Kenney, et al., 1995). As such, HBcAg can be used for displaying foreign protein domain onto the surface of HBV nucleocapsid, which makes them a promising carrier for presentation of foreign epitopes (Kenney, et al., 1995).

Some of the modifications that have been performed to HBcAg which include the addition of foreign sequences to the N or C terminus as well as the internal insertions. However, none of these modifications have prevented the HBcAg assembly into capsid. These modifications showed that the truncated HBcAg that can be used as a ligand for anti-HBe antibody detection (Schodel, et al., 1992). In order to develop HBcAg to become a vaccine carrier moiety, the foreign sequences attach site has been identified in recombinant expression systems. It requires a linker to attach the foreign sequences onto the N or C-terminus of the HBcAg. In addition, the fusion to these terminus did not interfere with HBcAg self-assemble ability; therefore, the antigenicity and shape of HBcAg are preserved (Schodel, et al., 1996).

### **2.2.3 Expression and production of HBcAg**

Hepatitis B core antigen (HBcAg) is known to be a virus-like particle (VLP) due to their ability to self-assemble, unable to self-replicate and does not contain pathogenic particles. In short, HBcAg structurally forms viral capsid

but with absence of viral genome. The production of HBcAg can be expressed directly from eukaryotic cells or prokaryotic cells (Suffian, et al., 2017). It can be done in either homologous or heterologous expression systems, which have been widely studied for their production in different types of expression systems such as plant viral expression system (Huang, et al., 2006), *Saccharomyces cerevisiae* (Chen, et al., 2005) and *E. coli* (Elghanam, et al., 2012; Milich, et al., 1997).

The bacterial expression system by using *E. coli* is the widely used expression system for HBcAg production because it provides a efficient, high production yield and low cost HBcAg recombinant capsid (Suffian, et al., 2017). In order to produce HBcAg suitable for drug delivery purpose, few short-comings need to be overcome in bacteria expression system such as the degradation of protein by host proteases, incorrect protein folding and difficulty in desired protein isolation from inclusion protein (Suffian, et al., 2017). Therefore, a series of optimizations need to be done to improve the overall productivity of bacterial expression system.

#### **2.2.4 N-terminally his-tagged HBcAg**

In the year 2007, under the observation with X-ray crystallography, it was found that the N-terminus of HBcAg particle is protruded out from the capsid (Tan, et al., 2007). Therefore, it is possible to insert a foreign sequence into this terminus by a linker. As a result, the binding of a foreign sequence (his-tag) to the N-terminus will be exposed these foreign sequences on the

surface of the capsid, which is beneficial for protein purification. For instance, an N-terminally his-tagged HBcAg, which was produced using *E. coli* expression system have been successfully recovered by using immobilized metal affinity chromatography (IMAC) (Yap, et al., 2009). The effect of this foreign sequences bound onto the N-terminus of HBcAg were studied. It was shown that the expression for constructed his-tagged HBcAg was high and it can be purified easily without the need of denaturation and renaturation of the capsid (Yap, et al., 2009). Furthermore, the fusion of his-tagged and the linker onto the N-terminus of HBcAg did not alter the self-assemble ability of the capsid as well as the antigenicity of the core particle.

On the other hand, N-terminally his-tagged HBcAg has also been purified using immobilized metal affinity-expanded bed adsorption chromatography (IMA-EBAC) from unclarified bacterial feedstock (Yap, et al., 2010). IMAC is a commonly used method for his-tagged protein purification that conjugated to aminodiacetic acid (IDA) ligands, then chelated onto the transition metal ions such as the nickel ion or copper ion. This metal ions act as a Lewis acid that play an important role in accepting the electron released from the histidyl residues of the his-tagged protein (Yap, et al., 2010). IMA-EBAC provides an alternative method for his-tagged HBcAg purification that produced 91% purity with purification factor of 3.64 (Yap, et al., 2010). Unfortunately, the recovery yield for his-tagged HBcAg directly from unclarified feedstock is not satisfying by using IMA-EBAC.

### **2.2.5 Conventional method for HBcAg extraction and purification**

Many methods have been used to purify HBcAg but most of the methods are too costly because they usually require processed protein solution, which free from contaminant prior to the purification process (Hjorth, 1997). These involve multiple steps of purification, whereby the protein feedstock is subjected to multiple clarification processes after it is harvested from bacterial broth to remove unwanted contaminants that will influence with the subsequently recovery step (Hjorth, 1997). Moreover, it is also time consuming, which eventually increases the overall production cost, particularly when large scale application is required (Rolland, et al., 2001).

Several HBcAg extraction and purification methods have been developed and described are ammonium-sulphate precipitation (Naito, et al., 1997; Palenzuela et al., 2002; Ng et al., 2006), size-exclusion chromatography (Tang, et al., 2007), sucrose-gradient ultracentrifugation (Huang, et al., 2006; Tan, et al., 2003), packed bed adsorption chromatography (Johansson, et al., 1996; Tan, et al., 2007) and high performance liquid chromatography (HPLC) (Tang, et al., 2007). Although these methods recovered HBcAg with high purity, there are some disadvantages that made these purification methods unfavorable.

For example, a study done by Palenzuela et al. (2002) utilized combination of ammonium sulphate precipitation and gel filtration chromatography on the Sepharose CL-4B column for HBcAg purification.

Multiple steps of purification were involved and the results showed that the purified HBcAg obtained was 90% in purity with 47% recovery yield. This result was not satisfying due to the low recovery yield obtained. Similar result was reported, whereby the ammonium sulphate precipitation required multiple steps of processes that produced a low recovery yield HBcAg. A total of 15% of HBcAg yield was lost due to the initial clarification steps for ammonium sulphate precipitation method (Ng, et al., 2006). Therefore, there is a critical demand for an economically friendly and rapid protocol for the purification of HBcAg such as aqueous two phase system (ATPS) to overcome these limitations.

### **2.3 Aqueous two phase system (ATPS)**

Aqueous two phase system (ATPS) is a promising type of liquid base fractionation purification technique that has been used to recover and purify different biological components such as acids (Wang, et al., 2017), antioxidants (Dordevic and Antov, 2017), metal ions, antibodies, dyes, enzymes and antibiotic (Fan, et al., 2017). It has also been used in separation of bio-product and bioconversion (Chen, et al., 2017). ATPS usually forms two immiscible phases by a polymer and a salt, a polymer and a polymer or an ionic liquid and a salt (Chen, et al., 2017; Fan, et al., 2017). Two immiscible phases will be formed under a specific temperature and system composition, whereby the polymer is enriched in the top phase and the salt or another type of polymer is enriched in the bottom phase (Fan, et al., 2017).

In polymer-salt ATPS, PEG of different molecular weight is the commonly used polymer in ATPS due to their low toxicity, low price and low volatile nature (Iqbal, et al., 2016). There are different factors that influence the phase separation in ATPS such as the concentration of polymer and salt, composition of salt, and molecular weight (MW) of polymer (Iqbal, et al., 2016). Phase separation behaviour also changes according to the type of salt due to their different properties (Iqbal, et al., 2016). Salt is crucial in ATPS due to their ability to absorb large amount of water and causes salting out phenomenon. Therefore, in polymer and salt ATPS, the phase separation is mainly caused by salting-out effect because it is mainly set up based on polymers and salts as the salting-out reagents (Dordevic and Antov, 2017; Iqbal, et al., 2016). Different types of ATPS have been used in the extraction and purification of different products as tabulated in Table 2.2.

### **2.3.1 Advantages of ATPS**

Aqueous two phase system has been extensively studied because this system provides a vast applications and advantages for biomolecules extraction and purification. ATPS can be operated in mild conditions (ordinary temperatures and pressures) for biological products extraction. This system mainly consists of water (70-90%) with low interfacial tension that enhances the diffusion process of some solutes and maintains their biological activity (Chen, et al., 2017; Fan, et al., 2017; Wang, et al., 2016). Therefore, denaturation risk for fragile biomolecules can be reduced compared to the traditional extraction systems (Fan, et al., 2017).

Furthermore, the biocompatibility, environmental friendly, process integration capability, scale up feasibility, high efficiency, ease of operation under large scale application with improved recovery yield and low cost are the main advantages of ATPS (Dordevic and Antov, 2017; Fan, et al., 2017; Wang, et al., 2017).

ATPS can be applied to handle large amounts of highly concentrated feedstock, therefore, it is suitable for large scale application for industrial and research purposes (Wang, et al., 2016). For instance, a capsaicin recovery yield of 95.5% from capsicum oleoresin was obtained using an ATPS consisting of ethylene-oxide propylene oxide (EOPO) and potassium phosphate (Fan, et al., 2017). In addition, high recovery yield of thaumatin extraction by ATPS was also reported, whereby the recovery yield was 96.02% (Ahmad, et al., 2008). High recovery yield usually seen in ATPS extraction and purification as this technique incorporates clarification, concentration and partial purification in a single step. Therefore, the steps required in purification process are reduced, thus the loss of protein can be minimized (Ahmad, et al., 2008).

**Table 2.2: Products extracted and purified with different types of ATPS.**

<b>Types of ATPS</b>	<b>Product extracted /purified</b>	<b>References</b>
Deep eutectic solvent (DES)-salt	Chlorogenic acid	Wang, et al., 2017
Ethanol-ammonium sulfate	Antioxidants (xylooligosaccharides and phenol compounds)	Dordevic and Antov, 2017
Ethylene oxide-propylene oxide (EOPO) copolymer- salt/ethanol	Capsaicin	Fan, et al., 2017
Poly(ethylene oxide) (PEO)-poly(propylene)(PPO)-Poly(ethylene oxide) (PEO)	Enzyme (Bromelain)	Rabelo, et al., 2004
PEG-phosphate	Enzyme (Collagenase)	Rosso, et al., 2012
PEG 4000-potassium citrate	Enzyme ( Lysozyme)	Lu, et al., 2013
Poly(hydroxyethylmethacrylate)-chitosan (pHEMA-chitosan)	Enzyme ( Lysozyme)	Yilmaz, 2005
PEG-phosphate	Enzyme [Glucose-6-phosphate dehydrogenase (G6PD)]	Ribeiro, et al., 2007
PEG-chlolinium salts	Antibiotic (tetracycline)	Pereira, et al., 2013
Aqueous two-phase micellar systems (ATPMS)	Antimicrobial peptide (Nisin)	Jozala, et al., 2012
Poly(ethylene oxide)(PEO)-sodium sulphate/lithium sulphate	Dye (carmine)	Mageste, et al., 2009
PEG 400-citrate	Plamidial DNA (pDNA)	Rahimpour, et al., 2006
Aqueous two-phase micellar systems (ATPMS)	Lipopolysaccharides (LPS)	Magalhaes, et al., 2007

### 2.3.2 Phase diagram

Phase diagram for ATPS is a graph that delineates the potential working area (two phases) for a particular two-phase system, where the pH, temperature and polymer/salt concentration are under a specific measurement (Kaul, 2000). The phase diagram provides information such as the concentration of phase-forming components necessary to form a system with two phases that are in equilibrium. In addition, the concentration of phase components in the top and bottom phases and the phase volumes ratio can also be determined from the phase diagram (Asenjo and Andrews, 2011; Raja, et al., 2011). The information provided by the phase diagram such as the binodal curves and tie line length enable researchers to make a systemic choice to be used as preliminary partitioning experiment (Kaul, 2000).

The binodal curve separates the diagram into two regions, which are known as biphasic region (above the binodal curve) and monophasic region (below the binodal curve) (Iqbal, et al., 2016). The line from T to B in Figure 2.2 is a tie-line that connects two or more nodes, which lies on the binodal curve. It is graphed to express the effect of system composition on partitioned biomolecules by calculating the tie-line length. The ratio of segments AB and AT, (Figure 2.2) can be estimated graphically by using the weight ratio  $V_t \rho_t / V_b \rho_b = AB/AT$ , where V and  $\rho$  are the volume and the density of the top (t) and bottom (b) phase, respectively (Iqbal, et al., 2016).

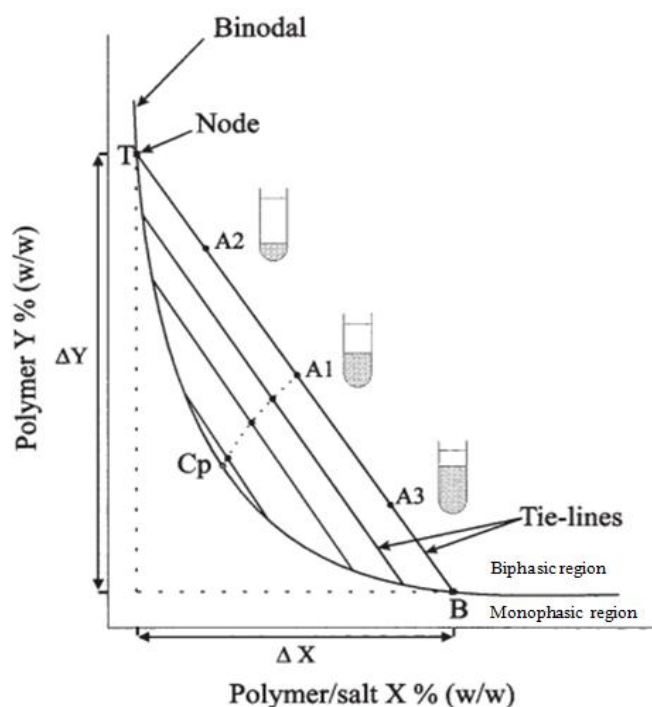


**Figure 2.2: The informations and details provides by the phase diagram.**

Bottom phase polymer/salt X (% w/w) is plotted on the x-axis and top phase polymer Y (% w/w) is plotted on the y-axis. A1, A2, and A3 represent the phase's compositions of three different systems lying on the same tie-line with different volume ratios. The final compositions of the top and bottom phase are represented by nodes T and B, respectively. The ratio of the segments AB (top phase) and AT (bottom phase) can be approximated graphically by the volume ratio of the two phases. The critical point, Cp is determined by extrapolation through the midpoints of a number of tie-lines. The difference in concentration of component X and Y between the two phases is represented by  $\Delta Y$  and  $\Delta X$  (Asenjo and Andrews, 2011; Iqbal, et al., 2016; Raja, et al., 2011; Kaul, 2000).

### 2.3.3 Factors that affected the partitioning of bio-molecules in ATPS

Partitioning behaviour of biomolecules in ATPS is usually influenced by several factors such as molecular weight (MW) of polymer, concentration of polymer, pH, ionic strength of the salt, hydrophobicity and temperature (Asenjo and Andrews, 2011; Johansson, et al., 2011). Apart from these factors,

phase separation rate in ATPS can also be affected by some physio-chemical properties such as density, viscosity and interfacial tension in the system (Iqbal, et al., 2016). The net effect of various interactions or bonding is different across two phases in ATPS, which resulted in the partitioning of protein into one phase (Asenjo and Andrews, 2011). Moreover, different type of bonds are also responsible for the protein interaction with surrounding molecules such as hydrogen, ionic and hydrophobic interactions with other weak forces (Asenjo and Andrews, 2011). Therefore, in order to achieve an effective separation of a particular biomolecule, optimization of these factors are necessary in order to achieve an optimal separation.

The MW of polymers highly influences the protein partitioning in ATPS, especially for system that is composed of polymer-salt (Raja, et al., 2011). High MW polymer requires low concentration of polymer for biphasic formation. Therefore, the binodal curves will shift towards the origin (Asenjo and Andrews, 2011). In contrast, low protein partitioning is expected in the phase with high MW polymer (Iqbal, et al., 2016). Besides that, difference in density, concentrations and viscosity between phases increase as the MW of polymer increases (Raja, et al., 2011). Hydrophobicity of the polymer increases as the MW of polymer growth due to the decrease in hydrophilic groups and increase of their hydrophobic chain area (Iqbal, et al., 2016).

Hydrophobicity is an important factor for protein partitioning. Beside the MW of polymer and TLL, addition of salt plays an important role in

manipulating the hydrophobicity in the system (Asenjo and Andrews, 2011). Usually both phases in ATPS are rather hydrophilic. However, the top phase (PEG enriched phase) is usually more hydrophobic than the bottom phase (Asenjo and Andrews, 2011). Therefore, this condition favours the partitioning of hydrophobic protein towards the top phase. Salts have ions with different hydrophobicities. Therefore, addition of salt into ATPS could force the counter ions to move into a phase with higher hydrophobicity, which eventually changes the binodal curve and phase diagram (Iqbal, et al., 2016).

The partitioning behaviour in biomolecules can also be significantly influenced by the pH in ATPS because it could alter the charge and surface properties of solutes (Asenjo and Andrews, 2011). If the pH in the system is higher than the isoelectric point, the protein will become negatively charged. On the other hand, if the pH drops below the isoelectric point, the protein will become positively charged (Iqbal, et al., 2016; Raja, et al., 2011). Higher pH values increase the affinity of protein into the PEG-rich phase and partition coefficient has been reported to increase or induce an additional affinity towards the PEG rich phase (Asenjo and Andrews, 2011; Iqbal, et al., 2016).

In general, temperature mainly influences the composition of two phases, or the phase diagram by affecting the partitioning through viscosity and density in ATPS. The two phase's areas also expand with increase in temperature (Iqbal, et al., 2016; Raja, et al., 2011). It has been shown that the

phase separation is very efficient in polymer-salt system at low temperature (Iqbal, et al., 2016).

## **2.4 Metal affinity partitioning**

Metal affinity partitioning is a potential affinity concept in bio-separation and it was first presented by Porath, et al. (1975) for the purification of proteins. This concept has an expanding range of applications, which has been incorporated into different protocols such as ATPS, chromatography and affinity adsorbent in order to develop a better method for protein and bio-molecules partitioning as shown in Table 2.3.

One of application for metal affinity is the development of metal affinity immobilized liposome partitioning chromatography (MA-ILC) for various peptides partitioning ranging in size from 5 to 40 residues (Nagami, 2014). The retention ability of peptides on the MA-ILC was shown to depend on the number of histidine residues in the peptides, but not their hydrophobicity. Therefore, this can be used as an effective method for analyze or separating peptides based on the metal affinity and the hydrophobicity interaction. Furthermore, metal affinity also applied in the development of immobilized metal ion affinity adsorbent on the binding of  $\alpha$ -amylase (Liao and Syu, 2009). The adsorbent was developed by chelating the IDA on cross-linked  $\beta$ -cyclodextrin, which further linked with copper ion to extract  $\alpha$ -amylase from the fermentation broth of *Bacillus amyloliquefaciens* (Liao and Syu, 2009). This method successfully recovered 81% of the enzyme activity with absorption ability for the metal affinity was up to 98%.

There are several advantages of using metal ions as the ligands for protein partitioning such as it provides easier product elution and ligand regeneration, metal ligands are stable under wide range of temperature and solvent conditions, specific binding with target protein, the interaction with target protein is reversible and they can be recycled without losing their performance (Silva and Franco, 2000). Moreover, the most general approach for protein immobilization is the use of recombinant tag such as histidine tag (his-tag). The generation of his-tagged to either N or C terminus of protein is the most commonly used metal partitioning affinity method in protein recombinant technology, which not only can be applied on protein in native states, but also those denatured protein and small peptide (Predki, 2007). This affinity is highly stable and it only can be reversed with the presence of high concentration of competing ligands such as imidazole.

**Table 2.3: Bio-separation methods based on affinity partitioning.**

Methods	Products	References
Immobilized affinity partitioning in ATPS	Green fluorescent protein (GFPuv)	Bernaumat and Bulow, 2006
Immobilized affinity partitioning in ATPS	Proteinase inhibitor ( $\chi_2$ -M)	Birkenmeir, et al., 1991
Metal affinity-immobilized liposome chromatography	Peptides	Nagami, et al., 2014
Immobilized metal ion affinity adsorbent based on cross-linked $\beta$ -cyclodextrin matrix	$\alpha$ -amylase	Liao and Syu, 2005
Dual affinity method in ATPS	Plasmid DNA (pUC19 plasmid)	Barbosa, et al., 2010
Affinity two phase partitioning	Primary antibody (caveolae)	Ramirez, et al., 2004
Immobilized metal ion affinity adsorbent ( $\beta$ -CD <sub>cl</sub> -IDA-Cu <sup>2+</sup> )	$\alpha$ -amylase	Liao and Syu, 2009

#### 2.4.1 Immobilized metal affinity partitioning (IMAP) in ATPS

Aqueous two phase system (ATPS) is an attractive alternative method for protein purification. However, one of the main drawback for ATPS is its low selectivity for protein partitioning and it still needs to be further explored for overall process improvement. Several methods such as the usage of ionic liquid phase (Pei, et al, 2009), trizine dye bound-polymer (Johansson and Andersson, 1984) and metal chelated polymer (Bernaumat and Bulow, 2005)

for protein partitioning enhancement in ATPS can be used to overcome this limitation.

Apart from these, immobilized metal ion affinity partitioning (IMAP) method has also been incorporated in ATPS to increase the selectivity of the metal-binding protein and improve the efficiency of ATPS. It also provides a fast and selective method for protein purification with ease in scale up and to potentially replace some other chromatography steps in downstream processing (Silva and Franco, 2000). This can be done by grafting a chelator, iminodiacetate (IDA) onto PEG to extract and purify products of interest such as lactate dehydrogenase (LDH) (Dongqiang, et al., 2000), green fluorescent protein (GFPuv) (Bernaudat and Bulow, 2006), proteinase inhibitor ( $\gamma_2$ -M) (Birkenmeir, et al., 1991) and *E. coli* inner membranes (Everberg, et al., 2006). Moreover, IDA is the most common and frequently used chelator for affinity partitioning compared to other chelators such as Tris (2-amino-ethyl)amine (TREN) and Tris (carboxymethyl)ethylene-diamine (TED) (Mondal and Gupta, 2006).

The first to apply metal ions as affinity ligands in ATPS was reported by Wuenschell, et al. (1990). Immobilized metal affinity partitioning (IMAP) in ATPS employed metal affinity ligands using a chelator known as iminodiacetic acid (IDA), which is bonded with PEG. Then, the resulted PEG-IDA is chelated onto a transition metal such as copper ions that is potentially

useful to selectively extract proteins by targeting cysteine, tryptophan or histidine that is accessible on the protein surface (Botros, et al., 1992). Although many amino acid residues can participate in binding, the actual protein retention in IMAP is basically based on the availability of histidyl residues (Gaberč-Porekar and Menart, 2001).

As for histidine, the imidazole group of it play an important role in binding onto the metal ions and a single histidine is good enough for binding metal affinity ligands (Mondal and Gupta, 2006). A specific binding by metal ions towards the amino acids which enable the extraction of targeted proteins into the PEG rich phase while the contaminant proteins remain in the other phase (Ruiz, et al., 2012). This provides a fast and selective alternative to enhance the protein partitioning, which further improve the purification factor and yield of the targeted protein (Silva and Franco, 2000).

#### **2.4.2 Recent findings of IMAP in ATPS**

Immobilized metal affinity partitioning (IMAP) has been incorporated into ATPS for biomolecules and protein purification. Recently, a research has been carried out for xylanase partitioning using metal affinity polymer-salt ATPS (Fakhari, et al., 2017). The immobilized metal affinity component known as PEG-IDA-Cu(II) has been synthesized according to methods described by Pesliakas, et al. (1994), whereby only PEG 6000 was selected for modified PEG production and it was activated using epichlorohydrin, which

covalently attach to IDA and then chelated on copper ion. The influence of the PEG and salt concentration, PEG-IDA-Cu(II) concentration, system pH, and crude enzyme concentration were evaluated based on the interaction on enzyme, enzyme yield and enzyme specific activity. Results obtained shown that the system with 10% PEG, 12% sodium sulfate, 50% ligand PEG-IDA-Cu<sup>2+</sup>, pH 8 and 6% crude enzyme loading extracted the highest xylanase specific activity (79.95) at top phase, where enzyme specific activity at top phase elevated with increasing polymer concentration, pH and crude concentration (Peliakas, et al., 1994).

On the other hand, in 2015, similar method has also been used for selective extraction of histidine derivative (Oshima, et al., 2015). However, instead of PEG-IDA-Cu(II), the chelating ligands used in this study were commercially purchased with one or two available IDA groups. Metal affinity using the synthesized complex between Cu(II) and commercially available chelating ligands in both studies, respectively, were found to be positive and effective for the extraction in ATPS. The histidine derivatives were efficiently extracted into the PEG-rich phase by binding to the metal ion through their imidazole groups. This study found that neutral or slightly basic systems were suitable for metal affinity partitioning for histidine derivatives due to the deprotonation of the imidazole groups, which facilitated the binding. As a result, they concluded that this method was a great alternative separation tool for histidine derivatives.

Furthermore, a random peptide was fused to the N-terminal of the green fluorescent protein (GFPuv) and extracted using the IMAP in a PEG/salt system (Bernaumat and Bulow, 2006). This proved that the presence of histidine and hydrophobic residues in the tag greatly improved the partitioning of recombinant protein in ATPS using metal affinity. The study use only a partially substituted PEG-salt system, where the results shown the protein partitioning still increasing at 20 to 30% PEG-IDA-Cu(II) substituted. Unfortunately, due to the limited polymer available, only 20% of PEG-IDA-Cu(II) is used for further study.

## CHAPTER 3

### MATERIALS AND METHODS

#### 3.1 Materials

##### 3.1.1 WB-HBcAg *Escherichia coli* cells

WB-HBcAg *E. coli* BL21 cells harbouring the plasmid pHis- $\beta$ -L-HBcAg coding for N-terminally his-tagged HBcAg recombinant protein contains a 6x his tag, an Xpress<sup>TM</sup> epitope tag, an enterokinase cleavage site, an octapeptide of  $\beta$ -galactosidase (Met-Thr-Met-Lle-Thr-Asp-Ser-Leu) and a tripeptide linker (Glu-Phe-His) at N-terminus of the truncated HBcAg (Yap, et al., 2009) was obtained from professor Dr. Tan Wen Siang from Faculty of Biotechnology and Biomolecular Science, Universiti Putra Malaysia (UPM).

##### 3.1.2 Chemicals and stock solutions

The chemicals and media used and their respective manufacturers are listed in Table 3.1. All chemicals were used as obtained without further purification.

**Table 3.1: Source of chemicals and media used in the study.**

<b>Chemicals</b>	<b>Manufacturers</b>
2-β-mercaptoethanol	Merck, Germany
4-(2-hydroxyethyl)-1-piperazineethanesulfonic acid (HEPES)	Merck, Germany
Absolute ethanol	Merck, Germany
Acrylamide	Nacalai Tesque, Japan
Albumin (bovine serum) fraction V	EMD Milipore, USA
Ammonium persulphate	Sigma Aldrich, USA
Ammonium sulphate	Bio-Basic Inc, Canada
Bis-acrylamide	Sigma Aldrich, USA
Boron trifluoride diethyl etherate (BFEE)	Merck, Germany
Bromophenol blue	Bio-Basic Inc, Canada
Chloroform	Merck, Germany
Coomassie brilliant blue G-250	Merck, Germany
Coomassie brilliant blue R-250	Nacalai Tesque, Japan
Copper sulphate	Merck, Germany
Diethanolamine	Merck, Germany
Diethyl ether	Merck, Germany
Epichlorohydrin	Merck, Germany
Ethylenediaminetetraacetic acid tetrasodium (EDTA)	ACROS organic, USA
Glycerol	SYSTEM <sup>®</sup> , Malaysia
Glycine	Bio-Basic Inc, Canada
Imidazole	Merck, Germany
Iminodiacetic acid (IDA)	Merck, Germany
Luria-Bertani (LB) Lennox agar	Conda Pronadisa, Spain
Luria-Bertani (LB) Lennox broth	Conda Pronadisa, Spain
Magnesium chloride	Merck, Germany
Methanol	Merck, Germany
Nickel sulphate	Merck, Germany
PEG 2000	Bio-Basic Inc, Canada
PEG 4000	Bio-Basic Inc, Canada
PEG 6000	Bio-Basic Inc, Canada
p-nitrophenyl phosphate disodium (pNPP-Na)	Bio-Basic Inc, Canada
Potassium phosphate dibasic	MPBio, USA
Potassium phosphate monobasic	Nacalai Tesque, Japan
Sodium acetate	Merck, Germany
Sodium bicarbonate	Bio-Basic Inc, Canada
Sodium carbonate anhydrous	Merck, Germany
Sodium chloride	Merck, Germany
Sodium dodecyl sulphate (SDS)	Bio-Basic Inc, Canada
Sodium hydroxide (NaOH)	Merck, Germany
Sodium sulphate	Bio-Basic Inc, Canada
Sodium thiosulphate	Merck, Germany
Sucrose	EMD Milipore, USA
Tetramethylethylenediamine (TEMED)	Sigma Aldrich, USA
Tris	Bio-Basic Inc, Canada
Toluene	Merck, Germany
Tween 20	SYSTEM <sup>®</sup> , Malaysia

## 3.2 Methods

### 3.2.1 Methodology overview

The general overview of the methods used in the recovery of his-tagged HBcAg from unclarified feedstock in this study is shown in Figure 3.1. First of all, modified PEG (PEG-IDA-metal) was synthesized prior to the construction of phase diagram for ATPS. Then, phase diagram composed of different modified PEG-salts systems were generated. Information such as the binodal curves and tie-lines were generated on the phase diagram. Next, cultivation of *E. colicells* were done to produce unclarified bacterial feedstock. Phase inversion, phase separation, tie-line length (TLL), phase volume ratio, system pH, biomass concentration and addition of neutral salt were optimized for the recovery of his-tagged HBcAg. Proteins from both top and bottom phases were obtained and analyzed using SDS-PAGE, the Bradford assay and densitometric analysis to determine the optimal parameters for his-tagged HBcAg recovery. Then, ATPS-purified his-tagged HBcAg was subjected to enzyme-linked immunosorbent assay (ELISA) and transmission electron microscope (TEM) for qualitative analysis. Last but not least, ATPS-purified his-tagged HBcAg and sucrose gradient ultracentrifuge-purified his-tagged HBcAg were compared in terms of their overall performance.

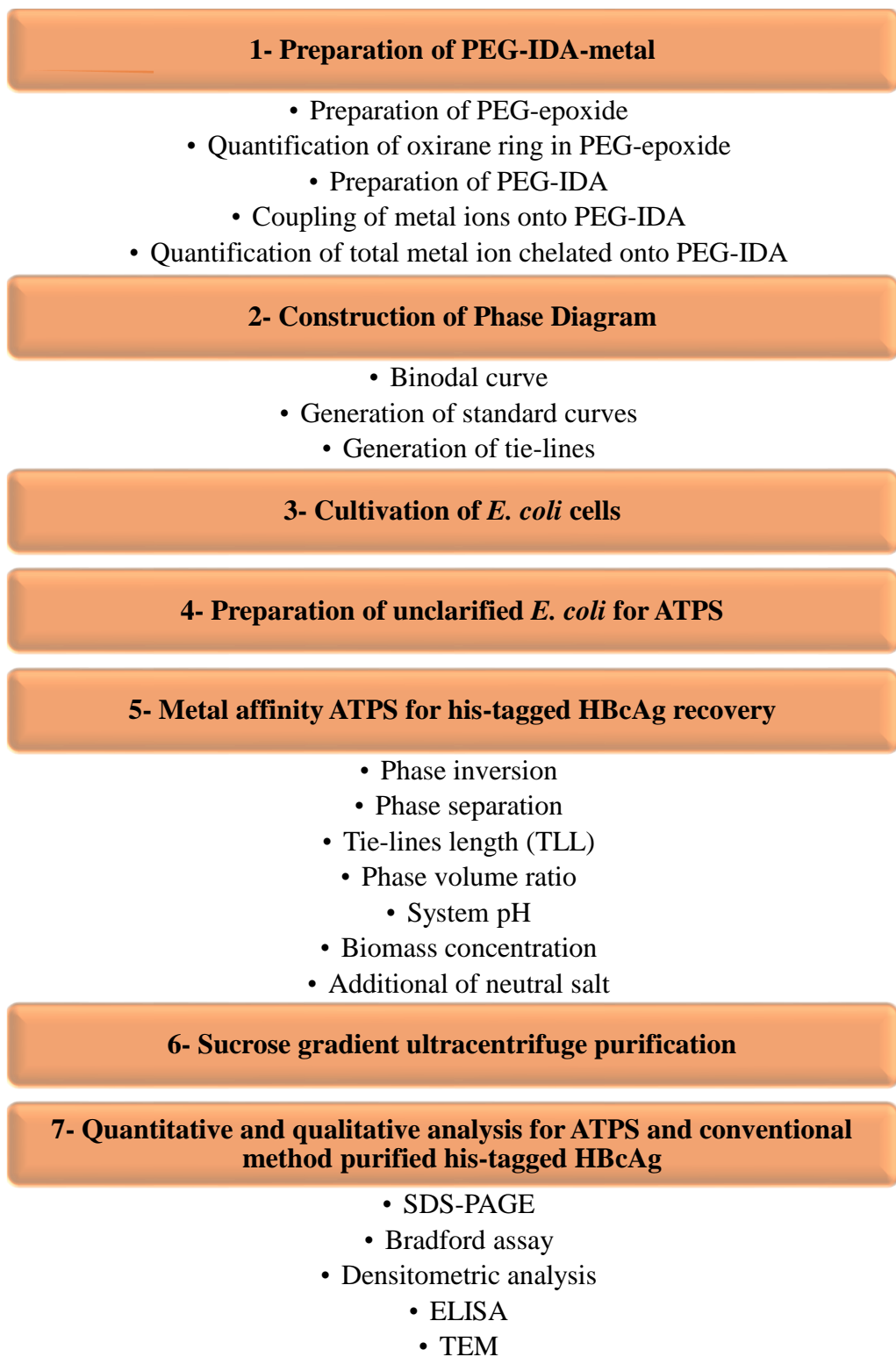


**Figure 3.1: General overview of the methodology**

### **3.2.2 Synthesis of PEG-IDA-metal**

#### **3.2.2.1 Preparation of PEG-epoxide**

Solid PEG 2000, PEG 4000 and PEG 6000 were activated using epichlorohydrin. Briefly, 5 g of PEG was dissolved in 25 mL of toluene. Then, boron trifluoride diethyl etherate (0.1–0.5 M) and epichlorohydrin (0.1–0.5 M) were added drop-wise to the reaction mixture and incubated at room temperature for 12–48 h. Next, 0.2–1.4 % (v/v) of 40% NaOH solution was slowly added and the mixture was stirred at room temperature for 1–5 h. The reaction mixture was then decanted, and washed with 25 mL of diethyl ether. As a result, a precipitate was formed. The precipitate was then filtered through a filter paper and dried. The dried product was then dissolved in 15 mL toluene and precipitated again with 25 mL of diethyl ether and dried. After two rounds of precipitation and drying, PEG-epoxide was obtained.

#### **3.2.2.2 Quantification of oxirane concentration in epoxidated PEG**

In this study, a method described by Sundberg and Porath, (1974) was used to quantify the amount of oxirane formed. This method involves a reaction between the oxirane ring and sodium thiosulphate. Briefly, 1 g of oxirane-containing product was added to 15 mL of 1.3 M sodium thiosulphate solution and the pH was kept constant by addition of 0.1 M hydrochloric acid (HCl) until the pH of the mixture reached pH 7. The amount of oxirane present in the solution was then calculated from the volume recorded for HCl needed in order to achieve pH 7.

1ml of HCL = 10 $\mu$ mol of oxirane ring

### **3.2.2.3 Preparation of PEG-IDA**

Five grams of PEG-epoxide was dissolved in 35 mL of 2 M sodium carbonate containing 0.1-0.5 M of IDA and the mixture was stirred for 24 h at 60° C. The mixture was cooled to room temperature before the extraction step with 100 mL chloroform was performed. The chloroform phases were formed and isolated. Then, the solvent was removed by using a rotary evaporator (Rotar-Vapor R205, BUCHI USA). PEG-IDA derivative was obtained after two round of crystallization in absolute ethanol at 4° C.

### **3.2.2.4 Coupling of metal ions onto PEG-IDA**

The metal ions complex of PEG-IDA was produced by dissolving 5 g PEG-IDA in 25 mL of 0.05 M sodium acetate buffer (pH 4) containing 0.1-0.5 M of Cu<sup>2+</sup> or Ni<sup>2+</sup>. The solution was stirred at room temperature for 1 h and then extracted twice with 100 mL of chloroform. The chloroform phase was isolated and the solvent was removed by using a rotary evaporator. The PEG-IDA-metal derivative was obtained after precipitation in absolute ethanol at 4° C.

### **3.2.2.5 Quantification of total metal ion chelated onto PEG-IDA**

The Cu<sup>2+</sup> and Ni<sup>2+</sup> concentrations in the metal chelated-PEG derivatives were measured by using atomic absorption spectrophotometer (AAS) (Agilent Technologies 200 AA, USA). Briefly, light source of AAS was stabilized for 10 min and an appropriate wavelength was then adjusted for copper ions (324.8

nm) and nickel ions (232.0 nm) for detection. Standard solutions were prepared by diluting the stock metal solution (0 to 1000mg/L) to construct a standard curve. Metal ions concentration present in the PEG-IDA-metal was then calculated based on the standard curves obtained.

### **3.2.3 Construction of phase diagram**

#### **3.2.3.1 Binodal curves**

Binodal curves were constructed to provide the potential area for biphasic and monophasic phase formation in ATPS. The binodal curves were determined by using the cloud point method or the titration method as described by Tou, et al. (2014). A total of 12 binodal curves were constructed, which include PEG 2000-IDA-Cu(II) against  $(\text{NH}_4)_2\text{SO}_4$ ; PEG 2000-IDA-Cu(II) against  $\text{Na}_2\text{SO}_4$ ; PEG 2000-IDA-Cu(II) against KPB; PEG 4000-IDA-Cu(II) against  $(\text{NH}_4)_2\text{SO}_4$ ; PEG 4000-IDA-Cu(II) against  $\text{Na}_2\text{SO}_4$ ; PEG 4000-IDA-Cu(II) against KPB; PEG 6000-IDA-Cu(II) against  $(\text{NH}_4)_2\text{SO}_4$ ; PEG 6000-IDA-Cu(II) against  $\text{Na}_2\text{SO}_4$  and PEG 6000-IDA-Cu(II) against KPB. The determination of the binodal curves were carried out in 15 mL centrifuge tubes (Greiner Bio-one, Germany). A five gram system with known concentrations of polymers and salt was prepared as shown in Table 3.2 and deionized water was used to top up the mixture to 5 gram. The mixture of polymer and salt was vortexed (VELP Scientifica, Italy) until it turned turbid. The mass of this mixture was determined in gram by using an analytical balance (KERN, ABJ-220-4M, Germany). Then, deionized water was added drop-wise until the mixture became clear and the final weight of each tube was

recorded and the final composition for both phases was calculated. The final composition constituent of the bottom phase was plotted as abscissa while the final composition of component in top phase was plotted as ordinate on a graph under exponential extrapolation pattern with triplicate data.

**Table 3.2: The system composition of 5g system which consists of modified PEG with various salts[(NH<sub>4</sub>)<sub>2</sub>SO<sub>4</sub>, Na<sub>2</sub>SO<sub>4</sub>, and KPB] at 23°C, pH 7.0.**

<b>Number of systems</b>	<b>Modified PEG % (w/w)</b>	<b>(NH<sub>4</sub>)<sub>2</sub>SO<sub>4</sub> concentration % (w/w)</b>	<b>Na<sub>2</sub>SO<sub>4</sub> % (w/w)</b>	<b>KPB % (w/w)</b>
<b>1</b>	45	36	18	36
<b>2</b>	40	32	16	32
<b>3</b>	35	28	14	28
<b>4</b>	30	24	12	24
<b>5</b>	25	20	10	20
<b>6</b>	20	16	8	16
<b>7</b>	15	12	6	12
<b>8</b>	10	8	4	8
<b>9</b>	5	4	2	4

### **3.2.3.2 Generation of standard curves**

The standard curves for conductivity were generated for salts and the refractive index (RI) standard curves were generated for both polymers and salts. Standard curves were used to determine the concentration of PEG and salts for tie-line (TL) construction. The conductivity standard curves were obtained by measuring a series of standard salt stock solutions ranging from 0 to 6% (w/w) using a conductivity meter (Eutech CON 700, Thermo Scientific, Singapore) at 23°C. This meter was calibrated using 1413  $\mu\text{S}/\text{cm}$  EC solution (Hanna Instruments, USA). Standard curves were generated after triplicate data were obtained and the mean values were calculated and expressed as  $\text{mS}/\text{cm}$ . On the other hand, the refractive index standard curves were generated using a series of stock solutions ranging from 0 to 6% (w/w) and 0 to 40% (w/w) for salts and polymers, respectively, by using a refractometer (Atago, PAL-1, Japan). The Brix values obtained were then converted to RI values based on the Sucrose Conversion Table (Appendix A). The RI obtained for both PEG and salt from samples were calculated by subtracting the RI of water from the total refractive index obtained for both the PEG and salts. The mean values were calculated and the RI standard curves were plotted.

### **3.2.3.3 Tie-lines (TL)**

Tie-line (TL) was constructed for every system to connect two nodes on binodal curves to provide the composition information of phase component in both phases. In order to determine the tie lines, a series of systems of known

composition were prepared for every PEG-IDA-Cu (II) and salts systems as listed in Table 3.3.

**Table 3.3 Details of phase compositions for each PEG-salt system.**

Modified PEG-salt system	Phase compositions					
	Salt %(w/w)	PEG %(w/w)	Salt (g)	PEG (g)	Feedstock (g)	Water (g)
PEG 2000-IDA-Cu(II)-(NH <sub>4</sub> ) <sub>2</sub> SO <sub>4</sub>	11.10	16.00	1.388	1.60	1.00	1.012
PEG 2000-IDA-Cu(II)-Na <sub>2</sub> SO <sub>4</sub>	7.90	15.00	1.975	1.50	1.00	0.525
PEG 2000-IDA-Cu(II)-KPB	13.50	13.00	1.679	1.30	1.00	1.021
PEG 4000-IDA-Cu(II)-(NH <sub>4</sub> ) <sub>2</sub> SO <sub>4</sub>	10.75	16.00	1.344	1.60	1.00	1.056
PEG 4000-IDA-Cu(II)-Na <sub>2</sub> SO <sub>4</sub>	8.20	14.00	2.050	1.40	1.00	0.550
PEG 4000-IDA-Cu(II)-KPB	14.50	16.00	1.813	1.60	1.00	0.587
PEG 6000-IDA-Cu(II)-(NH <sub>4</sub> ) <sub>2</sub> SO <sub>4</sub>	10.60	16.00	1.325	1.60	1.00	1.075
PEG 6000-IDA-Cu(II)-Na <sub>2</sub> SO <sub>4</sub>	7.90	14.00	1.975	1.40	1.00	0.625
PEG 6000-IDA-Cu(II)-KPB	13.00	14.00	1.625	1.40	1.00	0.975

The two phases formed were separated for further analysis. This isolated phase was then measured with the conductivity meter (Eutech CON 700, Thermo Scientific, Singapore) and a refractometer (Atago, PAL-1, Japan) to determine the concentration of salts and polymers in both phases, respectively. The final concentration of the phase component was calculated based on the standard curve as described in Section 3.2.3.2. All measurements were calculated based on triplicate values. Tie-line length (TLL) was calculated as:

$$\text{TLL} = \sqrt{\Delta x^2 + \Delta y^2}$$

where  $\Delta x$  represents the difference of salt concentration between top and bottom phases, and  $\Delta y$  represents the difference PEG-IDA-Cu (II) concentration between top and bottom phases. Meanwhile, the slope of TLL (STL) was calculated as:

$$\text{STL} = \frac{\Delta X}{\Delta Y}$$

where  $\Delta x$  represents the difference of salt concentration between top and bottom phases, and  $\Delta y$  represents the difference PEG-IDA-Cu (II) concentration between top and bottom phases. STL was calculated to facilitate the construction of tie-line and ideally, the STL of each tie-line under the same binodal curve should be the same. On the other hand, critical point (p) on the phase diagram was obtained based on extrapolation through the midpoints of few tie-lines. The midpoint of tie-line was calculated by:

$$\text{Midpoint} = \frac{\Delta X}{2}, \frac{\Delta Y}{2}$$

where  $\Delta x$  represents the difference of salt concentration between top and bottom phases, and  $\Delta y$  represents the difference PEG-IDA-Cu(II) concentration between top and bottom phases.

### 3.2.4 Cultivation of *E. coli* cells

WB-HBcAg *E. coli* BL-21 cells expressing the his-tagged HBcAg was streaked on Luria Bertani (LB) agar, pH 7, containing 100  $\mu\text{g/mL}$  ampicillin (USB corporation, USA) and incubated overnight (16-18 h) at 30°C. The next day, a single colony of *E. coli* cells from the plate was picked and inoculated into 250 mL LB broth, pH 7, containing 100  $\mu\text{g/mL}$  ampicillin. The culture was grown at 30°C with shaking (Daihan Labtech, Korea) at 200 rpm for 16-18h. The overnight culture was then inoculated (1:50) into another 1000 mL LB broth containing 100  $\mu\text{g/mL}$  ampicillin and was further grown for another 3-5 h with shaking at 200 rpm, at 30°C. When  $\text{OD}_{600}$  of the culture reached approximately 0.6-0.8 (UV-Vis spectrophotometer, Genesys 20, Thermo Science, USA), the induction of protein expression was initiated by addition of isopropyl- $\beta$ -D-thiogalactopyranoside (IPTG) with a final concentration of 0.5 mM. The culture was then further incubated for 16-18h with vigorous shaking at 200 rpm, at 30°C. Next, the culture was harvested by centrifugation (JA 14 rotor, Avanti®J-E, Beckman Coulter, USA) at 3,836  $\times g$  for 15 min at 4°C. The pellet was collected and the harvested pellet (biomass) was weighed and stored at -20°C until use.

### **3.2.5 Preparation of unclarified *E. coli* feedstock for ATPS**

The harvested pellet (biomass) was suspended in 25 mM 4-(2-hydroxyethyl)-1-piperazineethanesulfonic acid (HEPES) at pH 7 to obtain a crude feedstock with a final biomass concentration of 25% (w/v). The cell suspension was then sonicated by using an ultrasonicator (Cole Parmer Sonicator mode 130, USA) to disrupt and release the his-tagged HBcAg. The sonication was carried out with a probe (6 mm in diameter) and resonated at high frequency sound wave at 20 kHz with repeated 20 s disruption periods, followed by 20 s rest period in an ice bath with amplitude of 35 - 40% for 30 min. The tube was inverted every 5 min during the resting interval to ensure the *E. coli* cells were disrupted evenly. Then, this unclarified feedstock was stored at 4°C until further use.

### **3.2.6 Preparation of ATPS**

A 15 mL graduated centrifuge tube was used to perform the ATPS by adding known compositions of modified PEG, salt and unclarified feedstock containing 5% biomass (w/v) into the system. The final mass of the 5 g system was achieved by adding deionized water. The system was then mixed well using a vortex mixer (Velp Scientifica, Italy) and followed by centrifugation at 2,000 xg for 5 min at 23°C to induce phase separation. The top and bottom phases were carefully withdrawn after the system has reached an equilibrium and the volume for both phases was recorded. The samples were then subjected to quantification using SDS-PAGE, the Bradford assay and densitometric analysis as described later in Section 3.2.10. Different combinations of

modified PEGs-salts systems were constructed for the direct recovery of HBcAg in this study as listed in Table 3.2. Systems with phase volume ratio of 1.0 on TLL 1 (TLL nearest to binodal curve) were selected based on the phase diagram constructed. Three systems with the highest recovery yield, purity and purification factor of HBcAg were selected for further optimizations.

### **3.2.7 Removal of PEG and salt from samples**

Removal of PEG and salt from both phases was necessary prior to quantification. Samples from the PEG-riched top-phase was subjected to overnight dialysis in dialysis buffer composed of 25 mM HEPES (pH 8.0), 100 mM NaCl and 250 mM imidazole using a Snakeskin pleated dialysis tubing with 10,000 molecular weight cut off (MWCO) (Thermo Scientific, USA) at 4°C. The dialysis buffer was changed once throughout the dialysis. The dialysed samples were then concentrated using centrifugal concentrators [(10,000 MWCO), Vivaspin™ 6, Sartorius stedim, Germany]. On the other hand, samples from the salt-riched bottom phase was directly subjected to ultrafiltration using a centrifugal concentrator [(10,000 MWCO), Vivaspin™ 6, Sartorius stedim, Germany] with dialysis buffer at 6000 xg, at 4°C.

### **3.2.8 Methods scouting for his-tagged HBcAg recovery**

Several parameters that affect the partitioning of his-tagged HBcAg in ATPS were optimized in this study such as the phase inversion mode, phase separation mode, tie-line, phase volume ratio, system pH, biomass concentration and addition of neutral salt. The optimization of the partitioning

of his-tagged HBcAg was carried out systematically by changing one parameter at a time to identify its effect on his-tagged HBcAg recovery.

### **3.2.8.1 Phase inversion mode**

Process parameters such as phase inversion and phase separation also play important roles in ATPS. Three systems with the highest recovery yield, purity and purification factor of HBcAg were prepared (as described in Section 3.2.6) and subjected to phase inversion optimization using either a multi-function 3D rotator (Grant Bio PS-M3D, Cambridge) or a vortex mixer. Optimization of phase inversion duration was performed for 1, 3 and 5 min followed by centrifugation at 2,000 xg, for 5 min at 23°C. Samples from both top and bottom phases were carefully withdrawn and subjected to quantitative analysis as described in Section 3.2.10.

### **3.2.8.2 Phase separation mode**

The three best systems were also prepared for phase separation mode optimization. First mode, the sample was left on the bench until phase equilibrium was achieved. The second method was carried out by centrifugation at 2,000 xg, for 5 min at 23°C. Next, different centrifugal forces (1,000 xg, 2,000 xg, and 3,000 xg), durations (1 min, 3 min and 5 min) and temperatures (4°C and 23°C) were optimized accordingly to determine the best conditions for HBcAg recovery. Samples from both the top and bottom phases were carefully withdrawn and the samples were subjected for quantitative analysis for his-tagged HBcAg as described in Section 3.2.10.

### **3.2.8.3 Tie-line length (TLL)**

Three best systems were selected for TLL optimizations. The effect of three tie-lines per system with different lengths were studied. The coordinates used for optimization located on three different TLLs with phase volume ratio of 1.0 were selected from the respective phase diagram. TLL was labelled as TLL 1, 2 and 3 based on their distance from the origin of phase diagram in an ascending order. TLL 1 was the nearest to origin followed by TLL 2 and TLL 3. The ATPS composition was prepared based on Table 3.4. ATPS was prepared according to Section 3.2.6. Other than TLL, parameters such as optimized phase inversion and separation modes, system pH (8.0), phase volume ratio (1.0), and final biomass concentration (5% (w/v)) in the system were kept constant. Samples from both the top and bottom phases were carefully withdrawn and subjected for quantitative analysis for his-tagged HBcAg as described in Section 3.2.10.

**Table 3.4: Phase compositions for TLL optimization.**

PEG-salt system	TLL	Salt % (w/w)	PEG % (w/w)	Salt (g)	PEG (g)	Unclarified feedstock (g)	Water (g)
PEG 2000-	1	13.50	13.00	1.69	1.30	1.00	1.01
IDA-	2	14.00	14.50	1.75	1.45	1.00	0.80
Cu(II)-KPB	3	14.50	16.00	1.81	1.60	1.00	0.59
PEG 4000-	1	14.50	16.00	1.81	1.60	1.00	0.59
IDA-	2	15.40	17.00	1.93	1.70	1.00	0.37
Cu(II)-KPB	3	16.00	18.00	2.00	1.80	1.00	0.20
PEG 6000-	1	13.00	14.00	1.63	1.40	1.00	0.97
IDA-	2	13.20	15.00	1.65	1.50	1.00	0.85
Cu(II)-KPB	3	13.50	17.00	1.69	1.70	1.00	0.61

#### 3.2.8.4 Phase volume ratio

Three best systems were selected for phase volume ratio optimizations. Phase volume ratio is one of the crucial parameters that affect the partitioning of protein. The selected system was prepared and carried out as described in Section 3.2.6. Three different phase volume ratios [(top phase: bottom phase)- (2.3, 1.0 and 0.4)] were prepared according to Table 3.5. Parameters such as optimized TLL, system pH (8.0), and final biomass concentration in the system (5% (w/v)) were kept constant. Samples from both the top and bottom

phases were carefully withdrawn and quantified. The system with the highest recovery yield, purity and purification factor of his-tagged HBcAg was chosen for further optimizations.

**Table 3.5: Phase compositions of PEG 4000-IDA-Cu(II)-KPB system in the optimization of phase volume ratio.**

Phase volume ratio (top/bottom)	Salt % (w/w)	PEG % (w/w)	Salt (g)	PEG (g)	Unclarified feedstock (g)	Water (g)
2.3 <sup>1</sup>	12.00	23.00	1.50	2.30	1.00	0.20
1.0 <sup>1</sup>	14.50	16.00	1.81	1.60	1.00	0.59
0.4 <sup>1</sup>	22.00	8.00	2.75	0.80	1.00	0.45

<sup>1</sup>System with optimized TLL.

### 3.2.8.5 System pH

System pH 6, 7, and 8 were investigated separately to determine the effects of different system pH on his-tagged HBcAg recovery. All stock solutions of PEG and salts were prepared and adjusted to pH 6, 7 and 8, accordingly. The pH of the buffers was adjusted using 0.1M HCl or NaOH. The pH of unclarified feedstock was also adjusted to pH 6, 7 and 8, accordingly prior to addition into the system. In this study, all ATPS were prepared based on Table 3.6 by using the method described in Section 3.2.6 using their respective stock solutions with specific pH. Samples from each phase were carefully withdrawn and quantified as described in Section 3.2.10.

**Table 3.6: Phase compositions of PEG 4000-IDA-Cu(II)-KPB in the optimization of system pH.**

<b>System pH</b>	<b>Salt % (w/w)</b>	<b>PEG % (w/w)</b>	<b>Salt (g)</b>	<b>PEG (g)</b>	<b>Unclarified feedstock (g)</b>	<b>Water (g)</b>
6.0	14.50	16.00	1.81	1.60	1.00	0.59
7.0	14.50	16.00	1.81	1.60	1.00	0.59
8.0	14.50	16.00	1.81	1.60	1.00	0.59

### **3.2.8.6 Biomass concentration**

Different final biomass concentrations (1, 2, 3, 4, 5, and 6% (w/v)) were applied in ATPS to evaluate the effect of biomass concentration in partitioning of his-tagged HBcAg as listed in Table 3.7. In order to prepare feedstock containing different biomass concentrations, stock solution of unclarified feedstock was set at 40% (w/v) and disrupted using ultrasonication. In this study, 1 g of unclarified feedstock was loaded into each system. Subsequently, the experiment was carried out using the method described in Section 3.2.6. Samples were taken from both top and bottom phases from each system and analyzed using the methods described in Section 3.2.10. The system with the highest recovery yield, purity and purification factor was selected for further optimization.

**Table3.7: Preparation of stock solution of unclarified feedstock in optimization of biomass concentration.**

<b>System final biomass concentration</b>	<b>Amount of unclarified feedstock added in ATPS</b>	<b>Final volume of ATPS</b>
<b>% (w/v)</b>	<b>(g)</b>	<b>(g)</b>
1.0	1.0	5.0
2.0	1.0	5.0
3.0	1.0	5.0
4.0	1.0	5.0
5.0	1.0	5.0
6.0	1.0	5.0

### **3.2.8.7 Additional of neutral salt**

Different concentrations of NaCl (25, 50, 100, 200, and 500 mM) were added separately into different systems to investigate the effects of NaCl addition in HBcAg recovery as listed in Table 3.8. A 5 M of NaCl stock solution was used in this study. The experiment was carried out as described in Section 3.2.6. Subsequently, the tubes were mixed and separated using the optimized conditions. Each phase was subjected to analysis using SDS-PAGE and quantified as described in Section 3.2.10.

**Table 3.8: Phase compositions of PEG 4000-IDA-Cu(II)-KPB system in the optimization of NaCl addition.**

NaCl (mM)	Salt % (w/w)	PEG % (w/w)	Salt (g)	PEG (g)	NaCl (g)	Unclarified feedstock (g)	Water (g)
0	14.50	16.00	1.81	1.60	0.00	1.00	0.59
25	14.50	16.00	1.81	1.60	0.03	1.00	0.56
50	14.50	16.00	1.81	1.60	0.05	1.00	0.54
100	14.50	16.00	1.81	1.60	0.10	1.00	0.49
200	14.50	16.00	1.81	1.60	0.20	1.00	0.39
500	14.50	16.00	1.81	1.60	0.50	1.00	0.09

### 3.2.9 Conventional purification method for his-tagged HBcAg recovery

His-tagged HBcAg purified using ammonium sulphate precipitation and sucrose-gradient ultracentrifugation methods were performed and compared with the ATPS purified his-tagged HBcAg. Briefly, a total of 1 L *E. coli* culture was employed in this study. The biomass was resuspended using 50 mM Tris-HCl at pH 8.0 to a final concentration of 5% (w/v) and subjected to cell disruption using ultrasonication. Next, the sonicated cell lysate was clarified by high speed centrifugation at 12,300  $\times g$  for 20 min at 4°C (JA 14 rotor, Beckman Coulter, USA).

The supernatant was then collected and precipitated with 35% saturation of  $(\text{NH}_4)_2\text{SO}_4$  (0.189g/mL) at 4°C overnight on a hotplate stirrer (Stuart hotplate stirrer, UK). The overnight mixture was then centrifuged at 12,300 xg for 20 min at 4°C (JA 14 rotor, Beckman Coulter, USA). The pellet was collected and dissolved in dialysis buffer [50 mM Tris (pH 8.0) and 100 mM NaCl]. The dissolved pellet was then loaded into dialysis tubing with 10,000 MWCO (Thermo Scientific, USA) and dialyzed overnight in dialysis buffer at 4°C with stirring on a hot plate (Stuart hotplate stirrer, UK). The dialysis buffer was changed once during the dialysis. The dialyzed sample was collected and then subjected to sucrose-gradient ultracentrifugation. Discontinuous sucrose gradient of 8–40% (w/v) was used to fractionate his-tagged HBcAg.

Stock solutions of sucrose were prepared (8, 16, 32 and 40% (w/v)). The discontinuous sucrose-gradient was prepared by layering sucrose solutions with different densities into the ultracentrifuge tubes (Ultracentrifuge 12ML PA Tube, Thermo Scientific, USA). Approximately 300 µL of dialyzed samples was then layered on top of the gradient in the ultracentrifuge tube and centrifuged at 210,053 xg (TH-641 swing bucket rotor, WX ultra 100, Thermo Scientific, USA) for 5 h at 4°C. The collected fractions were pooled and dialysed overnight at 4°C to remove sucrose. Subsequently, the dialysed sample was concentrated with Vivaspin® centrifugal concentrators [(300,000 MWCO, Vivaspin™ 6, Cole-Plamer, USA)] and centrifuged at 6,000xg (4°C). The

concentrated sample was then analyzed using SDS-PAGE and quantified based on the Bradford assay and densitometric analysis as described in Section 3.2.10.

### **3.2.10 Quantitative analysis of ATPS-purified his-tagged HBcAg**

#### **3.2.10.1 Tricine-sodium dodecyl sulphate-polyacrylamide gel electrophoresis (Tricine-SDS-PAGE) analysis**

The protein sample from each phase was fractionated using SDS-PAGE (Mini-Protean 3, Bio-Rad, USA) with a discontinuous tricine buffer system as described by Schagger, (2006). Acrylamide gel composed of 16% (w/v) of resolving gel and a stacking gel of 4% (w/v) were used in the present study. Firstly, the apparatus was set up accordingly for gel preparation of 0.75 mm thickness. A 16% (w/v) resolving gel containing 890  $\mu$ L autoclaved deionized water, 10 mL AB-3 buffer [49.5% T, 3% C, 48% (w/v) acrylamide, 1.5% (w/v) bisacrylamide], 10 mL 3x gel buffer [3 M Tris, 1 M HCl, 0.3% (w/v) SDS, pH 8.45], 100  $\mu$ L 10% (w/v) ammonium persulfate (APS), and 10  $\mu$ L TEMED was prepared. The solution was then mixed thoroughly and pipetted into the spaces formed by gel plates. The gel surface was layered with butanol and left to polymerize for 30 min. The butanol was then rinsed off with deionized water and the gel surface was dried using filter paper.

On the other hand, a 4% (w/v) stacking gel containing 8.9 mL autoclaved deionized water, 1 mL AB-3 [49.5% T, 3% C, 48% (w/v) acrylamide, 1.5% (w/v) bisacrylamide], 3 mL 3x gel buffer [3 M Tris, 1 M HCl, 0.3% (w/v) SDS, pH 8.45], 90  $\mu$ L 10% (w/v) ammonium persulfate (APS),

and 9  $\mu$ L TEMED was prepared. Stacking gel solution was mixed thoroughly and pipetted on top of the polymerized resolving gel. A 10-well comb was then carefully inserted into the stacking gel and the gel was allowed to polymerize for 15 min. The gel was transferred into the tank together with gel gasket after polymerization was completed. The anode and cathode tank were then filled with anode buffer [1 M Tris, 0.025 M HCl, pH 8.9] and cathode buffer [1 M Tris, 1 M tricine, 1% SDS, pH 8.25]. The comb was gently removed before the sample was loaded into the well.

For sample preparation, the samples were mixed with SDS-containing sample buffer [12% (w/v) SDS, 30% (v/v) glycerol, 0.01% bromophenol blue, 6%  $\beta$ -mercaptoethanol, 0.05% coomassie blue G-250, 150 mM Tris-HCl, pH 7.0] and boiled for 10 min. These samples were spun down using a tabletop low speed mini centrifuge (AccuBiotech, China) at 1,000  $\times$ g for 1 min. Subsequently, the protein marker (Benchmark, Invitrogen) and boiled samples were loaded into their wells. The gel was electrophoresed at a constant current (16 mA/gel) until the dye front ran off (Powerpac basic, Bio-rad, USA). Next, the gels were removed gently by separating the two plates and then incubated in fixing solution (50% methanol, 10% acetic acid, 100 mM ammonium acetate) prior to staining. The gels were then stained with 0.025% (w/v) Coomassie Brilliant Blue R-250 (Nacalai Tesque, Japan) and destained twice with destaining solution (10% (v/v) acetic acid) until visible bands and a clear background were observed.

### **3.2.10.2 The Bradford assay**

The total protein concentration from each phase was quantified using the Bradford assay (Bradford, 1976). Bovine serum albumin (BSA) was used as the standard. 1 mg/mL BSA and 1× Bradford dye [0.05% Coomassie Blue G250, 95% (v/v) absolute ethanol, 85% (v/v) ortho phosphoric acid] were prepared before the assay was carried out. A 96-well medium-binding flat bottom plate (Greiner bio-one, Germany) was used in this study. Briefly, 15 µL Tris buffer saline (TBS) [NaCl (150 mM), Tris-HCl (50 mM, pH 7.6)] was added into each well. For BSA standard, TBS and BSA added were 0, 2, 4, 6, 8, 10 µg/µL and 20, 18, 16, 14, 12, 10 µL, respectively. Next, 5 µL of samples obtained from each phase were added into their respective wells. The Bradford dye (200 µL) was then added into all wells and mixed thoroughly. The protein was measured at 595 nm using a microtitre plate reader (I-CON software, Infinite M200, Tecan Group Ltd., Switzerland). All measurements were carried out in duplicates.

### **3.2.10.3 Densitometric analysis**

The quantification of HBcAg was carried out using the Alpha Innotech FluorChem® FC2 system (Cell Bioscience, USA). The FluorChem® FC2 Imaging system offers a complete range of image acquisition modes suitable for imaging the fluorescent and chemiluminescent gels and blots. After SDS-PAGE, the gel was placed in the MultiImage II Light Cabinet (DE-500) and the image of the gel was captured. Subsequently, the density of the HBcAg at 21 kDa was measured and compared against the total lane's density for all lanes

involved by using Alpha Innotech software. The software then automatically detected the protein band peak and the protein density was measured. The amount of his-tagged HBcAg was calculated based on the density (recorded as%) of his-tagged HBcAg band on the SDS-PAGE gel against the total amount of protein obtained from the Bradford assay.

### **3.2.11 Qualitative analysis of ATPS-purified his-tagged HBcAg**

#### **3.2.11.1 Enzyme-linked immunosorbent assay (ELISA)**

The antigenicity of the his-tagged HBcAg recovered from ATPS was determined by enzyme-linked immunosorbent assay (ELISA) (Ng, et al., 2007). ELISA was carried out for ATPS-purified his-tagged HBcAg where the HBcAg purified using sucrose-gradient ultracentrifugation was used as a positive control, while modified PEG was used as a negative control. U-shaped high binding 96 wells microtitre plate (Greiner bio-one, Germany) was first coated with HBcAg (10-1000 ng; 120  $\mu$ L) overnight with gentle agitation at 4°C (NB-1015/BIOTEK, Handy LAB System). The coated wells were washed three times (15 min/time) with TBST [NaCl (150 mM), Tris-HCl (50 mM, pH 7.6), Tween 20 (0.05%)] to wash off any unbound protein. The coated wells were then blocked with 10% milk diluents (KPL, USA) for 2 h at room temperature. Next, the wells were washed three times with TBST and primary antibody (6X his-tag mouse monoclonal antibody) (1:2500, 100  $\mu$ L, Gene Tex, USA) was added and incubated for 1 h at room temperature. Subsequently, the wells were then washed with TBST for 3 times (15 min/time) and followed by addition of anti-mouse IgG conjugated with alkaline phosphatase (1:2500, 100  $\mu$ L) and

incubated for 1 h at room temperature. The unbound antibodies were washed off with TBST (three times) with 15 min each time. HBcAg was detected by adding p-nitrophenyl phosphate substrate (1 mg/mL, 200  $\mu$ L, Biobasic). The absorbance was read at 405 nm using a microtitre plate reader (M200, Tecan group, Switzerland) after 15-20 min. The assay was performed in triplicates.

### **3.2.11.2 Transmission electron microscope (TEM)**

The morphology of the ATPS and ultracentrifugation purified his-tagged HBcAg was determined using transmission electron microscope (TEM). Firstly, the purified his-tagged HBcAg was absorbed to a carbon coated grid (FCF 300-Cu, Formvar<sup>®</sup> carbon film on a 300 mesh copper grid, Electron Microscopy Sciences, Hatfield, PA, USA) for 3-5 min. Next, the grid was gently dried using a filter paper and negatively stained using 2% uranyl acetate for 5 min. The grid was then allowed to dry for 5 min before subjected to observation under LEO912AB energy filtered TEM (EFTEM, Carl Zeiss, Inc, Thornwood, USA).

### **3.2.12 Calculations**

Recovery yield of his-tagged HBcAg refers to amount of his-tagged HBcAg obtained in ATPS over the initial amount of his-tagged HBcAg in the feedstock:

$$\text{Recovery yield (\%)} = \frac{\text{Amount of his – tagged HBcAg}}{\text{Initial amount of his – tagged HBcAg}} \times 100$$

Purity of his-tagged HBcAg is regarded as the amount of recovered his-tagged HBcAg over the total amount of protein in percentage:

$$\text{Purity (\%)} = \frac{\text{Amount of recovered his – tagged HBcAg}}{\text{Total amount of protein}} \times 100$$

Purification factor is defined as the purity of his-tagged HBcAg in the ATPS divided by the purity of the his-tagged HBcAg in the unclarified feedstock:

$$\text{Purification factor} = \frac{\text{Purity of his – tagged HBcAg after ATPS}}{\text{Purity of his – tagged HBcAg in the feedstock}} \times 100$$

## CHAPTER 4

### RESULTS

#### 4.1 Preparation of PEG-epoxide

Several important parameters such as the activation duration, boron trifluoride ethyl-etherate (BFEE) concentration, epichlorohydrin concentration and sodium hydroxide (NaOH) concentration need to be optimized in the preparation of PEG-epoxide. The epoxide yield is directly proportional with the binding efficiency of iminodiacetic acid (IDA) with epoxide before the chelation of metal ions.

##### 4.1.1 Activation duration

The activation duration was the first parameter to be optimized in the preparation of PEG-epoxide in this study. The activation duration from 1 to 6h after addition of NaOH into the reaction mixture was investigated. The concentration of BFEE concentration, epichlorohydrin concentration and NaOH concentration remained constant. The concentration of oxirane ring detected in all PEG-epoxide increased and maintained constant after the maximum level was reached (Table 4.1).

PEG 2000-epoxide produced the highest oxirane ring of approximately 240.6 μmol/g PEG compared to PEG 4000-epoxide and PEG 6000-epoxide that recorded 178.4 μmol/g PEG and 177.5 μmol/g PEG, respectively. The reaction between PEG 2000 and epichlorohydrin was rapid whereby an hour of activation yielded a total of 186.8 μmol/g PEG oxirane ring. The optimal activation duration for achieving the highest oxirane ring production in the products was selected for further optimization. Therefore, the optimal activation duration for both PEG 2000 and PEG 4000 was 2 h, whereas for PEG 6000, it was 3 h (Table 4.1).

**Table 4.1: Effect of activation duration on oxirane ring production.**

Activation time, (h)	Oxirane rings amount, (μmol/g PEG)		
	PEG 2000 <sup>1</sup>	PEG 4000 <sup>1</sup>	PEG 6000 <sup>1</sup>
1	186.8±4.2	65.3±2.2	58.7±1.8
2	<b>240.6±3.6</b>	<b>178.4±3.2</b>	115.8±3.0
3	240.4±4.0	129.8±4.0	<b>177.5±3.8</b>
4	232.6±5.8	144.9±3.4	132.7±3.6
5	228.7±4.8	130.7±4.2	136.0±4.0
6	234.3±4.2	140.2±5.6	143.0±2.2

<sup>1</sup>Each data is mean ± standard deviation of triplicate determinations  
The bold values represented the chosen parameters in their respective optimization.

#### **4.1.2 Boron trifluoride ethyletherate (BFEE) concentration**

The synthesis route for PEG-epoxide production involved multiple components and parameters. Boron trifluoride ethyl-etherate (BFEE) was one of the crucial components for the first sub step to open the ring of epichlorohydrin as well as to provide the acidic conditions for the reaction mixture. The optimal condition was determined by measuring the oxirane ring concentration present in the PEG-epoxide produced using BFEE concentration ranging from 0.2 to 1.2% (v/v) as tabulated in Table 4.2. The activation duration, epichlorohydrin concentration and NaOH concentration were remained constant. Results showed that increase of BFEE concentration increased the yield of oxirane ring production in PEG-epoxide. The concentration of oxirane ring detected started to decline after the maximum level was achieved. In general, PEG 2000 produced the highest oxirane concentration in the presence of different concentrations of BFEE compared to PEG 4000 and PEG 6000.

However, the oxirane ring concentration for PEG 2000 epoxide started to decline after it achieved 250.6  $\mu\text{mol/g}$  PEG in the presence of 1% (v/v) of BFEE. PEG 4000-epoxide and PEG 6000-epoxide produced the optimal concentration of oxirane ring at 0.8% (v/v) of BFEE. The oxirane ring concentration obtained in both PEG 4000 and PEG 6000 were 28.8% and 29.1%, respectively lower than the one obtained with PEG 2000-epoxide under 0.8% (v/v) of BFEE. Therefore, the optimal BFEE concentrations obtained for

these three different PEG were selected to be used as a constant in the next parameter optimization.

**Table 4.2: Effect of BFEE concentration on oxirane ring production.**

BFEE concentration, % (v/v)	Oxirane rings amount, ( $\mu\text{mol/g}$ PEG)		
	PEG 2000 <sup>1</sup>	PEG 4000 <sup>1</sup>	PEG 6000 <sup>1</sup>
0.2	76.5 $\pm$ 2.4	136.0 $\pm$ 3.2	84.7 $\pm$ 2.2
0.4	136.2 $\pm$ 4.4	130.1 $\pm$ 4.6	92.8 $\pm$ 5.4
0.6	199.1 $\pm$ 5.6	117.6 $\pm$ 4.2	87.7 $\pm$ 4.2
0.8	240.4 $\pm$ 6.2	<b>178.4<math>\pm</math> 5.2</b>	<b>177.5<math>\pm</math>5.4</b>
1.0	<b>250.6<math>\pm</math> 22</b>	124.3 $\pm$ 4.6	149.9 $\pm$ 3.8
1.2	233.5 $\pm$ 3.6	71.0 $\pm$ 5.0	150.8 $\pm$ 5.2

<sup>1</sup>Each data is mean  $\pm$  standard deviation of triplicate determinations  
The bold values represented the chosen parameters in their respective optimization.

#### 4.1.3 Epichlorohydrin concentration

Epichlorohydrin concentration is important as it is the main component for the production of PEG-epoxide. Similar to BFEE, epichlorohydrin concentration was optimized by measuring the oxirane ring concentration in the PEG-epoxide produced using different concentrations of epichlorohydrin, ranging from 0.2 to 1.2% (v/v). The results showed that increase in epichlorohydrin concentration increased the yield of oxirane ring production in PEG-epoxide (Table 4.3).

Generally, the concentration of oxirane ring detected started to decline after the maximum level was achieved. The highest oxirane ring concentration obtained for PEG 2000 was about 250.6 $\mu$ mol/g PEG and it was 28.8% and 29.1% higher compared to that obtained from PEG 4000 and PEG 6000, respectively at 0.8% (v/v) of epichlorohydrin. The highest oxirane ring production for PEG 4000 and PEG 6000 was recorded as 226.3 $\mu$ mol/g PEG and 220.2  $\mu$ mol/g PEG, respectively at 1% (v/v) of epichlorohydrin. Therefore, the optimal epichlorohydrin concentrations of 0.8%, 1.0% and 1.0% for PEG 2000, PEG 4000 and PEG 6000, respectively, were used for the subsequently optimization.

**Table 4.3: Effect of epichlorohydrin concentration on oxirane ring production.**

Epichlorohydrin concentration, % (v/v)	Oxirane rings amount, ( $\mu$ mol/g PEG)		
	PEG 2000 <sup>1</sup>	PEG 4000 <sup>1</sup>	PEG 6000 <sup>1</sup>
0.2	72.2 $\pm$ 2.8	66.5 $\pm$ 2.4	64.6 $\pm$ 2.2
0.4	158.5 $\pm$ 4.6	80.5 $\pm$ 4.0	157.1 $\pm$ 5.0
0.6	236.3 $\pm$ 6.2	156.8 $\pm$ 6.6	126.7 $\pm$ 4.4
0.8	<b>250.6<math>\pm</math>6.6</b>	178.4 $\pm$ 5.2	177.5 $\pm$ 5.4
1.0	242.2 $\pm$ 5.6	<b>226.3<math>\pm</math>4.2</b>	<b>220.2<math>\pm</math>5.6</b>
1.2	223.0 $\pm$ 3.4	193.1 $\pm$ 4.4	160.16 $\pm$ 3.8

<sup>1</sup>Each data is mean  $\pm$  standard deviation of triplicate determinations  
The bold values represented the chosen parameters in their respective optimization.

#### 4.1.4 Sodium hydroxide (NaOH) concentration

The effects of NaOH concentration on the synthesis of epichlorohydrin activated PEG was investigated. Based on the Table 4.4, it was demonstrated that the yield of oxirane rings was proportional to the increase of NaOH concentration. There was no oxirane ring detected when 0.2% (v/v). NaOH was used in activation (Table 4.4). Activation of epichlorohydrin started to take place at 0.4% (v/v) of NaOH. The highest oxirane ring concentration was observed when 1.2% (v/v) of NaOH was added, which recorded a concentration of 269.3 $\mu$ mol/g PEG, 252.1  $\mu$ mol/g PEG and 238.5  $\mu$ mol/g PEG for PEG 2000-epoxide, PEG 4000-epoxide and PEG 6000-epoxide, respectively. Therefore, these optimal NaOH concentrations were selected for the following optimization.

**Table 4.4: Effect of NaOH concentration on oxirane ring production.**

NaOH, % (v/v)	Oxirane rings amount, ( $\mu$ mol/g PEG)		
	PEG 2000 <sup>1</sup>	PEG 4000 <sup>1</sup>	PEG 6000 <sup>1</sup>
0.2	0.00	0.00	0.00
0.4	16.6 $\pm$ 2.2	22.9 $\pm$ 2.8	9.1 $\pm$ 3.0
0.6	42.64 $\pm$ 4.2	59.7 $\pm$ 3.4	37.8 $\pm$ 2.2
0.8	128.5 $\pm$ 3.0	143.1 $\pm$ 4.4	112.7 $\pm$ 4.2
1.0	250.6 $\pm$ 3.8	226.3 $\pm$ 4.8	220.2 $\pm$ 5.2
1.2	<b>269.3 <math>\pm</math>5.2</b>	<b>252.1<math>\pm</math>5.8</b>	<b>238.5<math>\pm</math>4.6</b>
1.4	263.5 $\pm$ 3.0	238.5 $\pm$ 3.6	203.1 $\pm$ 5.4

<sup>1</sup>Each data is mean  $\pm$  standard deviation of triplicate determinations  
The bold values represented the chosen parameters in their respective optimization.

## 4.2 Preparation of PEG-IDA and PEG-IDA-metal ions

### 4.2.1 Iminodiacetic acid (IDA) concentration

Iminodiacetic acid (IDA) concentration is one of the major factors that affect the preparation of PEG-IDA. In the present study, IDA concentration on the synthesis of PEG-IDA was optimized by measuring the metal ion concentration bound onto the PEG-IDA product. The results of metal concentration at different IDA concentrations ranging from 0.1 to 0.5 mol/L in the reaction mixture are shown in Figure 4.1. Increased in IDA concentration resulted in higher metal concentration bound to the PEG-IDA.

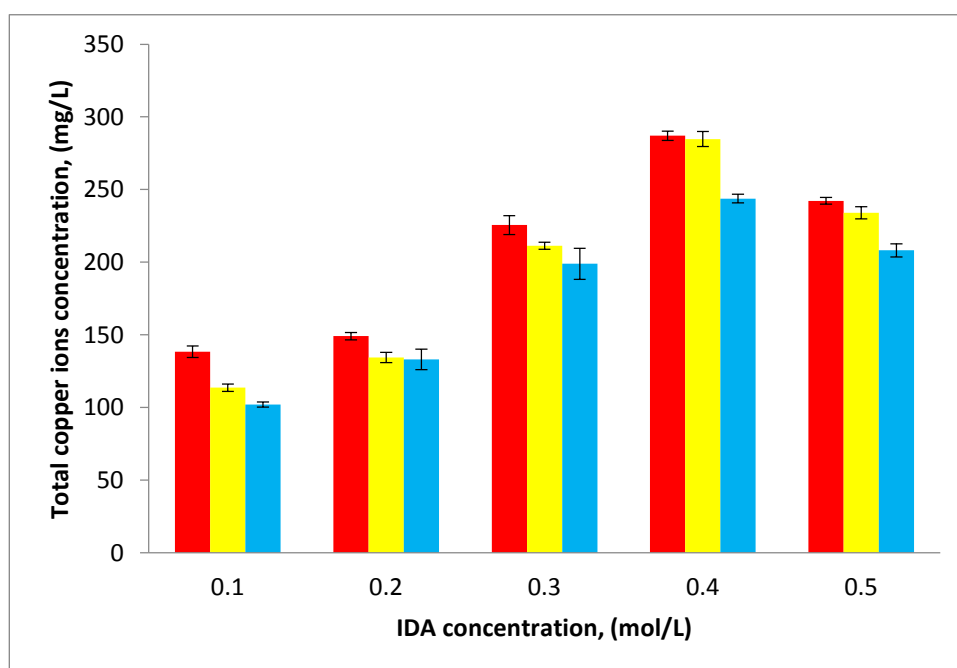


**Figure 4.1 Effect of IDA concentration on the total copper ions detected in the final product.** ■ represents total copper ions coupled to PEG 2000-IDA, ■ represents total copper ions coupled to PEG 4000-IDA and ■ represent total copper ions coupled to PEG 6000-IDA. Error bars plotted on each data point represented the standard deviation of triplicate determinations.

In general, based on each IDA concentration tested, PEG 2000-IDA demonstrated the highest binding efficiency to metal ions, followed by PEG 4000-IDA. In contrast, PEG 6000-IDA showed the lowest binding concentration with metal ions. Based on Figure 4.1, the total concentration of metal ions obtained for PEG 2000, PEG 4000 and PEG 6000 were 287.1 mg/L, 284.8 mg/L, and 243.8 mg/L, respectively, in the presence of 0.4 M IDA. Therefore, 0.4 mol IDA was selected for the next step of optimization.

#### **4.2.2 Types of metal ions**

Copper and nickel ions were used for the synthesis of PEG-IDA-metal. They were studied and optimized by measuring the metal ions concentration bound to the PEG-IDA. The results are as shown in Figure 4.2 and the highest concentration of bound metal was selected for the production of PEG-IDA-metal. The highest concentration of copper ions detected that was bound to PEG 2000-IDA that recorded a concentration of 225.6 mg/L and it was 11.8% higher than the one bound to PEG 6000-IDA.

In addition, metal ion detected in PEG 4000-IDA-Cu(II) was 225.1 mg/L, which was almost similar to the one detected in PEG 2000-IDA-Cu(II). However, the concentration was 0.5 mg/L lower than latter. On the other hand, the concentration of nickel ions bound to PEG 2000-IDA-Ni(II), PEG 4000-IDA-Ni(II) and PEG 6000-IDA-Ni(II), nickel ions were 108.55 mg/L, 114.46 mg/L and 95.59 mg/L, respectively. Therefore, the results clearly showed that the copper ions detected in the final product was approximately 2 times higher

than the nickel ions as shown in Figure 4.2. Therefore, PEG-IDA-Cu(II) was selected for phase diagram construction with different types of phase forming salts.

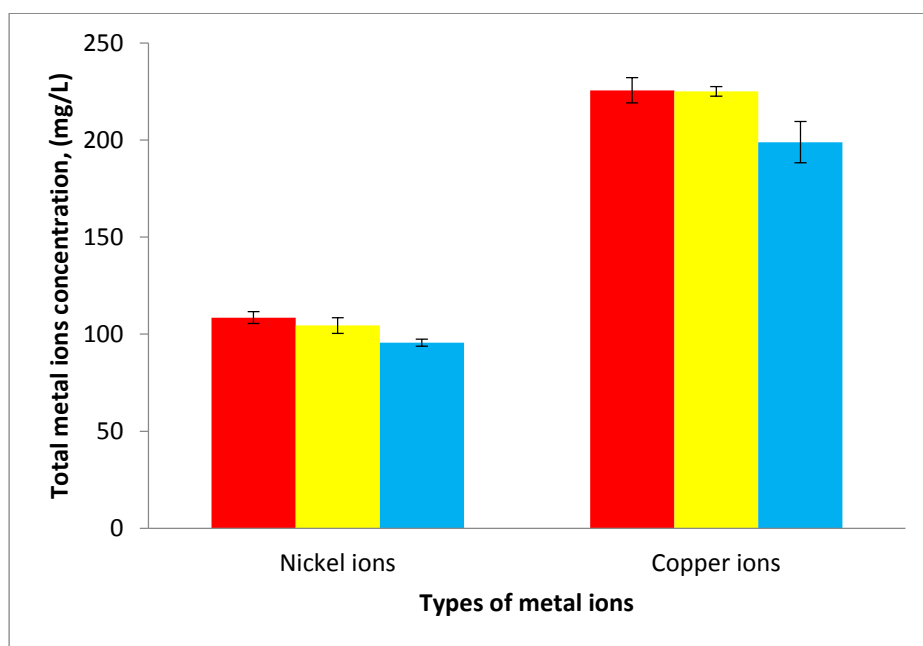


**Figure 4.2 Concentration of metal ions bound to PEG-IDA.** ■ represents the total metal ions coupled to PEG 2000-IDA, ■ represents the total metal ions coupled to PEG 4000-IDA and ■ represents the total metal ions coupled to PEG 6000-IDA. Error bars plotted on each data point represented the standard deviation of triplicate determinations.

### 4.3 Construction of phase diagram

#### 4.3.1 Binodal curve

Binodal curve is used as a divider to separate two regions with monophasic region (area below the curve) and diphasic region (area above the curve). The final system compositions were calculated and recorded for PEG 2000-IDA-Cu(II), PEG 4000-IDA-Cu(II), PEG 6000-IDA-Cu(II) with three phase-

forming salts ( $\text{Na}_2\text{SO}_4$ ,  $(\text{NH}_4)_2\text{SO}_4$  and potassium phosphate buffer (KPB)). The recorded data were used to plot binodal curves with PEG-IDA-Cu(II) concentration as ordinate while salt concentration as abscissa. All the binodal curves generated for different PEG-IDA-Cu(II) and the phase-forming salts are shown in Figure 4.3, Figure 4.4 and Figure 4.5.

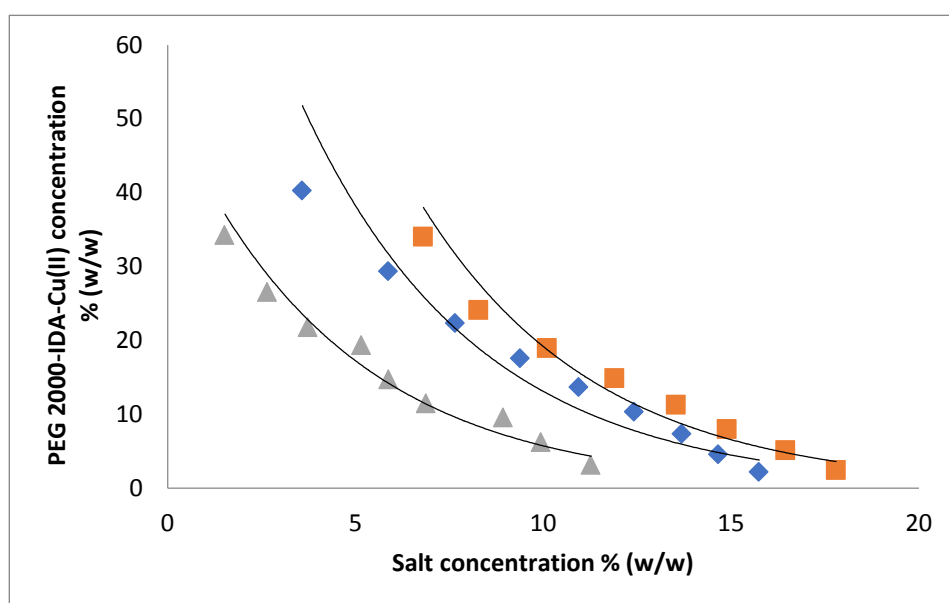


**Figure 4.3: Binodal curves of different phase-forming salts with PEG 2000-IDA-Cu (II).**  $(\text{NH}_4)_2\text{SO}_4$  represents as ( $\blacklozenge$ ),  $\text{Na}_2\text{SO}_4$  represents as ( $\blacktriangle$ ) and lastly KPB represented as ( $\blacksquare$ ) against PEG 2000-IDA-Cu(II). Error bars plotted on each data point represents the standard deviation of triplicate determinations.

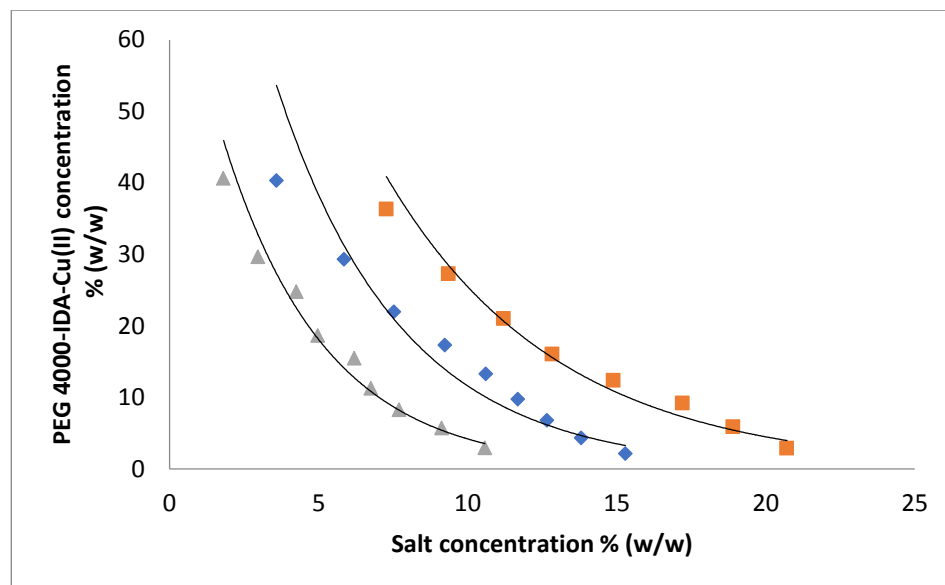


**Figure 4.4: Binodal curves of different phase-forming salts with PEG 4000-IDA-Cu (II).**  $(\text{NH}_4)_2\text{SO}_4$  represents as (  $\blacklozenge$  ),  $\text{Na}_2\text{SO}_4$  represents as (  $\blacktriangle$  ) and lastly KPB represented as (  $\blacksquare$  ) against PEG 4000-IDA-Cu(II). Error bars plotted on each data point represents the standard deviation of triplicate determinations.

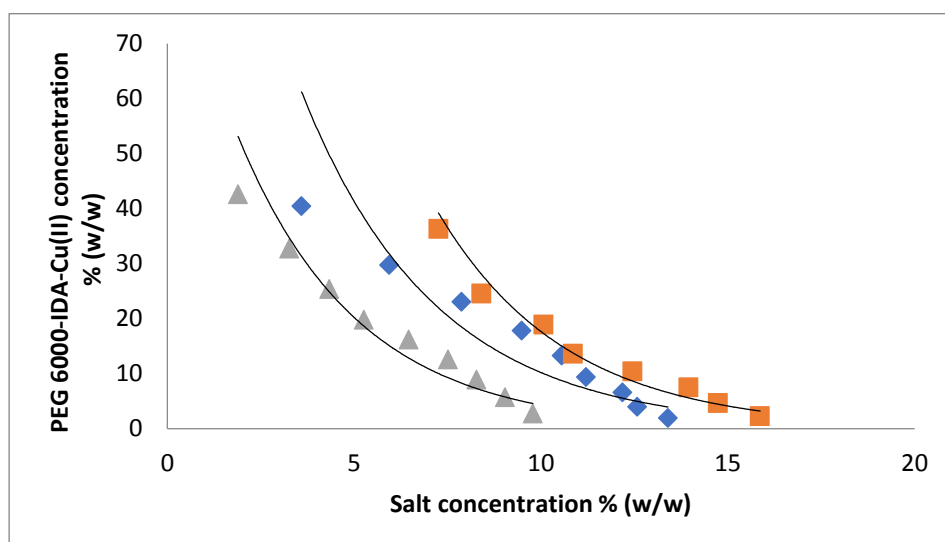


**Figure 4.5: Binodal curves of different phase-forming salts with PEG 6000-IDA-Cu (II).**  $(\text{NH}_4)_2\text{SO}_4$  represents as (  $\blacklozenge$  ),  $\text{Na}_2\text{SO}_4$  represents as (  $\blacktriangle$  ) and lastly KPB represented as (  $\blacksquare$  ) against PEG 6000-IDA-Cu(II). Error bars plotted on each data point represents the standard deviation of triplicate determinations.

Based on Figures 4.3-4.5, ATPS constituted of  $\text{Na}_2\text{SO}_4$  provided the largest heterogeneous region compared to other salts, hence lower concentrations of  $\text{Na}_2\text{SO}_4$  were needed to form two phases. Whereas, KPB systems showed the smallest heterogeneous region, thus higher concentrations of salts were needed to form two phases in ATPS. Therefore, a comparison between  $\text{Na}_2\text{SO}_4$  and different MW PEG-IDA-Cu(II) were done as shown in Figure 4.6. Results showed that PEG 6000-IDA-Cu(II) curve was the nearest to the origin while PEG 2000-IDA-Cu(II) was the farthest from the origin on the graph. In ATPS, a system located nearest to the origin is preferred as it requires the lowest concentrations of phase-forming components for biphasic formation.

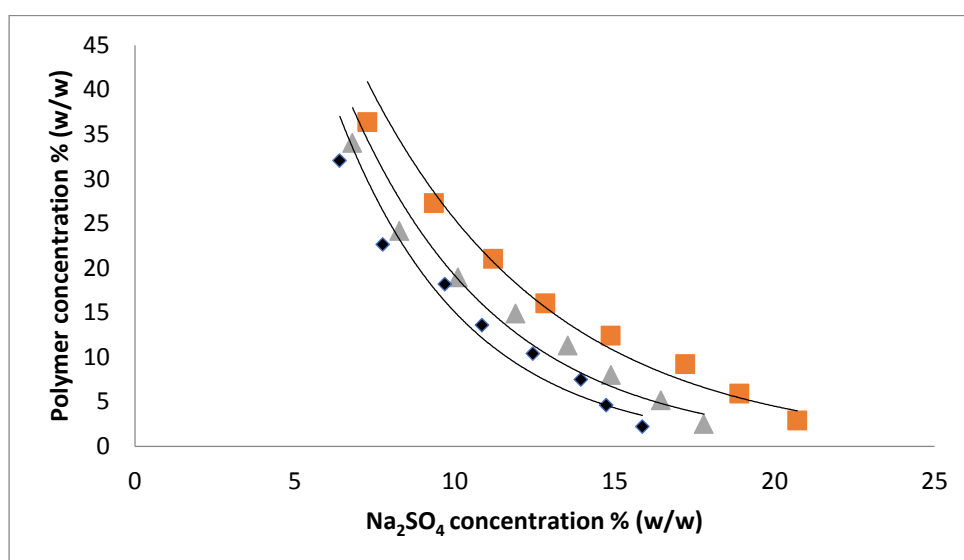


**Figure 4.6: Binodal curves of different PEG-IDA-Cu (II) against  $\text{Na}_2\text{SO}_4$ .** PEG 2000-IDA-Cu(II) represents as (  $\blacklozenge$  ), PEG 4000-IDA-Cu(II) represents as (  $\blacktriangle$  ), and PEG 6000-IDA-Cu(II) represents as (  $\blacksquare$  ) on PEG-salt system to study the effect of different PEG MW on binodal curves. Error bars plotted on each data point represented the standard deviation of triplicate determinations.

### 4.3.2 Standard curves for tie-lines generation

#### 4.3.2.1 Standard curves for salt conductivity

Standard curves for phase-forming salts,  $(\text{NH}_4)_2\text{SO}_4$ ,  $\text{Na}_2\text{SO}_4$  and KPB were generated in this study as shown in Figure 4.7, Figure 4.8 and Figure 4.9, respectively. The concentration range for all phase-forming salts were from 0 to 8% (w/w). These  $R^2$  values for the standard curves were more than 0.9, which indicated all data points fall on the best fitted line. Error bars of each data point represent the standard deviation of triplicate determinations. The standard deviation for all the data were less than 0.05, where the error bars were too small to be observed in the standard curves. These standard curves were used to determine the salt concentration for tie-line generation.

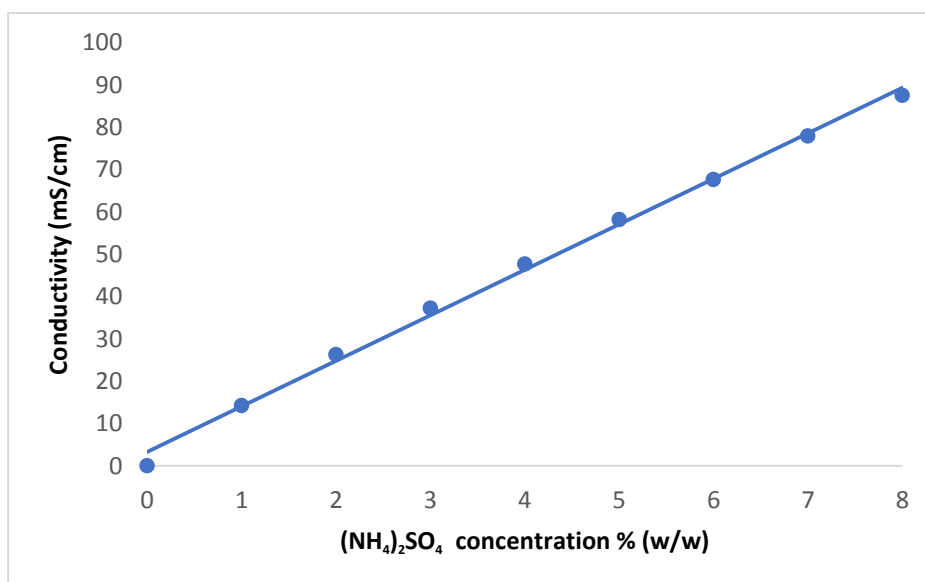


**Figure 4.7: Standard curve for conductivity measurement (mS/cm) of  $(\text{NH}_4)_2\text{SO}_4$  concentration % (w/w).** The equation for the standard curve is  $y = 10.75x - 7.4686$  ( $R^2 = 0.9968$ ).

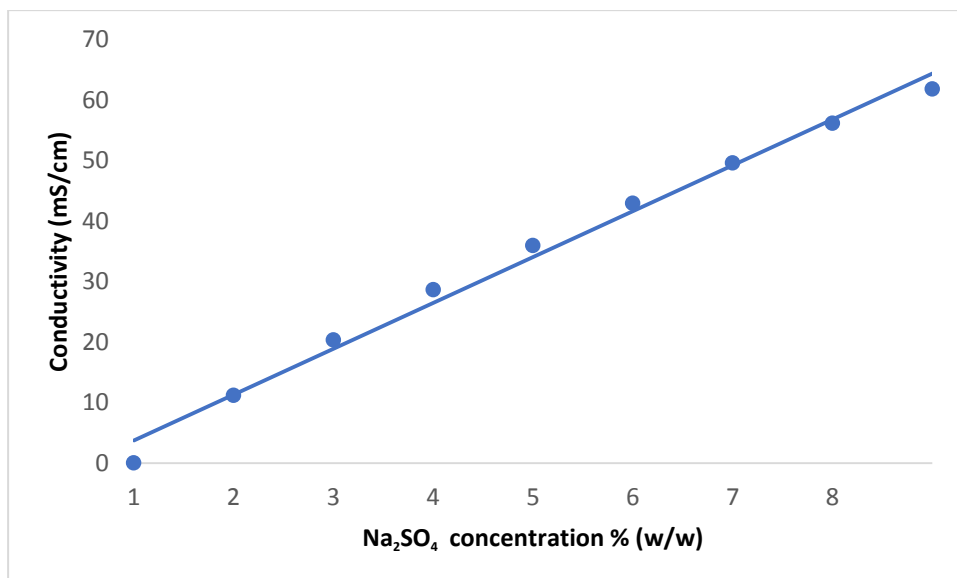


**Figure 4.8: Standard curve for conductivity measurement (mS/cm) of Na<sub>2</sub>SO<sub>4</sub> (% (w/w)).**The equation for the standard curve is  $y = 7.5893x - 3.8689$  ( $R^2 = 0.9906$ ).

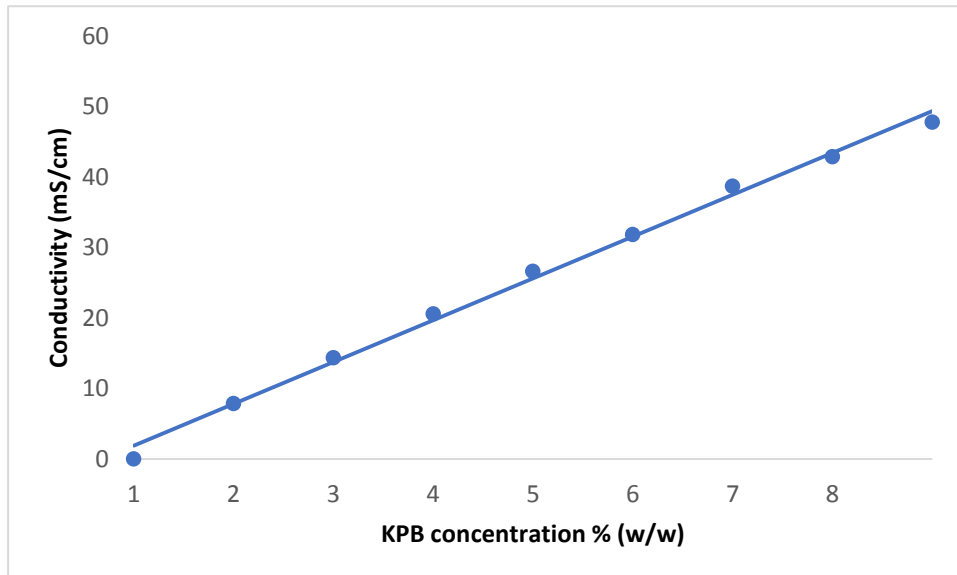


**Figure 4.9: Standard curve for conductivity measurement (mS/cm) of KPB(% (w/w)).**The equation for the standard curve is  $y = 5.9311x - 4.0553$  ( $R^2 = 0.9953$ ).

#### 4.3.2.2 Standard curves for refractive index of PEG

Standard curves for the refractive index of PEG 2000-IDA-Cu(II), PEG 4000-IDA-Cu(II) and PEG 6000-IDA-Cu(II) are as shown in Figure 4.10, Figure 4.11 and Figure 4.12, respectively. They were used to measure polymer concentration for tie-line generation. The concentration range for all modified polymers used was from 0 to 6% (w/w). The  $R^2$  values obtained for this standard curve were more than 0.9, which indicated all data points fall on the best fitted line. Error bars of each data point represent the standard deviation of triplicate determinations. The standard deviation for all the data were less than 0.05 where the error bars were too small to be observed in the standard curves.

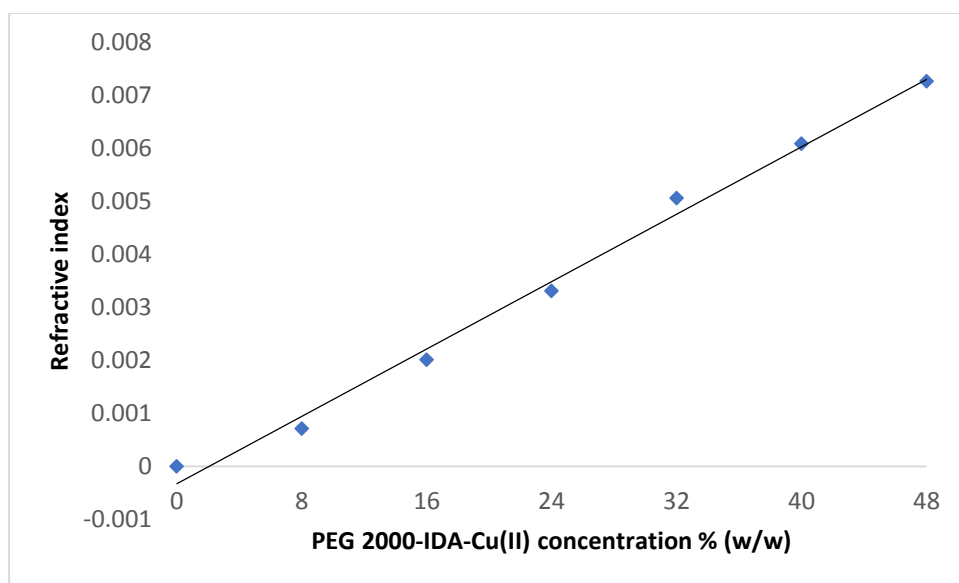


**Figure 4.10: Standard curve for the refractive index of PEG 2000-IDA-Cu(II)(% (w/w)).** Each data point is mean  $\pm$  standard deviation of triplicate determinations. The equation for the standard curve is  $y = 0.0013x - 0.0016$  ( $R^2 = 0.9928$ ).

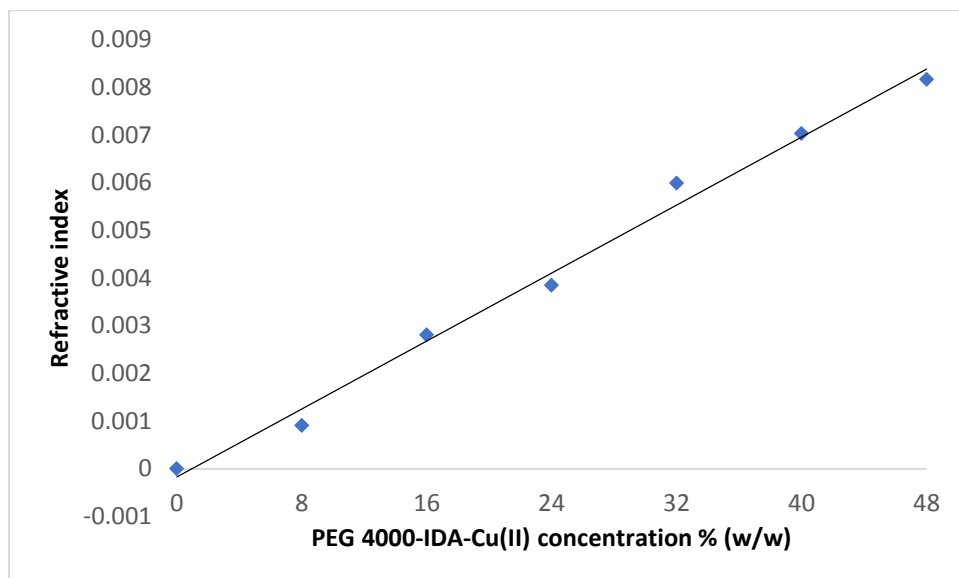


**Figure 4.11: Standard curve for the refractive index of PEG 4000-IDA-Cu(II)(% (w/w)).** Each data point is mean  $\pm$  standard deviation of triplicate determinations. The equation for the standard curve is  $y = 0.0014x - 0.0016$  ( $R^2 = 0.9915$ ).

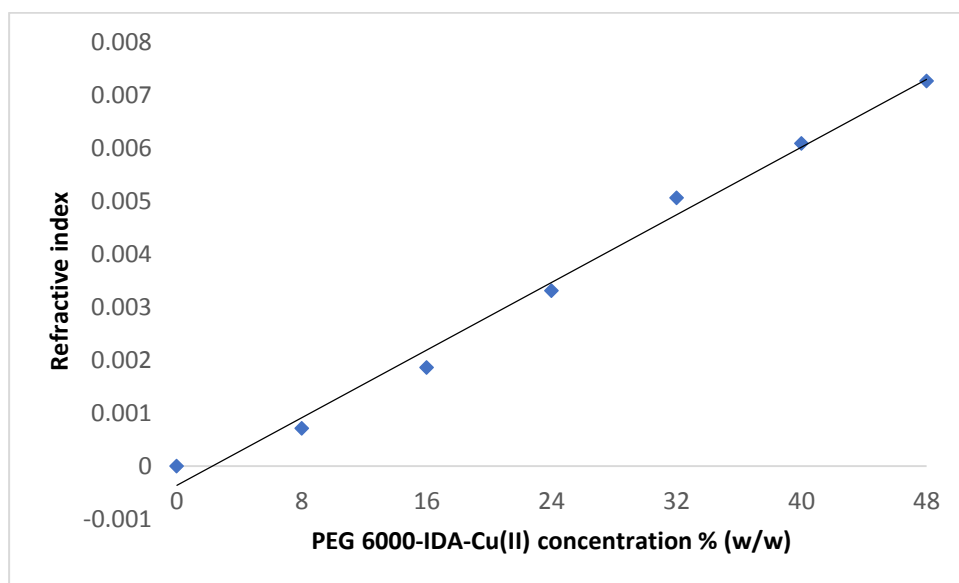


**Figure 4.12: Standard curve for the refractive index of PEG 6000-IDA-Cu(II)(% (w/w)).** Each data point is mean  $\pm$  standard deviation of triplicate determinations. The equation for the standard curve is  $y = 0.0013x - 0.0016$  ( $R^2 = 0.9911$ ).

### 4.3.2.3 Standard curves for refractive index of phase-forming salts

The total refractive index obtained from the top phase of ATPS is contributed by both refractive index of polymers and salts. Therefore, it is crucial to measure the salt refractive index to obtain the exact polymer concentration in the top phase. The refractive index standard curve for phase-forming salts  $(\text{NH}_4)_2\text{SO}_4$ ,  $\text{Na}_2\text{SO}_4$  and KPB were generated as shown in Figure 4.13, Figure 4.14 and Figure 4.15, respectively. The concentration range used for standard curves generation for all phase-forming salts were from 0 to 12% (w/w). These  $R^2$  values obtained were more than 0.9, which indicated that all data points fall on the best fitted line. Error bars of each data point represent the standard deviation of triplicate determinations.

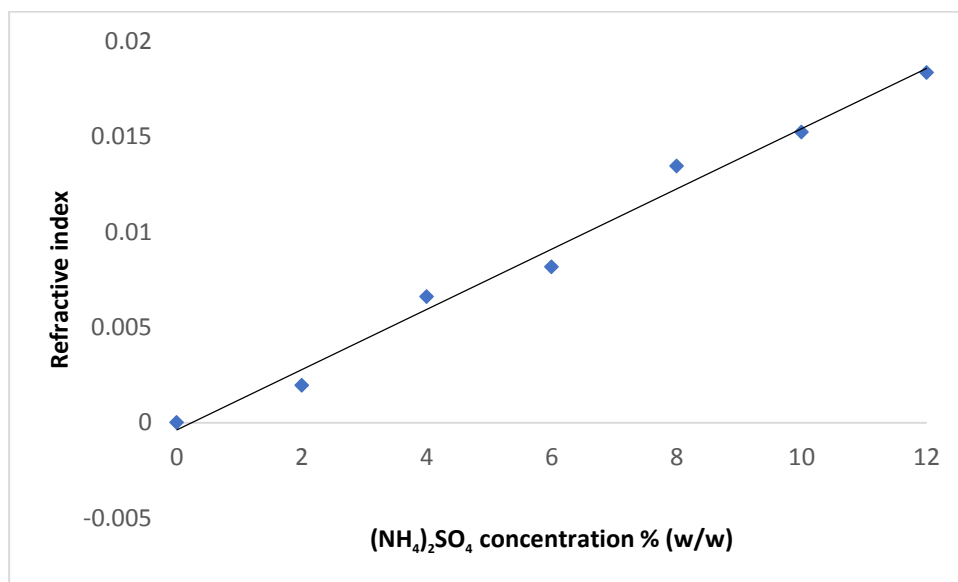


**Figure 4.13: Standard curve for refractive index of  $(\text{NH}_4)_2\text{SO}_4$  (% (w/w)).** The equation for the standard curve is  $y = 0.0032x - 0.0035$  ( $R^2 = 0.9872$ ).

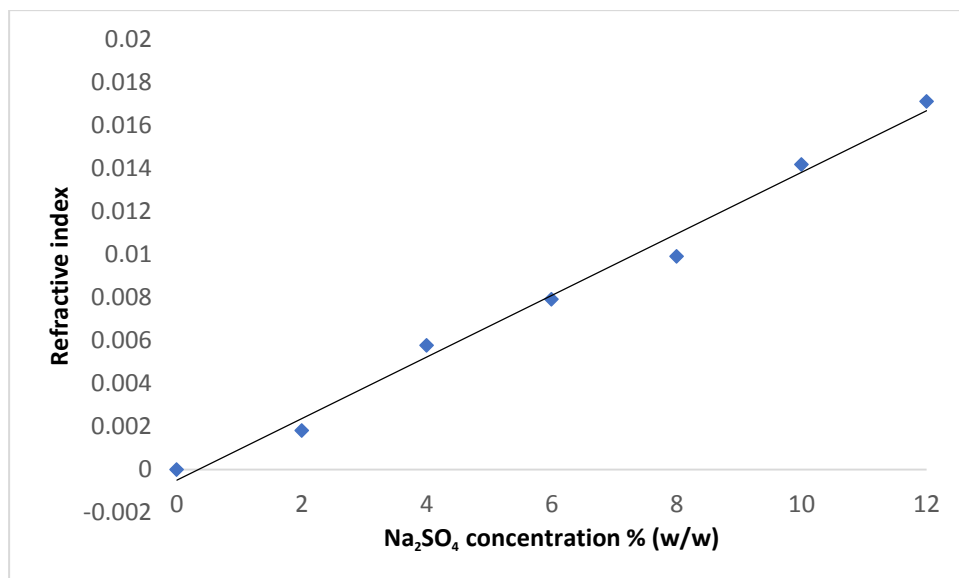


**Figure 4.14:** A standard curve for refractive index of Na<sub>2</sub>SO<sub>4</sub> (% (w/w)). The equation for the standard curve is  $y = 0.0029x - 0.0034$  ( $R^2 = 0.9901$ ).

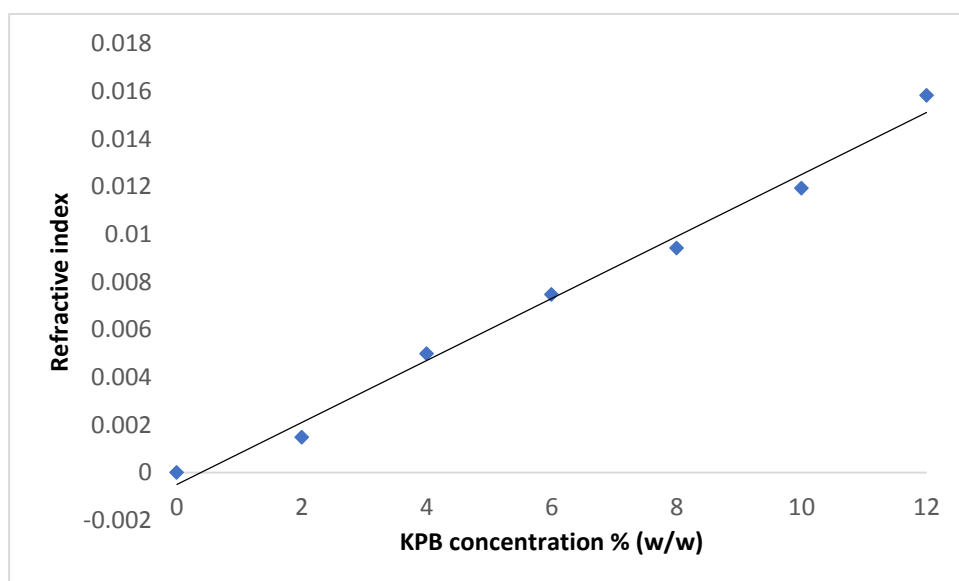


**Figure 4.15:** A standard curve for refractive index of KPB (% (w/w)). The equation for the standard curve is  $y = 0.0026x - 0.0031$  ( $R^2 = 0.9905$ ).

### 4.3.3 Generation of tie-lines

System with a phase volume ratio of 1.0 (top: bottom) for each binodal curve was used to generate tie-lines. The final concentrations of PEG-IDA-Cu(II) and salts in the top and bottom phases were determined based on the standard curves generated. A total of three tie-lines were generated for each binodal curve. PEG 6000-IDA-Cu(II)-Na<sub>2</sub>SO<sub>4</sub> system was selected as it was nearest to the origin, which provided the largest heterogeneous region and required the lowest concentration of phase components to form two-phases.

A complete phase diagram which consisted of PEG 6000-IDA-Cu(II)-Na<sub>2</sub>SO<sub>4</sub> binodal curve and three tie-lines is shown in Figure 4.16. The rest of the phase diagrams which composed of different modified PEG and phase-forming salts were also plotted (Appendix B). Three experimental tie lines labelled as TL 1, 2 and 3 and the points on the lines represented the final compositions of salts and modified PEG in top and bottom phases. TL labelled as 1, 2 and 3 also determined the distance of binodal curve from nearest to farthest from the origin. Critical point (C<sub>p</sub>) of PEG 6000-IDA-Cu(II)-Na<sub>2</sub>SO<sub>4</sub> system was also calculated and plotted.

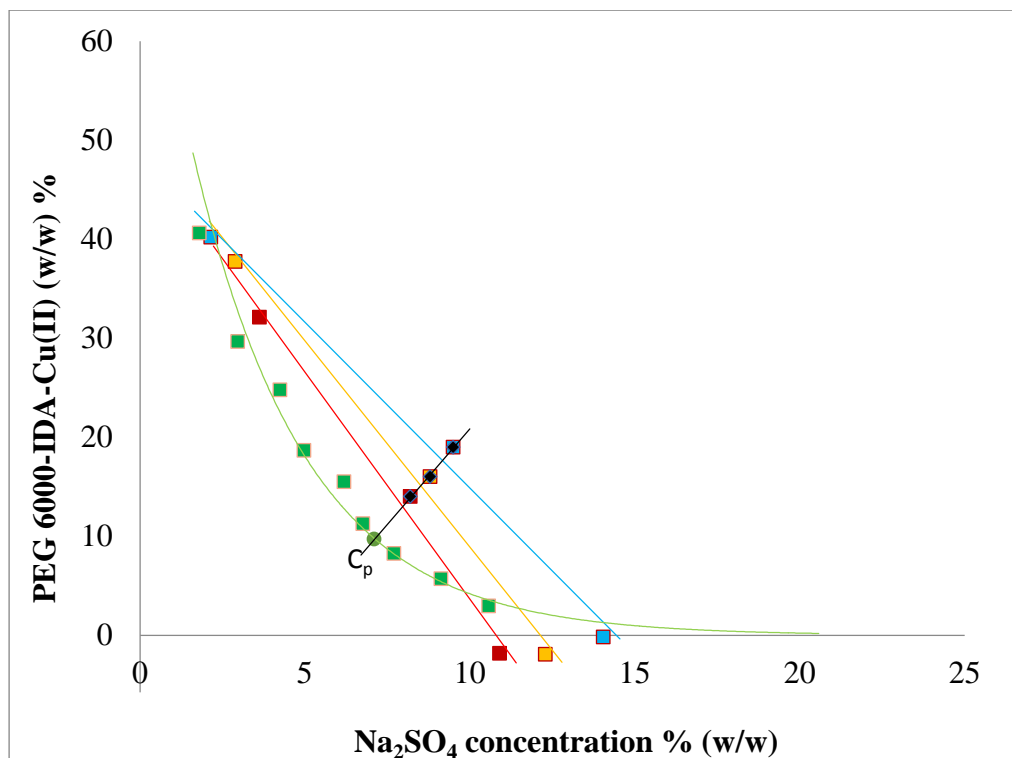


**Figure 4.16: A phase diagram for PEG 6000-IDA-Cu(II)- $\text{Na}_2\text{SO}_4$  system.** The binodal curve for PEG 6000-IDA-Cu(II) was plotted against  $\text{Na}_2\text{SO}_4$ . Tie-lines were represented as TL 1, TL 2 and TL3.  $C_p$  on binodal curve was determined and represents as critical point. TL 1, 2, and 3 represent the distance of binodal curves from nearest to farthest from origin. Error bars: triplicate determinations.

#### 4.3.3.1 Tie-line length (TLL) and slope of tie-line length (STL)

Tie-line length (TLL) and slope of tie-line (STL) were calculated and listed in Table 4.5. These results illustrated that TLL value increased as the tie-line shifted farther away from the binodal curve. Therefore, this indicated that the phase compositions for each phase component increased as TLL increased. In this study, TLL nearest to the binodal curve was favoured as it required the lowest concentration of phase components to form two-phases compared to other TLLs. Besides, it can be observed that STL values were inversely related to TLL values (Table 4.5). STL values decreased as the TLLs increased for all

PEG-salt systems. Besides that, STL values for all tie-lines of PEG 6000-IDA-Cu(II)-Na<sub>2</sub>SO<sub>4</sub> system were generally slightly higher compared to (NH<sub>4</sub>)<sub>2</sub>SO<sub>4</sub> and KPBSalts systems.

**Table 4.5:Varies tie-line and their corresponding TLL and STL.**

Tie-line	Composition (%)		STL	TLL
	Salt	Polymer		
PEG 2000-IDA-Cu(II) – Ammonium sulphate				
1	11.1	16	-0.37	27.49
2	11.5	18	-0.42	33.19
3	12	19	-0.43	34.56
PEG 2000-IDA-Cu(II) – KPB				
1	13.5	13	-0.43	26.62
2	14	14.5	-0.43	30.96
3	14.5	16	-0.46	35.81
PEG 2000-IDA-Cu(II) – Sodium sulphate				
1	7.9	15	-0.27	32.34
2	8.1	16	-0.30	36.83
3	8.4	17	-0.33	38.09
PEG 4000-IDA-Cu(II) – Ammonium sulphate				
1	10.75	16	-0.35	30.60
2	11.4	18	-0.39	38.82
3	12	20.5	-0.40	37.02

<b>Table 4.5 (continued)</b>				
<b>Tie-line</b>	<b>Composition (%)</b>		<b>STL</b>	<b>TLL</b>
	<b>Salt</b>	<b>Polymer</b>		
PEG 4000-IDA-Cu(II) – KPB				
1	14.5	16	-0.50	39.49
2	15.4	17	-0.52	43.04
3	16	18	-0.54	42.25
PEG 4000-IDA-Cu(II) – Sodium sulphate				
1	8.2	14	-0.27	38.18
2	8.8	16	-0.30	45.33
3	9.5	19	-0.30	48.07
PEG 6000-IDA-Cu(II) – Ammonium sulphate				
1	10.6	16	-0.24	31.64
2	11	17	-0.28	34.79
3	11.4	19	-0.30	37.17
PEG 6000-IDA-Cu(II) – KPB				
1	13	14	-0.35	27.11
2	13.2	15	-0.34	33.74
3	13.5	17	-0.37	39.02
PEG 6000-IDA-Cu(II) – Sodium sulphate				
1	7.9	14	-0.24	33.75
2	8.1	15.5	-0.25	41.97
3	8.4	17	-0.32	39.30

The symbol “-” represents negative values.

## 4.4 Optimization of his-tagged HBcAg partitioning

### 4.4.1 Effect of phase inversion on his-tagged HBcAg partitioning

Phase inversion methods used in this study included a 3D rotator and a vortex mixer. Effects of two different inversion methods and duration on the recovery of his-tagged HBcAg from unclarified *E. coli* feedstock are tabulated in Table 4.6. The optimal system was selected based on the recovery yield, purity and purification factor obtained from the PEG rich top phase in ATPS.

**Table 4.6: Effects of different modes of phase inversion on purity, purification factor, and recovery yield of his-tagged HBcAg from unclarified feedstock using 14%(w/w)PEG 6000-IDA-IDA-Cu(II) and 7.9%(w/w)Na<sub>2</sub>SO<sub>4</sub> system.**

Phase inversion mode	Time (min)	Phase	Purity (%) <sup>1</sup>	Purification factor	Recovery yield (%) <sup>1</sup>
<b>Vortex mixer</b>	1	Top	58.3 ± 0.3	1.82	69.9 ± 2.1
		Inter	32.2 ± 0.5	1.00	24.3 ± 3.2
		Bottom	19.7 ± 0.2	0.62	6.0 ± 2.3
	<b>5</b>	<b>Top</b>	<b>62.3 ± 0.5</b>	<b>1.95</b>	<b>71.9 ± 1.5</b>
		Inter	30.5 ± 0.6	0.95	21.0 ± 1.9
		Bottom	17.0 ± 0.3	0.53	5.0 ± 0.7
3D rotator	1	Top	59.4 ± 0.5	1.86	68.3 ± 4.1
		Inter	32.4 ± 0.3	1.01	22.7 ± 2.0
		Bottom	17.2 ± 0.3	0.54	9.0 ± 3.8
	5	Top	61.9 ± 0.6	1.93	69.1 ± 1.4
		Inter	29.8 ± 0.2	0.93	23 ± 3.4
		Bottom	12.1 ± 0.7	0.38	7.0 ± 2.2

<sup>1</sup>Each data is mean ± standard deviation of triplicate determinations.

The bold values represented the chosen parameters in their respective optimization.

Phase inversion using a vortex mixer for 5 min produced the optimum recovery yield (71.9%) of his-tagged HBcAg with 62.3% in purity and a purification factor of 1.95 (Table 4.6). On the other hand, phase inversion using the 3D rotator produced a slightly lower purity and purification factor of 61.9% and 1.93, respectively compared to the one obtained using the vortex mixer. In addition, the duration of inversion was taken into consideration as it plays an important role in the partitioning of his-tagged HBcAg in ATPS. In general, the purity, purification factor and recovery yield of his-tagged HBcAg obtained using both inversion methods for 1 min was lower than that obtained from 5 min of mixing. Therefore, mixing with a vortex mixer for 5 min was selected as the optimum phase inversion method for his-tagged HBcAg recovery from unclarified bacterial feedstock.

#### **4.4.2 Phase separation mode**

Two types of phase separation methods were investigated in this study, which included leaving the system to separate naturally and through centrifugation. However, leaving the system to separate on its own was not feasible to use as it required an extremely long separation duration, which took up to two days. Therefore, centrifugation method was selected as the separation method. Different centrifugation forces, centrifugation durations and temperatures were optimized in order to obtain the optimal recovery of his-tagged HBcAg. The effects of these parameters on the recovery of his-tagged HBcAg are tabulated in Table 4.7.

**Table 4.7: Effects of different phase separation methods on the purity, purification factor, and recovery yield of his-tagged HBcAg from unclarified *E. coli* feedstock using 14%(w/w)PEG 6000-IDA-Cu(II) and 7.9% (w/w)Na<sub>2</sub>SO<sub>4</sub> system.**

Parameters	Duration (min)	Force ( xg)	Temperature (°C)	Phase	Purity (%) <sup>1</sup>	Purification factor <sup>1</sup>	Recovery yield (%) <sup>1</sup>
<b>Force (xg)</b>	1	1000	<b>4</b>	Top	61.7 ± 0.3	2.0	47.9 ± 1.3
				Inter	26.5 ± 0.4	0.8	47.5 ± 0.5
				Bottom	9.4 ± 0.5	0.3	5.5 ± 0.3
	<b>1</b>	<b>2000</b>	<b>4</b>	<b>Top</b>	<b>67.3 ± 0.7</b>	<b>2.2</b>	<b>61.0 ± 1.2</b>
				Inter	21.5 ± 0.7	0.7	28.6 ± 0.2
				Bottom	10.3 ± 0.8	0.3	9.1 ± 0.4
	1	3000	<b>4</b>	Top	66.6 ± 0.1	2.1	58.9 ± 0.8
				Inter	20.2 ± 0.8	0.7	26.2 ± 0.3
				Bottom	13.9 ± 0.4	0.4	17.0 ± 0.1
<b>Duration (min)</b>	1	2000	<b>4</b>	Top	67.3 ± 0.7	2.2	61.0 ± 0.2
				Inter	21.5 ± 0.7	0.7	28.6 ± 0.2
				Bottom	9.3 ± 0.8	0.3	9.1 ± 0.0
	<b>3</b>	<b>2000</b>	<b>4</b>	<b>Top</b>	<b>69.7 ± 0.4</b>	<b>2.3</b>	<b>65.5 ± 1.3</b>
				Inter	19.5 ± 0.9	0.6	20.7 ± 0.1
				Bottom	10.7 ± 0.7	0.4	11.3 ± 0.9
	5	2000	<b>4</b>	Top	66.5 ± 0.5	2.2	63.0 ± 0.7
				Inter	22.7 ± 0.5	0.7	23.8 ± 0.8
				Bottom	12.0 ± 0.4	0.4	10.9 ± 0.1
<b>Temperature (°C)</b>	3	2000	23	Top	61.2 ± 0.6	2.1	64.2 ± 1.3
				Inter	27.3 ± 0.3	0.8	25.3 ± 0.7
				Bottom	12.1 ± 0.7	0.3	9.1 ± 0.2
	<b>3</b>	<b>2000</b>	<b>4</b>	<b>Top</b>	<b>69.7 ± 0.4</b>	<b>2.3</b>	<b>65.5 ± 0.3</b>
				Inter	19.5 ± 0.9	0.6	20.7 ± 0.1
				Bottom	10.7 ± 0.7	0.4	11.3 ± 0.3

<sup>1</sup>Each data is mean ± standard deviation of triplicate determinations.

The bold values represented the chosen parameters in their respective optimization.

First of all, centrifugal force was optimized under constant centrifugation duration (1 min) and temperature (4°C). The purity, purification factor and recovery yield for his-tagged HBcAg using 2000 xg centrifugal force were the highest among all centrifugal forces tested, which recorded a purity of 67.3%, a purification factor of 2.2 and 61% of recovery yield. Therefore, 2000 xg centrifugation force was used to optimize the centrifugation duration.

Based on the results obtained, 5 min centrifugation duration produced the lowest purity followed by 1 min and the highest was achieved with 3 min of centrifugation. The recovery yield obtained for 3 min centrifugation was 4.5% and 2.5% higher than 1 min and 5 min durations, respectively. Therefore, for the next optimization for centrifugal temperature, 2000 xg centrifugal force and 3 min centrifugation were used. Two different temperatures such as room temperature (23°C) and 4°C were investigated. The results showed that temperature at 4°C was the optimal temperature to be used. The his-tagged HBcAg recovered at this temperature was 8.5% and 1.3% higher than the purity and yield obtained at room temperature, respectively.

## **4.5 Methods scouting for his-tagged HBcAg recovery in IMAP-ATPS**

### **4.5.1 Different PEG-IDA-Cu(II)-salt systems**

Different combinations of PEG-IDA-Cu(II)-salt systems were applied to study the effect of different systems toward the recovery yield, purity, and purification factor of purified his-tagged HBcAg. A total of nine systems with TLL 1, 5 % (w/v) biomass concentration and a phase volume ratio of 1.0 were

used to determine the three best systems for the recovery of his-tagged HBcAg.

The results are tabulated in Table 4.8.

**Table 4.8: Purity, purification factor, and recovery yield of his-tagged HBcAg using different PEG-IDA-Cu(II)-salt systems.**

PEG-salt systems	Phase	Purity (%) <sup>2</sup>	Purification factor <sup>2</sup>	Recovery yield (%) <sup>2</sup>
<b>PEG 2000-IDA-Cu(II)-Na<sub>2</sub>SO<sub>4</sub></b>	<b>Top</b>	<b>74.4 ± 0.5</b>	<b>2.4</b>	<b>68.7 ± 0.5</b>
	Inter	16.7 ± 0.4	0.5	15.6 ± 0.2
	Bottom	13.2 ± 0.5	0.4	11.3 ± 0.1
PEG 4000- IDA-Cu(II)-Na <sub>2</sub> SO <sub>4</sub>	Top	72.2 ± 0.4	2.3	67.6 ± 0.66
	Inter	16.7 ± 0.4	0.5	17.7 ± 0.4
	Bottom	8.3 ± 0.2	0.3	12.1 ± 0.3
PEG 6000- IDA-Cu(II)-Na <sub>2</sub> SO <sub>4</sub>	Top	69.7 ± 0.4	2.3	65.5 ± 0.3
	Inter	19.5 ± 0.9	0.6	20.7 ± 0.1
	Bottom	10.7 ± 0.7	0.4	12.3 ± 0.3
PEG 2000- IDA-Cu(II)-(NH <sub>4</sub> ) <sub>2</sub> SO <sub>4</sub>	Top	69.4 ± 0.5	2.2	75.4 ± 0.1
	Inter	23.9 ± 0.3	0.8	23.5 ± 0.1
	Bottom	5.2 ± 0.1	0.2	7.7 ± 0.1
PEG 4000- IDA-Cu(II)-(NH <sub>4</sub> ) <sub>2</sub> SO <sub>4</sub>	Top	60.5 ± 0.6	2.0	72.5 ± 0.5
	Inter	24.1 ± 0.6	0.8	20.9 ± 0.4
	Bottom	11.5 ± 0.2	0.4	8.5 ± 0.3
PEG 6000- IDA-Cu(II)-(NH <sub>4</sub> ) <sub>2</sub> SO <sub>4</sub>	Top	60.1 ± 0.6	1.9	73.1 ± 0.2
	Inter	25.2 ± 0.5	0.8	21.1 ± 0.2
	Bottom	8.0 ± 0.2	0.3	6.2 ± 0.3

Table 4.8 (continued)

PEG-salt systems	Phase	Purity (%) <sup>2</sup>	Purification factor <sup>2</sup>	Recovery yield (%) <sup>2</sup>
<b>PEG 2000-IDA-Cu(II)-KPB<sup>1</sup></b>	<b>Top</b>	<b>73.7 ± 0.3</b>	<b>2.4</b>	<b>77.3 ± 0.8</b>
	Inter	16.4 ± 0.4	0.5	14.3 ± 0.1
	Bottom	6.5 ± 0.2	0.2	6.7 ± 0.1
<b>PEG 4000-IDA-Cu(II)-KPB<sup>1</sup></b>	<b>Top</b>	<b>74.7 ± 0.8</b>	<b>2.4</b>	<b>76.0 ± 0.2</b>
	Inter	13.2 ± 0.3	0.4	12.0 ± 0.1
	Bottom	11.0 ± 0.2	0.4	11.4 ± 0.1
PEG 6000-IDA-Cu(II)-KPB <sup>1</sup>	Top	66.8 ± 0.6	2.2	74.8 ± 0.2
	Inter	20.5 ± 0.4	0.7	11.9 ± 0.5
	Bottom	7.4 ± 0.3	0.2	10.1 ± 0.2

<sup>1</sup>KPB represented potassium phosphate buffer.

<sup>2</sup>Each data is mean ± standard deviation of triplicates determinations.

The bold values represented the chosen parameters in their respective optimization.

Based on Table 4.8, most of the his-tagged HBcAg was partitioned to the PEG-IDA-Cu(II)-rich top phase but some of the his-tagged HBcAg was also partitioned to the interphase and bottom phases. Therefore, the criteria of selection for the three optimal systems were based on the recovery yield, purity and purification factor of his-tagged HBcAg obtained from the PEG-IDA-Cu(II)-rich top phase. Among all the PEG-salt systems investigated, three PEG-salt systems that recorded the highest recovery yield, purity and purification factor of his-tagged HBcAg were PEG 2000-IDA-Cu(II)-Na<sub>2</sub>SO<sub>4</sub>, PEG 2000-IDA-Cu(II)-KPB, and PEG 4000-IDA-Cu(II)-KPB systems.

Based on the results, it was observed that most of the his-tagged HBcAg was partitioned into the PEG-IDA-Cu(II) rich top phase when low MW PEG-IDA-Cu(II) was used. The recovery yield, purity and purification factor for his-tagged HBcAg gradually decreased with the increased in the MW of PEG-IDA-Cu(II). PEG 6000-IDA-Cu(II)-Na<sub>2</sub>SO<sub>4</sub>, which was previously used in phase inversion and separation optimization was found to produce lower recovery yield, purity and purification factor for his-tagged HBcAg recovery compared to the three best selected systems as shown in Table 4.8. Moreover, higher amount of his-tagged HBcAg was partitioned into inter and bottom phases in PEG-IDA-Cu(II)-Na<sub>2</sub>SO<sub>4</sub> system.

Besides, none of the PEG-IDA-Cu(II)-(NH<sub>4</sub>)<sub>2</sub>SO<sub>4</sub> systems was selected to proceed with the subsequent optimization due to their low purity and purification factor of the purified his-tagged HBcAg compared to other systems although the recovery yield was high (Table 4.8). All three PEG-IDA-Cu(II)-(NH<sub>4</sub>)<sub>2</sub>SO<sub>4</sub> systems have shown that large proportion of the his-tagged HBcAg was partitioned into the inter phase instead of top phase, which was the highest among all systems tested that recorded 23.5%, 20.9% and 21.1% for PEG 2000-IDA-Cu(II)-(NH<sub>4</sub>)<sub>2</sub>SO<sub>4</sub>, PEG 4000-IDA-Cu(II)-(NH<sub>4</sub>)<sub>2</sub>SO<sub>4</sub>, and PEG 6000-IDA-Cu(II)-(NH<sub>4</sub>)<sub>2</sub>SO<sub>4</sub>, respectively.

This phenomenon was not favoured in ATPS as his-tagged HBcAg partitioned into top phase was the main aim in this study. Therefore, the PEG-IDA-Cu(II)-(NH<sub>4</sub>)<sub>2</sub>SO<sub>4</sub> systems was not selected for further optimization.

Systems that yielded the highest purity of his-tagged HBcAg were selected for the next optimization. These selected systems were PEG 2000-IDA-Cu(II)-Na<sub>2</sub>SO<sub>4</sub>, PEG 2000-IDA-Cu(II)-KPB, and PEG 4000-IDA-Cu(II)-KPB systems that yielded a purity of 74.4%, 73.7% and 74.7%, respectively and these systems were selected for tie-line length (TLL) optimization as described in Section 4.5.2.

#### **4.5.2 Tie-line length (TLL)**

Effects of TLL on the recovery of his-tagged HBcAg was tested using three selected systems (PEG 2000-IDA-Cu(II)-Na<sub>2</sub>SO<sub>4</sub>, PEG 2000-IDA-Cu(II)-KPB, and PEG 4000-IDA-Cu(II)-KPB) with 5 % (w/v) biomass concentration and the results are tabulated in Table 4.9. In this study, TLL 1, 2 and 3 represented the TLL distance from the nearest to farthest from the binodal curve.

The purity, purification factor and recovery yield of his-tagged HBcAg of the three selected systems improved as TLL increased except for TLL 2 and TLL 3 in PEG 4000-IDA-Cu(II)-KPB system. The purity and recovery yield for both TLL were almost similar but TLL 2 in this system recorded a slightly higher purity and recovery yield compared to TLL 3 with differences of not more than 2% in both the purity and recovery yield. Moreover, an increase in TLL also observed an increase in his-tagged HBcAg partitioning to the PEG-IDA-Cu(II) rich top phase and a decrease in his-tagged HBcAg partitioning to the bottom phase in the systems.

**Table 4.9: Effect of different TLL in PEG 2000-IDA-Cu(II)-Na<sub>2</sub>SO<sub>4</sub>, PEG 2000-IDA-Cu(II)-KPB, and PEG 4000-IDA-Cu(II)-KPB systems on purity, purification factor, and recovery yield of his-tagged HBcAg.**

ATPS system	TLL <sup>1</sup>	Polymer: salt (% (w/w))	Phase	Purity (%) <sup>2</sup>	Purification factor <sup>2</sup>	Recovery yield (%) <sup>2</sup>		
PEG 2000-IDA-Cu(II)-Na <sub>2</sub> SO <sub>4</sub>	1	7.9:15.0	Top	74.4 ± 0.5	2.4	68.7 ± 0.5		
			Inter	16.7 ± 0.4	0.5	15.6 ± 0.2		
			Bottom	13.2 ± 0.5	0.4	11.3 ± 0.1		
	2	8.1:16.0	Top	76.5 ± 1.3	2.5	69.9 ± 0.4		
			Inter	12.6 ± 0.5	0.4	16.8 ± 0.5		
			Bottom	11.5 ± 0.4	0.4	9.7 ± 0.3		
			3	8.4:17.0	Top	77.7 ± 0.9	2.5	71.0 ± 0.7
					Inter	11.7 ± 0.1	0.4	17.9 ± 0.3
					Bottom	10.0 ± 0.3	0.3	8.3 ± 0.1
PEG 2000-IDA-Cu(II)-KPB	1	13.5:13.0	Top	73.7 ± 0.3	2.4	77.3 ± 0.8		
			Inter	16.4 ± 0.4	0.5	14.3 ± 0.1		
			Bottom	6.5 ± 0.2	0.2	6.7 ± 0.1		
	2	14.0:14.5	Top	78.9 ± 1.0	2.6	81.1 ± 1.1		
			Inter	15.2 ± 0.2	0.5	14.6 ± 0.5		
			Bottom	5.4 ± 0.3	0.2	5.1 ± 0.1		
			<b>3</b>	<b>14.5:16.0</b>	<b>Top</b>	<b>81.2 ± 0.8</b>	<b>2.6</b>	<b>82.9 ± 0.9</b>
					Inter	15.7 ± 0.1	0.5	13.5 ± 0.5
					Bottom	5.0 ± 0.1	0.2	4.4 ± 0.3
PEG 4000-IDA-Cu(II)-KPB	1	14.5:16.0	Top	74.7 ± 0.8	2.4	76.0 ± 0.2		
			Inter	13.2 ± 0.3	0.4	12.0 ± 0.1		
			Bottom	11.0 ± 0.2	0.4	11.4 ± 0.1		
	2	15.4:17.0	Top	77.8 ± 0.3	2.5	82.6 ± 0.9		
			Inter	12.9 ± 0.5	0.4	12.5 ± 0.4		
			Bottom	5.9 ± 0.2	0.2	4.3 ± 0.2		
			3	16.0:18.0	Top	77.1 ± 0.7	2.5	81.9 ± 0.3
					Inter	12.6 ± 0.2	0.4	13.4 ± 0.4
					Bottom	5.4 ± 0.3	0.2	4.1 ± 0.4

<sup>1</sup>TLL with number 1, 2 and 3 represented TLL distance nearest to farthest from origin of binodal curve.

<sup>2</sup> Each data is mean ± standard deviation of triplicate determinations.

The bold values represented the chosen parameter.

A gradual increase in purity and recovery yield with increase in TLL was clearly observed in PEG 2000-IDA-Cu(II)-Na<sub>2</sub>SO<sub>4</sub> system. An increase of 0.9% purity and 1.2% recovery yield were obtained as the TLL increased from TLL 1 to TLL 2. Moreover, an increase of 0.8% purity and 1.1% recovery yield of his-tagged HBcAg was observed as TLL increased from TLL 2 to TLL 3. As a result, TLL 3, which recorded a purity of approximately 78% and 71% recovery yield, was the best composition to be used in Na<sub>2</sub>SO<sub>4</sub> salt system. However, when this was compared with the other salt systems, it was not selected for the next optimization step as the other salt systems acquired a higher purity, purification factor and recovery yield.

As for PEG 2000-IDA-Cu(II)-KPB system, similar trend was observed whereby the TLL was directly proportional to the purity and recovery yield of his-tagged HBcAg. The purity for his-tagged HBcAg obtained under TLL 1 system was 74.7% and this was slightly increased to 78.9% when TLL 2 was used. A purity of 81.2% was obtained when TLL 3 system was used. In the similar system, the recovery yields obtained for TLL 1, 2 and 3 were 77.3%, 81.1% and 82.9%, respectively. The system with the highest purity and recovery yield was chosen to study the effects of phase volume ratio parameters on his-tagged HBcAg recovery. Therefore, PEG 2000-IDA-Cu(II)-KPB system with TLL 3 composition was selected for this purpose.

### 4.5.3 Phase volume ratio

The composition of TLL 3 in PEG 2000-IDA-Cu(II)-KPB system with 5 % (w/v) biomass concentration was employed in the optimization of phase volume ratio. Three phase volume ratios were studied, which were 2.3, 1.0 and 0.4 and the results are tabulated in Table 4.10.

**Table 4.10: Effects of phase volume ratio of TLL 3 in PEG 2000-IDA-Cu(II)-KPB system system on the partitioning of his-tagged HBcAg.**

Systems	Salt% (PEG w/w)	PEG% (w/w)	Phase volume ratio (top/bottom)	Phase	Purity (%) <sup>1</sup>	Purification factor <sup>1</sup>	Recovery yield (%) <sup>1</sup>
<b>TLL 3 for PEG 2000-IDA-Cu(II)-KPB</b>	<b>12.0</b>	<b>24.5</b>	<b>2.3</b>	<b>Top</b>	<b>82.8 ± 1.6</b>	<b>2.7</b>	<b>86.9 ± 1.3</b>
				Inter	15.4 ± 0.4	0.6	10.7 ± 0.3
				Bottom	3.1 ± 0.2	0.4	2.5 ± 0.1
	14.5	16.0	1.0	Top	81.2 ± 0.8	2.6	82.9 ± 0.9
				Inter	15.7 ± 0.1	0.5	13.5 ± 0.5
				Bottom	5.0 ± 0.1	0.2	4.4 ± 0.3
	21.5	12.0	0.4	Top	49.9 ± 2.3	1.4	47.1 ± 1.2
				Inter	37.7 ± 0.5	0.8	40.9 ± 0.2
				Bottom	11.2 ± 0.2	0.4	10.6 ± 0.4

<sup>1</sup>Each data is mean ± standard deviation of triplicate determinations.

The bold values represented the chosen parameter.

The highest recovery yield, purity and purification factor of his-tagged HBcAg were achieved using TLL 3 in PEG 2000-IDA-Cu(II)-KPB system with a phase volume ratio of 7:3. A total of 86.9% of his-tagged HBcAg was recovered with a purity of 82.8% and a purification factor of 2.6. In contrast, it was observed that the purity, purification factor and recovery yield of his-tagged HBcAg in 0.4 phase volume ratio were extremely low compared to those obtained with phase volume ratios of 1.0 and 2.3. This was due to the presence of high amount of contaminant protein that were partitioned along with his-tagged HBcAg to the top phase. Therefore, PEG 2000-IDA-Cu(II)-KPB system with TLL 3 composition and a phase volume ratio of 2.3 was selected for the optimization of NaCl addition.

#### **4.5.4 Additional of NaCl**

Sodium chloride is frequently used as neutral salt in ATPS to improve the partitioning of target protein between the phases. Therefore, in this study, the effect of NaCl addition was investigated. Different concentrations of NaCl were added (25, 50, 100, and 200 mM) into PEG2000-IDA-Cu(II)-KPB with TLL 3 system, 5 % (w/v) biomass concentration and a phase volume ratio of 2.3. Based on the results, the recovery yield of his-tagged HBcAg was inversely proportional with NaCl concentrations.

Based on Table 4.11, the purity, purification factor and recovery yield decreased with the increase in NaCl concentration in the system. The system with addition of 200 mM NaCl, which yielded 60.8% purity, 2.0 purification

factor and 41.5% of recovery yields were the lowest compared to the other systems with lower NaCl concentrations. Furthermore, this system also partitioned the highest amount of his-tagged HBcAg into the interphase and bottom phase, with recovery yields of 27.3% and 25.1%, respectively.

**Table 4.11: Effects of addition of different concentrations of NaCl on the partitioning of his-tagged HBcAg using 24.5%(w/w) PEG 2000-IDA-Cu(II) and 12%(w/w) KPB system.**

Concentration of NaCl (mM)	Phase	Phase volume ratio (Top/bottom)	Purity (%) <sup>1</sup>	Purification factor <sup>1</sup>	Recovery yield (%) <sup>1</sup>
<b>0</b>	<b>Top</b>	<b>2.3</b>	<b>82.8 ± 1.6</b>	<b>2.7</b>	<b>86.9 ± 2.3</b>
	Inter		15.4 ± 0.4	0.5	10.7 ± 0.3
	Bottom		3.1 ± 0.2	0.1	2.5 ± 0.1
25	Top	2.0	76.1 ± 0.1	2.4	71.6 ± 3.2
	Inter		12.0 ± 0.4	0.6	15.2 ± 0.5
	Bottom		8.5 ± 0.2	0.7	7.1 ± 0.3
50	Top	1.9	71.0 ± 0.6	1.8	68.4 ± 2.4
	Inter		14.7 ± 0.7	0.9	15.8 ± 0.6
	Bottom		8.1 ± 0.4	0.7	8.4 ± 0.3
100	Top	1.6	63.4 ± 0.4	1.5	66.1 ± 3.0
	Inter		18.9 ± 1.0	0.7	17.1 ± 0.8
	Bottom		11.0 ± 0.5	0.6	10.9 ± 0.5
200	Top	1.4	60.8 ± 0.3	2.0	41.5 ± 2.1
	Inter		19.9 ± 1.3	1.0	27.3 ± 1.3
	Bottom		19.0 ± 0.6	0.7	25.1 ± 1.1

<sup>1</sup>Each data is mean ± standard deviation of triplicate determinations.

The bold values represented the chosen parameter.

Addition of NaCl into the system did not only cause the partitioning of his-tagged HBcAg from the top phase to the other phases, but it also altered the phase volume ratio. The phase volume ratio declined with increase in NaCl concentration. Therefore, this further explained the low recovery yield of his-tagged HBcAg detected in the top phase with NaCl concentrations ranging from 25 to 200 mM. As a result, PEG 2000-IDA-Cu(II)-KPB system with TLL 3 and phase volume ratio of 2.3 without addition of NaCl was selected for further optimizations.

#### **4.5.5 System pH**

The effect of pH on the partitioning of his-tagged HBcAg was investigated in this study. A series of system pH (6, 7, and 8) with 5 % (w/v) biomass concentration and TLL 3 has been employed to determine the best system pH for the recovery of his-tagged HBcAg. The results shown in Table 4.12 demonstrate that the purity, purification factor and recovery yield of his-tagged HBcAg increased as the system pH increased from pH 6 to 8. The optimum recovery of his-tagged HBcAg of 91.3% with a purity of 93.6% and a purification factor of 3 was achieved at pH 8. Apart from that, there was no biphasic formation when system pH 5 was employed in this study, thus, pH 5 was not suitable to be used in ATPS, hence no data was tabulated in Table 4.12. In addition, a decrease in phase volume ratio was also observed with increase in system pH from pH 6 to 8. Although the phase volume ratio for pH 7 and pH 8 were almost similar, the purity and yield recovered at pH 8 were higher compared to pH 7. Therefore, it was selected for the subsequent optimization.

**Table 4.12: Effect of system pH on the partitioning of his-tagged HBcAg using 24.5%(w/w) PEG 2000-IDA-Cu(II) and 12%(w/w) KPB system.**

System pH	Phase	Phase volume ratio (Top/bottom)	Purity (%) <sup>1</sup>	Purification factor	Recovery yield (%) <sup>1</sup>
6	Top	10.5	71.4 ± 0.3	2.3	60.8 ± 2.8
	Inter		20.5 ± 1.0	0.7	25.3 ± 1.7
	Bottom		6.7 ± 0.4	0.2	7.5 ± 0.4
7	Top	2.3	82.8 ± 1.6	2.7	86.9 ± 2.3
	Inter		15.4 ± 0.4	0.5	10.7 ± 0.3
	Bottom		3.1 ± 0.2	0.1	2.5 ± 0.1
8	Top	<b>2.2</b>	<b>93.6 ± 3.7</b>	<b>3.0</b>	<b>91.3 ± 2.9</b>
	Inter		6.3 ± 0.2	0.2	5.9 ± 0.6
	Bottom		0.6 ± 0.1	0.0	1.1 ± 0.1

<sup>1</sup>Each data is mean ± standard deviation of triplicate determinations.

The bold values represented the chosen parameter.

#### 4.5.6 Biomass concentration

Different biomass concentrations (3, 4, 5, 6 and 7% (w/v)) were used to study the effects of biomass concentration % (w/v) on the recovery of his-tagged HBcAg recovery by using ATPS in this study. Previously, all optimizations were carried out with a final biomass concentration of 5%(w/v). Based on Table 4.13, the optimum biomass concentration for his-tagged HBcAg partitioning was achieved in the system loaded with unclarified feedstock containing 5%(w/v) biomass concentration. This system recovered 93.6% in purity of his-tagged HBcAg with 91.3% recovery yield and a purification factor of 3.0.

**Table 4.13: Effect of biomass concentrations on the partitioning of his-tagged HBcAg using 24.5% (w/w) PEG 2000-IDA-Cu(II) and 12% (w/w) KPB system.**

Final biomass concentration % (w/v)	Phase	Purity (%) <sup>1</sup>	Purification factor <sup>1</sup>	Recovery yield (%) <sup>1</sup>	Phase volume ratio
3	Top	87.3 ± 3.2	2.8	84.2 ± 3.1	2.4
	Inter	7.3 ± 0.4	0.2	10.9 ± 1.0	
	Bottom	6.3 ± 0.2	0.2	4.1 ± 0.4	
4	Top	86.7 ± 4.3	2.8	87.1 ± 2.5	2.2
	Inter	6.8 ± 0.6	0.2	7.9 ± 0.2	
	Bottom	6.9 ± 0.3	0.2	5.7 ± 0.3	
<b>5</b>	<b>Top</b>	<b>93.6 ± 3.7</b>	<b>3.0</b>	<b>91.3 ± 2.9</b>	<b>2.2</b>
	Inter	6.3 ± 0.2	0.2	5.9 ± 0.6	
	Bottom	0.6 ± 0.1	0.0	1.1 ± 0.1	
6	Top	84.6 ± 4.1	2.7	81.8 ± 2.6	2.0
	Inter	10.3 ± 0.9	0.3	10.9 ± 1.2	
	Bottom	4.6 ± 0.2	0.2	3.1 ± 0.5	
7	Top	76.3 ± 2.4	2.5	71.7 ± 3.6	1.6
	Inter	15.3 ± 1.1	0.5	19.4 ± 1.7	
	Bottom	7.0 ± 0.2	0.2	7.3 ± 0.9	

<sup>1</sup>Each data is mean ± standard deviation of triplicate determinations.

The bold values represented the chosen parameter.

Table 4.13 demonstrates that the purity, recovery yield and purification factor of his-tagged HBcAg increased as the biomass concentration was increased from 1 to 5% (w/v). As the biomass concentration increased to 6 from 5% (w/v), the purity, recovery yields and purification factor for his-tagged HBcAg started to decline. Biomass concentration of 7% (w/v) produced the

lowest purity, recovery yield and purification factor with the values of 76.3%, 71.7% and 2.5, respectively. These values were generally about 1.2 times lower than those obtained using the optimal condition (5%(w/v) biomass concentration). Phase volume ratio was also observed to be inversely proportional with the biomass concentration as tabulated in Table 4.13. The highest phase volume ratio was obtained when 3% biomass concentration was used. However, the ratio decreased to as low as 1.6 when 7% biomass concentration was used, with a total phase volume ratio reduction of 33.33%.

#### **4.5.7 Optimized conditions for ATPS**

The optimum recovery of his-tagged HBcAg with the highest purity, purification factor and recovery yield were obtained using ATPS composed of PEG 2000-IDA-Cu(II)-KPB system, TLL 3 with a volume ratio of 7:3, system pH8.0, without NaCl addition and loaded with 5% (w/v) unclarified feedstock. The conditions before the optimization was In a 5g ATPS system in this study, low MW polymer acquired higher performance in his-tagged HBcAg recovery as compared to high MW polymer. This is because the amount of modified PEG 2000 in a 5g ATPS is the highest, followed by PEG 4000 and PEG 6000. Therefore, it contained higher amount of modified PEG available to interact with his-tagged HBcAg in the top phase, which resulted in higher recovery yield in the system with low MW polymer. It was observed that the purity of his-tagged HBcAg in PEG-rich top phase (lane 2 and lane 5) has significantly increased after optimizations as well as improved in the recovery yield with most of the his-tagged HBcAg partitioned to PEG-rich top phase while the

contaminant proteins to the intermediate and bottom phase (lane 4 and lane 7) (Figure 4.17).

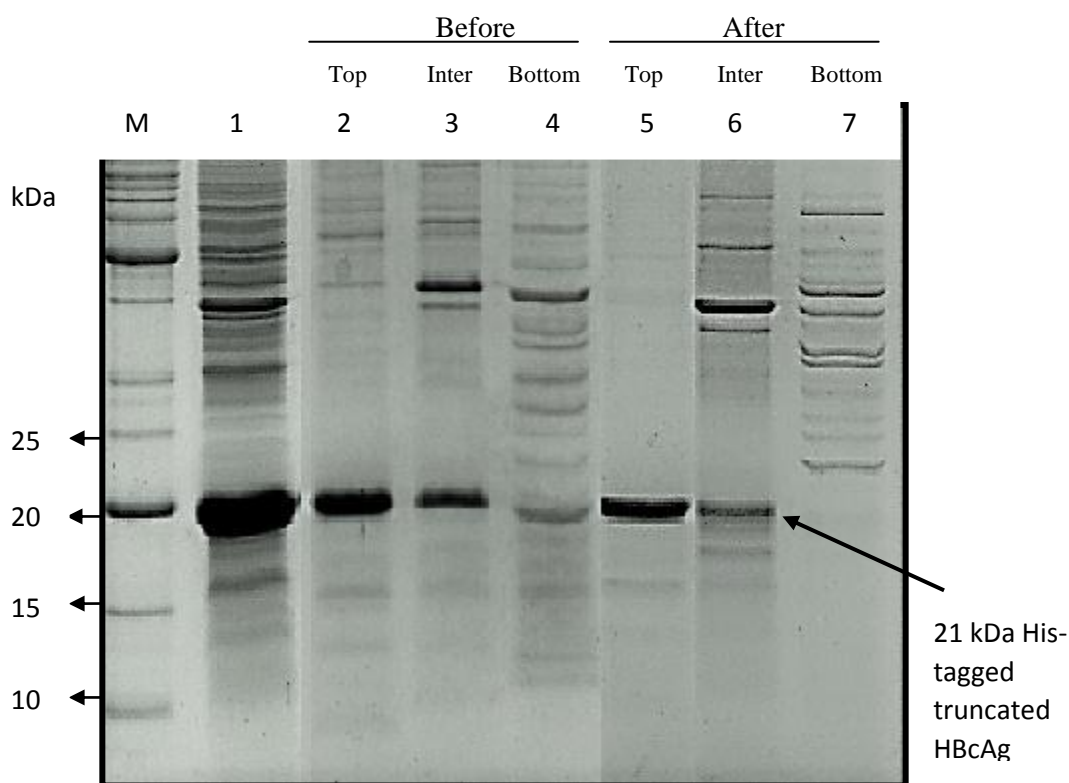


**Figure 4.17: SDS-PAGE gel of HBcAg recovered before and after optimizations on system parameters using PEG 2000-IDA-Cu(II)-KPB system.** Lane M is the molecular mass marker in kDa (BenchMark, Invitrogen), lane 1 is the unclarified feedstock, lane 2, 3 and 4 are the top, inter and bottom phase, respectively of PEG-2000-IDA-Cu(II)-KPB system before optimizations on system parameters, lane 5, 6 and 7 are top, inter and bottom phase, respectively of PEG-2000-IDA-Cu(II)-KPB system after optimizations on system parameters. The arrow shows the position of 21 kDa his-tagged truncated HBcAg.

These sucrose gradient ultracentrifugation and ATPS purified his-tagged HBcAg were compared in terms of number of unit operation, purity, recovery yield and purification factor (Table 4.14). The his-tagged HBcAg purified using sucrose gradient ultracentrifugation yielded slightly higher purity than the one

purified using ATPS. The purity and purification factor obtained from sucrose gradient ultracentrifugation purification were 96% and 3.2, respectively. On the other hand, the purity and purification factor of his-tagged HBcAg obtained using ATPS were 94% and 3.0, respectively. However, recovery yield of his-tagged HBcAg purified using sucrose gradient ultracentrifugation was 78.7% lower compared to ATPS method. The yield obtained from sucrose gradient ultracentrifugation was 12.6%, whereas the yield obtained from ATPS was 91.3%. Furthermore, sucrose gradient ultracentrifugation involves more operation steps compared to ATPS method as shown in Table 4.14.

**Table 4.14: Comparison between ATPS and sucrose gradient ultracentrifugation.**

Sucrose-gradient ultracentrifugation			
Unit operation	Recovery yield of his-tagged HBcAg (%) <sup>1</sup>	Purity of his-tagged HBcAg (%) <sup>1</sup>	Purification factor of his-tagged HBcAg
Unclarified homogenate	100 ± 0	30.5 ± 1.4	1.0
Centrifugation	41.1 ± 0.5	35.3 ± 0.4	1.2
Ammonium sulphate precipitation	25.3 ± 1.2	36.7 ± 0.4	1.2
Dialysis	23.6 ± 1.4	36.4 ± 0.8	1.2
Sucrose-gradient ultracentrifugation and dialysis	15.9 ± 0.7	94.5 ± 0.6	3.1
Concentration	12.6 ± 0.3	96.2 ± 1.3	3.2
ATPS			
Unclarified homogenate	100 ± 0	30.5 ± 1.4	1.0
ATPS & dialysis	91.3 ± 2.9	93.6 ± 3.7	3.0

<sup>1</sup>Each data is mean ± standard deviation of triplicate determinations.

#### 4.6 Antigenicity of purified his-tagged HBcAg

The antigenicity of the recovered his-tagged HBcAg using ATPS was determined using enzyme-linked immunosorbent assay (ELISA). Results were compared between the his-tagged recovered using ATPS and sucrose-gradient ultracentrifugation, whereby the latter was used as positive control in this study. Figure 4.18 shows that the antigenicity exhibited by ATPS-purified his-tagged HBcAg was comparable to the purified his-tagged HBcAg using sucrose-gradient ultracentrifugation. Therefore, ATPS did not affect the antigenicity of the purified his-tagged HBcAg.

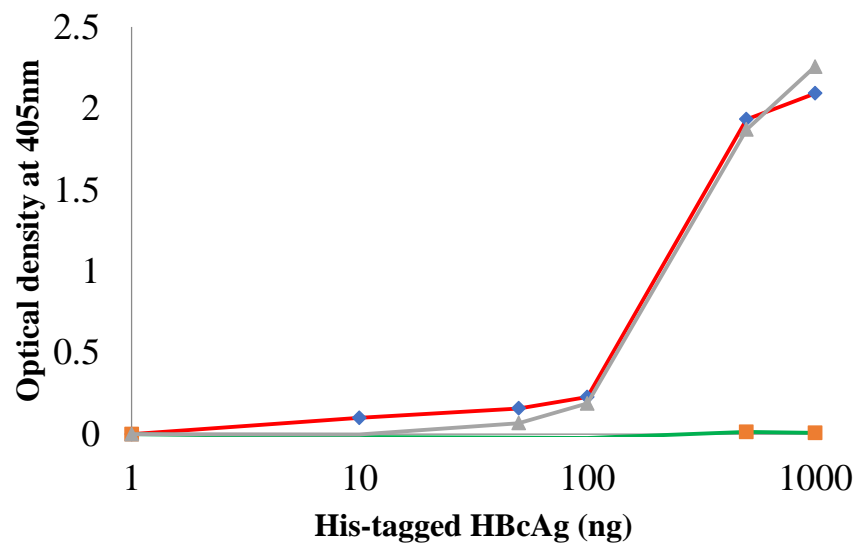


**Figure 4.18: Antigenicity determination of ATPS and sucrose gradient ultracentrifugepurified his-tagged HBcAg via ELISA.** The purified his-tagged HBcAg from ATPS (◆); positive control as purified his-tagged HBcAg from sucrose-gradient ultracentrifugation (▲); and PEG as negative control (■). All data denotes the mean  $\pm$  S.D. for triplicate determinants.

#### **4.7 Transmission Electron Microscope (TEM) on purified his-tagged HBcAg**

The ATPS and sucrose gradients ultracentrifugation purified his-tagged HBcAg were examined using TEM for capsid size and morphology as shown in Figures 4.19 and 4.20. Based on the micrographs, the ATPS and sucrose gradients purified his-tagged HBcAg were able to self-assemble into icosahedral capsids with average size of 30 nm in diameter.

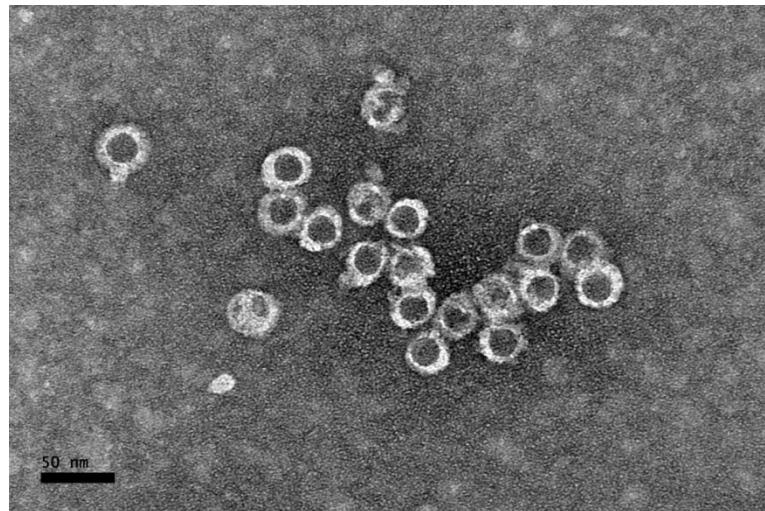


**Figure 4.19: Transmission electron micrograph of ATPSpurified his-tagged HBcAg particles.**

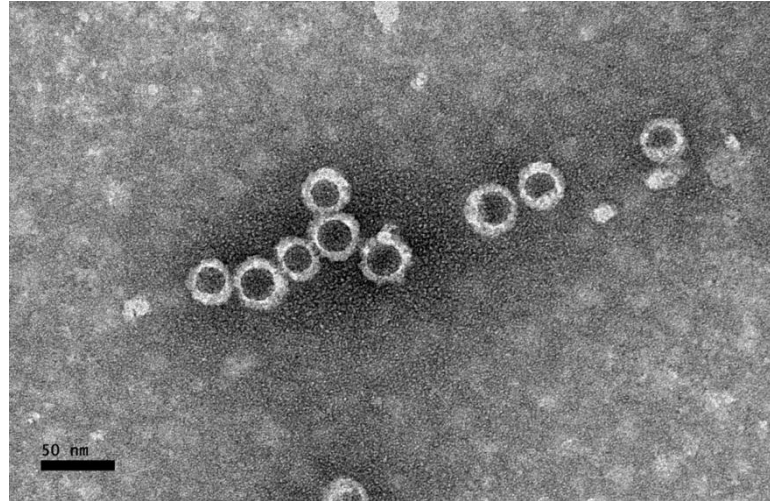


**Figure 4.20: Transmission electron micrograph of sucrose gradient ultracentrifuge purified his-tagged HBcAg particles.**

## CHAPTER 5

### DISCUSSION

#### **5.1 Preparation of PEG-epoxide, PEG-IDA, PEG-IDA-metal ions and the partitioning of metal affinity ligands in ATPS**

In the production of PEG-IDA-metal, first of all PEG was dissolved in toluene. Then, boron trifluoride ethyletherate and epichlorohydrin were added drop-wise to the reaction mixture and incubated at room temperature. Next, NaOH solution was slowly added and the mixture was stirred at room temperature. The reaction mixture was then decanted, and washed with diethyl ether. As a result, PEG-epoxide was obtained. Amount of oxirane rings was quantified by a method described by Sundberg and Porath, (1974), which involves a reaction between the oxirane ring and sodium thiosulphate and the pH was kept constant by addition of 0.1 M hydrochloric acid (HCl) until the pH of the mixture reached pH 7. The amount of oxirane present in the solution was then calculated from the volume recorded for HCl needed in order to achieve pH 7. One ml of HCL added equivalence to 10 $\mu$ mol of oxirane ring in the product. PEG-IDA-metal ion formed after PEG-epoxide was reacted with IDA and metal ion. Metal ions in the product were detected by using AAS.

It is commonly known that most of the proteins favour the salt rich bottom phase in ATPS. Therefore, metal partitioning can act as an efficient

method to selectively increase the partitioning of metal binding protein into PEG rich top phase in a PEG-salt ATPS (Lin, et al., 2000). Therefore, the affinity of copper ions (transition metal ions) was used to selectively partition the histidine amino acid residues that are accessible on the surface of his-tagged HBcAg into the top phase in this study. One of the earliest applications of metal affinity partitioning in ATPS was reported for heme protein extraction, which contained different numbers of histidine residues side chains by using PEG-IDA-Cu(II) (Wuenshell, et al., 1990). On the other hand, Birkenmeier, et al. (1991) also investigated the affinities of several transition metal ions for  $\alpha_2$ -macroglobulin, tissues plasminogen activator, superoxide dismutase and monoclonal antibodies purification using PEG-IDA-metal ions in ATPS. Therefore, before a metal affinity partitioning study can be carried out in ATPS, the main component, PEG-IDA-metal ion need to be synthesized.

Epichlorohydrin activation (Lin, et al., 2000) was used in the production of PEG-epoxide in this study and subsequently chelated with IDA and metal ion to obtain PEG-IDA-metal ions. Besides, there is another common method that can be used to produce PEG-IDA (Birkenmeier, et al., 1991; Laboureau, et al., 1996) where PEG-IDA was synthesized from monomethoxy-PEG (M-PEG). Three synthesis steps are required for the preparation of PEG-IDA using this method. Briefly, monomethoxy-PEG (M-PEG) is reacted with thionyl chloride to produce chloroacetylated methoxypoly(ethylene glycol) (Cl-M-PEG) under anhydrous hydrogen environment. Secondly, aminomethoxy-PEG (amino-M-PEG) is produced after Cl-M-PEG is treated with ammonia solution. Subsequently, amino-M-PEG is

reacted with bromoacetic acid under basic environment for PEG-IDA production. It is clearly shown that these synthesis pathways are complicated and tedious, and furthermore M-PEG must be used.

On the other hand, PEG-IDA can be prepared using a relatively simple route directly from PEG. Epichlorohydrin activation method utilizes PEG instead of M-PEG and it is activated with known concentration of epichlorohydrin, BFEE, NaOH to obtain PEG-epoxide (monosubstituted derivative), which subsequently coupled with IDA to obtain PEG-IDA. Synthesis route of epichlorohydrin activation method has been previously described (Dongqiang, et al., 2000). However, several parameters for each step involved need to be optimized for the optimal production of PEG-IDA.

The optimization processes for the synthesis of modified PEG is necessary for large scale production of PEG-IDA-Cu(II), which was required for the construction of binodal curves and phase diagrams as well as for method scouting for his-tagged HBcAg recovery in ATPS. However, very limited studies have been carried out on the optimization for modified PEG synthesis. Most of the studies just reported a direct synthesis of PEG-IDA-metal based on the method described by Pesliakas et al. (1994). Therefore, this study undertook a step by step optimization to synthesize and produce the desired modified PEG.

First of all, optimization of the activation duration is important prior to other parameters due to the consideration of the overall processing time in this study. An optimal activation time is necessary to improve the overall production time and yields. Speed of activation is influenced by two main factors such as the polymer length and concentration (Silberberg, 2013). When the molecular weight of the PEG increases, the length of the polymer chain will increase as well. This causes the extension of polymers interactions with neighbouring chains, which requires longer time to interact, and therefore, activation activity will decrease (Silberberg, 2013). This explains why the optimal activation duration increased when the molecular weight of PEG used in this study increased as shown in Table 4, whereby the optimal activation for PEG 2000, PEG 4000 and PEG 6000 were 2h, 2h and 3h, respectively. In a study by Dongqiang et al. (2000), the activation duration optimization was done on PEG 2000 in a range from 1 to 5h, whereby the optimal activation duration was 5h. There are a total of 3h differences between the result obtained in this study and Dongqiang et al. (2000). It was due to the difference in initial concentration of BFEE used in the activation, whereby 1.0% was used in this study, whereas only 0.5% was used by Dongqiang et al. (2000). As a result, the epichlorohydrin activation was faster in this study. However, there are no optimization reported on PEG 4000 and PEG 6000 activation thus far.

Effect of BFEE concentration on the production of PEG-epoxide is as shown in Table 4.2. BFEE is a crucial component and it acts as Lewis acid catalyst to open the epichlorohydrin ring and provides the acidic medium to

allow nucleophiles to attack the electrophilic C of the C-O bond of epichlorohydrin (Carey, 2000). The concentration of oxirane ring detected in PEG-epoxide increased with the increased in BFEE concentration in this study. However, the oxirane ring concentration started to decline after the optimal concentration was achieved. The reason behind this was because of extreme acidic condition cause by high concentration of BFEE in the reaction mixture. Moreover, it could also be due to the alkaline effect on the recycling process for the second sub-step reaction (Dongqiang, 2000). As a consequence, BFEE could not function optimally as a catalyst, thus disrupted the opening of the epichlorohydrin ring.

Epichlorohydrin concentration also plays an important role in the production of PEG-epoxide. Epichlorohydrin is an irritant and carcinogenic chlorinated epoxy compound that can react with a large range of nucleophiles. It has high reactivity against the nucleophiles, which is usually used as industrial solvent in the production of glycerol, plastic, epoxy glues and resins (Carey, 2003). Epichlorohydrin ring is opened in an acidic environment provided by BFEE to activate PEG in order to form PEG-epoxide. PEG-epoxide is chelated on IDA to produce PEG-IDA and further reaction in saturated metal ion to yield the final product PEG-IDA-metal. Therefore, the higher the epichlorohydrin concentration in the reaction mixture, the higher the production of PEG-epoxide as observed in this study. Similarly, there are no optimizations of epichlorohydrin reported by Dongqiang, et al. (2000) or by other researcher, thus far.

Epichlorohydrin has also been used as functional activating agent for the construction of polysiloxane-polyvinyl alcohol (POS-PVA) composite for immobilized lipase purification (Santos, et al., 2008). Epichlorohydrin has been shown to produce immobilized derivatives with higher stability and activity compared to other activation agent such as the glutaraldehyde, which usually has lower productivity, lower yield, and loss of native activity (Santos, et al., 2008). Epichlorohydrin seems to overcome those drawbacks and perform well in maintaining the immobilized protein activity, whereby glutaraldehyde caused hydrolytic activity of the enzyme decreased about 50% (Santos, et al., 2008). Single hydroxyl group is needed for epichlorohydrin to react while glutaraldehyde required two hydroxyl groups, therefore epichlorohydrin has more available active sites for protein partitioning in immobilization purification compared to glutaraldehyde. Therefore, epichlorohydrin was used in this study as the activation agent for the production of immobilized ligands. The immobilization yield is directly proportional to the reactivity of epoxy group of epichlorohydrin (Santos, et al., 2008).

On the other hand, NaOH is crucial in opening the ring of epichlorohydrin by attacking the electrophilic C of the C-O bond (Hoffman, 2005). The concentration of oxirane ring detected in the activated products increased gradually with the increase of NaOH concentration as shown in Table 4.4. In general, the optimal conditions for PEG-epoxide production involving three types of PEG (PEG 2000, PEG 4000 and PEG 6000) are listed

in Tables 4.1 to 4.4. The production of PEG 2000-IDA-metal also has been done in a research by Dongqiang, et al. (2000), where the optimization conditions recorded was similar with the finding in this study for PEG 2000. Other than PEG 2000, optimization on PEG 4000 and PEG 6000 were also included in this study.

PEG-epoxide produced in this study was then chelated to IDA to form PEG-IDA. The reaction between PEG-epoxide and IDA was efficient and easy because IDA consists of a nitrogen atom and two short chain carboxylic groups, which make it a great chelating agent for PEG and transition metal ions (Figure 4.1) (He, et al., 2014; Tishchenko, et al., 2002). Therefore, IDA concentration was observed to be directly proportional to the total metal ions concentration detected in the products. Structurally, PEG-IDA with tridentate form occupies a maximum of three coordination sites in the metal coordination sphere, leaving three coordination sites free for interaction with water or biomolecules such as hexacoordinate central metal ions (Birkenmeir, et al. 1991; Gaberc-Porekar and Menart, 2001). Therefore, IDA is suitable to be used for affinity partitioning and act as a linker between polymers and metal ions.

The free alcohol groups on the surface of PEG are to link chelating groups of IDA and the binding of metal ions. IDA is a tridentate chelator, which is widely used as the chelating agent compare to the tetradentate ligands such as NTA and carboxymethylated aspartic acid (CM-Asp). It is reported that tetradentate chelator have higher affinities for transition metal ions but

unfortunately they exhibit a low binding ability with protein with only two available coordination sites for protein (Gaberc-Porekar and Menart, 2001).

However, a slightly more detailed optimization for the synthesis of modified PEG, which involved PEG 2000 has been reported (Dongqiang, et al., 2000). Different metal ions such as the copper ion, nickel ion, zinc ion and cadmium ion have been investigated in a previous study to determine which metal ion could bind the highest to the PEG-IDA (Peliakas, et al., 1994). Two types of transition metal ions (copper ions and nickel ions) were investigated in the present study. Based on Figure 4.2, it is shown that higher concentrations of copper ions were bound to the modified PEG compared to nickel ions. Similar findings were also reported by Gaberc-Porekar and Menart, (2001), whereby nickel ion was known to bind less strongly than copper ions by iminodiacetate chelator. Due to the higher binding of copper ions onto the PEG-IDA compared to nickel ions, PEG-IDA-Cu(II) was selected for phase diagram construction with different types of phase forming salts.

On the other hand, purification of the protein is basically based on the coordination of the immobilized metal ion such as Cu(II), Ni(II), Zn(II), Co(II) and Fe(III) with the electron donor groups from the protein surface (Gaberc-Porekar and Menart, 2001). Strong binding between metal-chelated PEG and protein can be achieved by multiple active sites attachment of native or engineered surface histidine tag, which are inserted onto the N or C-terminus of a protein. The coordination of the metal ion can be bidentate or tridentate

depending on their occupied coordination bond, whereby this remaining sites are normally occupied by water and it can then be used to exchange with suitable electron donor (Gaberc-Porekar and Menart, 2001). In the case for IDA chelator, the order for binding are usually in the following order: Cu(II) > Ni(II) > Zn(II) > Co(III) and the affinity of the protein for metal ions are strongly depending on the metal ion involve (Gaberc-Porekar and Menart, 2001). Furthermore, a study also shown that Cu(II) ion provide more robust binding to the poly-histidine tag compared to Ni(II) ion, whereby Cu(II) ion shown to have specific absorption onto 6xHis tagged protein (Predki, 2007). In contrast, the surface of the modified PEG-Cu(II) shown to resist the nonspecific binding of other protein molecules (Predki, 2007). Therefore, in this study, IDA chelator was used to chelate onto the Cu(II) and Ni(II) as these chelator and metal ions have been shown to acquire higher affinities to retain the protein of interests (Gaberc-Porekar and Menart, 2001).

## **5.2 Binodal curve**

Binodal curve is needed to predict the two phase regions that can be utilized in ATPS for extraction and partitioning of biomolecules. This study had constructed a total of nine binodal curves for modified PEG 2000-IDA-Cu(II), PEG 4000-IDA-Cu(II) and PEG 6000-IDA-Cu(II) against three types of organic salts (ammonium sulphate, Na<sub>2</sub>SO<sub>4</sub> and KPB). Construction of phase diagram provides clear information such as the concentration of polymer and salt required for biphasic formation, concentration of polymer and salt in top

and bottom phases and the ratio difference between phases (Hatti-Kaul, 2000). These criteria are important in selecting a suitable system for protein partitioning. The area above the binodal curve known as biphasic region is responsible for two phase formation in ATPS. The area below the binodal curve is known as monophasic region, which represents the system forms a single phase in ATPS. The effects of two factors such as polymer MW and salt types, which affect the positioning of binodal curve in this study were compared.

### **5.2.1 Effects of different types of salts on binodal curves**

A total of three binodal curves were compared to identify the differences and effects of different salts on the positioning of binodal curves. The binodal curves for PEG 2000-IDA-Cu(II), PEG 4000-IDA-Cu(II) and PEG 6000-IDA-Cu(II) against three organic salts are shown in Figures 4.3 to 4.5. All the results showed a similar trend, where the sodium sulphate system occupied the nearest position to the origin followed by ammonium sulphate and the farthest from origin was KPB system. The Na<sub>2</sub>SO<sub>4</sub> system showed the largest heterogenous region among all the salts systems. Heterogenous region is represented by the size of the biphasic region for a particular binodal curve and this indicated the ability of the polymer and salt to form two phases in ATPS (Lladosa, et al., 2012). The larger the heterogenous region, the stronger the salting out power, hence lower concentration of polymers and salts are needed to obtain a biphasic phases (Silverio et al., 2013). Therefore, based on the results, it was shown that the Na<sub>2</sub>SO<sub>4</sub>binodal curve, which was nearest to

the origin acquired a stronger salting out power. In contrast, KPB binodal curve acquired the lowest salting out power among all the salts tested. The differences of salting out and hydrating power of salts during formation of biphasic systems can be further explained based on the Hofmeister series and the Hofmeister effect.

The Hofmeister series is a widely used homologous series to rank ion specific effect on biomolecular properties such as protein stability and aggregation propensity (Senske, et al., 2016). First of all, the Hofmeister series described that ions can be classified as kosmotropes (highly hydrated) and chaotropes (weakly hydrated), where kosmotropes is a structure maker according to their abilities to induce the structuring of water or a water attractor (Oechsle, et al., 2015). On the other hand, chaotropes are known as structure breaker, where the small ions will break the hydrogen bonding with their relatively high charge densities, which disturb the ordering of water molecules by their electrostatic nature (Zangi, 2010). In ATPS, a constant competition always occurs among salt and polymer, therefore, strong kosmotropic ions will increase the water molecules structuring by prevailing in the competition. This eventually resulted in salting out of polymer away from salt, which then lead to phase separation (Zangi, 2010).

These are the listed orders in the Hofmeister series,  $F^- > PO_4^{3-} > SO_4^{2-} > CH_3COO^- > Cl^- > Br^- > I^- > SCN^-$  for anions and  $(CH_3)_4N^+ > (CH_3)_2NH_2^+ > NH_4^+ > K^+ > Na^+ > Cs^+ > Li^+ > Mg^{2+} > Ca^{2+} > Ba^{2+}$  for cations (Patel, et al., 2014). The orders

showed that the hydration strength increases from  $F^-$  to  $SCN^-$  for anions but decreases from  $(CH_3)_4N^+$  to  $Ba^+$  for cations. In this study, only two anions ( $SO_4^{2-}$  and  $PO_4H^{2-}$ ) and three cations ( $NH_4^+$ ,  $K^+$  and  $Na^+$ ) were compared and discussed further because the three salts used for binodal curves construction in this study were  $(NH_4)_2SO_4$ ,  $Na_2SO_4$  and KPB.

As mentioned above, binodal curves for  $Na_2SO_4$  was located nearest to the origin with the largest heterogenous region (highest hydration power) followed by  $(NH_4)_2SO_4$  and KPB binodal curves. First of all, based on the Hofmeister series, the order for cations are  $NH_4^+ > K^+ > Na^+$ .  $NH_4^+$  has the strongest hydration power, followed by  $K^+$  and lastly the  $Na^+$ . However, the results obtained in this study were not similar to the Hofmeister series. This phenomenon can be explained due to the more dominant effect of anions over the cations in the Hofmeister effect (Kumar and Venkatesu, 2014; Patel, et al., 2014).

In the Hofmeister series, the orders for anions are  $PO_4^{3-} > SO_4^{2-}$ , thus,  $SO_4^{2-}$  is more kosmotropic (stronger hydration strength) compared to  $PO_4^{3-}$ . Therefore, these two anions ( $PO_4^{3-}$  and  $SO_4^{2-}$ ) involved were the main reason in explaining the contradicting finding as to why the  $Na_2SO_4$  system was more powerful than KPB system in term of salting out and hydration power. Although theoretically  $(NH_4)_2SO_4$  has higher kosmotropicity than  $Na_2SO_4$ , this study showed that the strength of hydration power was higher for  $Na_2SO_4$  system. This can be explained by Gibbs free energy of hydration ( $\Delta G_{hyd}$ )

regarding the overall phase separation ability of kosmotropic ions (Tou, et al., 2014).

Studies by Li et al. (2002) and Bulgariu and Bulgariu, (2008) showed that kosmotropicity of a salt is directly proportional to the value of  $\Delta G_{\text{hyd}}$ , where the smaller the values of  $\Delta G_{\text{hyd}}$ , the higher the kosmotropicity of the ion. Therefore, by comparing the cation  $\Delta G_{\text{hyd}}$  where -365 kJ/mol for  $\text{Na}^+$ , -304 kJ/mol for  $\text{K}^+$  and -284 kJ/mol for  $\text{NH}_4^+$  (Bulgariu and Bulgariu, 2008; Ferreira and Teixeira, 2011),  $\text{Na}_2\text{SO}_4$  has the highest salting out power with the lowest  $\Delta G_{\text{hyd}}$  value. Therefore, this particular salt system is favoured in ATPS construction as it requires the least concentration of salt for ATPS formation.

### **5.2.2 Effect of polymer MW on binodal curves**

In the current study, PEG 2000-IDA-Cu(II), PEG 4000-IDA-Cu(II) and PEG 6000-IDA-Cu(II) were used to plot the binodal curves against  $\text{Na}_2\text{SO}_4$  as shown in Figure 4.6. Then, the effect of polymer MW on the strength of hydration and salting out were compared according to the heterogenous region and their distance from origin as shown by each binodal curve. PEG 6000-IDA-Cu(II) binodal curve was the nearest curve to the origin with the highest heterogenous region followed by PEG 4000-IDA-Cu(II) and PEG 2000-IDA-Cu(II) binodal curves. Polymer MW is the main factor for these outcomes as it involves polymer solubility and the exclusion effect.

Vijayaragavan, et al. (2014) reported that the polymer MW, which was inversely proportional to the distance of their binodal curve to the origin, indicated higher salting out power for higher MW polymer. Polymer with higher MW acquires higher chain length, therefore, higher hydrophobicity due to lesser free volume that is available for water attraction. When longer polymer chain length is applied in ATPS, it leads to decrease in solubility of water in the top phase, hence, causes the polymer salting out effect and move the binodal curve closer to origin (Saravanan, et al., 2007; Silverio, et al., 2012). Consequently, lower concentration of phase forming component is required for ATPS formation as the MW of polymer increase.

### **5.3 Tie-line, TLL and STL**

The standard curves for salt conductivity and polymer refractive index (Figures 4.7 to 4.15) play an important role in constructing the tie lines on phase diagram. Tie-lines plotted on phase diagram were labelled as TL 1 to TL 3, which indicated their distance from the origin as shown in Figure 4.16. TLL values increased when the tie line is located farther away from the origin. Therefore, higher concentration of phase forming components will be needed for ATPS formation. It is important to determine the minimal concentration of phase forming component to develop an ATPS in order to reduce the cost either for research or industry purpose. Thus, this explained why the system located nearest to the origin will always be the optimal choice for ATPS construction. However, the phase separation rate is faster when TLL is increased (Brooks et al., 1985). Phase separation is affected by the physical

properties of ATPS such as density, viscosities and interfacial tension. Longer TLL provides high viscosities and density differences between salt and polymer, thus the separation rate is faster as compared to system with shorter TLL (Kumar et al., 2007). Therefore, it is suggested that an intermediate TLL with optimum phase separation rate should be selected for partitioning based on the phase diagram (Kumar et al., 2007).

STL value indicates the slope of the tie line plotted. These gradients demonstrate the difference between polymer and salt concentration within the same phase (Tubio et al., 2009). The TLL was inversely proportional to STL and STL value was directly proportional to salting-out power of salt (Table 4.5). Greater slope of STL indicates greater salting-out power of salt in ATPS (Salabat, et al., 2010). Higher value of STL was observed for Na<sub>2</sub>SO<sub>4</sub> systems where the STLs obtained were slightly higher compared to (NH<sub>4</sub>)<sub>2</sub>SO<sub>4</sub> and KPB systems (Table 4.5). Therefore, Na<sub>2</sub>SO<sub>4</sub> acquired the strongest salting-out power followed by (NH<sub>4</sub>)<sub>2</sub>SO<sub>4</sub> and KPB system. Therefore, phase diagram comprised of PEG 6000-IDA-Cu(II) against Na<sub>2</sub>SO<sub>4</sub> was selected for further optimization due to the lowest concentration of phase components needed for ATPS formation.

#### **5.4 Phase inversion and phase separation on his-tagged HBcAg recovery**

PEG 6000-IDA-Cu(II)-Na<sub>2</sub>SO<sub>4</sub> was selected to optimize the effect of phase inversion and separation on the recovery yield, purity and purification factor of his-tagged HBcAg from unclarified *E. coli* feedstock.

#### **5.4.1 Phase inversion mode**

In this study, two types of phase inversion methods were used, which are inversion with a 3D rotary shaker and a vortex mixer. Rotary shaker represents mild inversion while the vortex mixer represents vigorous inversion. Phase inversion is defined and occurred when a mixture or solution becomes continuously dispersed into droplets (Merchuka, et al., 1998). The intensity differences between these methods will lead to different types of dispersions with top phase continuous or bottom phase continuous.

Merchuka, et al. (1998) and Salamanca, et al. (1998) reported that systems with vigorous inversion (continuous top phase) required longer phase separation time as compared to mild inversion method (continuous bottom phase). Theoretically, a gentle inversion method with shorter separation time is more favoured (Merchuka, et al., 1998). Although mild inversion requires shorter separation period, the results in this study revealed that phase inversion with vigorous mixing (vortex mixer) produced higher recovery yield and purification factor as shown in Table 4.6. Asenjo and Andrew (2008) stated that addition of protein to the ATPS caused system alteration in terms of polarity and size of drops and hydrophobicity, which changed the surface properties. Therefore, his-tagged HBcAg introduced in the systems affected the overall inversion. Similar finding was reported in Tou, et al. (2014), whereby better results were observed in vortex inversion method instead of 3D rotary shaker method.

In addition, the duration for phase inversion also plays an important role in affecting his-tagged HBcAg partitioning into top PEG phase. Increase in duration of vigorous inversion by vortex mixing will increase the collision forces between the molecules in the system (Van Suijdam and Metz, 1981). Therefore, this has increased the chance of his-tagged HBcAg to specifically bind to the modified PEG (top phase). This explains why 5 min inversion with a vortex mixer produced higher recovery yield and purity for his-tagged HBcAg. Therefore, phase inversion with a vortex mixer for 5 min was selected as the optimum condition for phase inversion and this was applied throughout the subsequent optimization.

#### **5.4.2 Phase separation mode**

This study was carried out to investigate the effect of separation modes. The centrifugation separation method and the other one was left on the bench until equilibrium was achieved. As mentioned in Section 5.5.1, phase separation was longer in vigorous inversion method compared to gently inversion method. The system which was left on the bench to separate after vigorous inversion required extremely long separation period, which was up to 2 days. Therefore, this separation method was excluded for further optimization in this study. Asenjo and Andrews (2012) explained that the rate of separation is mainly caused by three forces such as the gravitational, flotation and frictional forces and the movements of a drop in the system is influenced by the balance of these forces. Furthermore, high viscosity could

also contribute to the slow separation rate (Salamanca et al., 1998; Asenjo and Andrews, 2012). The viscosity in a system is mainly caused by the polymer and it increases with the increased of concentration and MW of polymer used in ATPS. Therefore, in order to facilitate the process of phase separation in this study, centrifugation method was used to achieve full separation just in few minutes instead of days (Shiri, et al., 2013).

Different centrifugal forces 1000  $xg$ , 2000  $xg$  and 3000  $xg$  were employed in this study. Results showed that the highest recovery yield and purification factor were achieved at 2000  $xg$ . When the centrifugal force was increased to 3000  $xg$ , the overall recovery yield and purification started to decline. Theoretically, centrifugal force is mainly affected by protein size and density. The larger the protein size and the higher the density, the shorter the sedimentation rate of the protein (Tropp, 2012). In this study, most of the cell debris and unwanted protein were bigger than his-tagged HBcAg. Therefore, most of these contaminants would be sedimented to the salt rich bottom phase. When the centrifugal force was increased, some of the target protein might not be able to partition into the designated phase. This is because most of the proteins are diffusion limited and their diffusion balance would be disturbed when high centrifugation force is applied. As a result, this would cause undesired protein or cell debris to accumulate and partition into top phase as their buoyant density is balanced with high centrifugal force (Luechau, et al., 2010; Mukhopadhyay, 1997). Therefore, this explained why when higher centrifugal forces are applied for separation, the recovery yield and purity of his-tagged HBcAg in the top phase declined as shown in Table 4.7.

Centrifugation time also plays an important role in separating the two phases. In this study, the optimal centrifugal duration was achieved at 3 min by using centrifugal force at 2000 *xg*. However, the recovery yield and purification factor declined as the centrifugation time was prolonged to 5 min. Centrifugation helps the particles to achieve equilibrium in ATPS during separation but prolonged centrifugation will cause the desired protein to precipitate into the intermediate and bottom phase. Therefore, slightly higher his-tagged HBcAg was observed in intermediate and bottom phases for 5 mins centrifugation as compared to centrifugation for 3 mins. This phenomenon indicated that his-tagged HBcAg started to leave the top phase and precipitated into the intermediate and bottom phases.

On the other hand, two centrifugal temperatures, which were 4°C, and room temperature have been investigated in this study. It was observed that the optimal temperature for phase separation in this study was at 4°C. When the temperature rose from 4°C to room temperature (23°C), the recovery yield and purification factor decreased. Generally, it is common that low temperature is usually used to maintain the biological activities for protein and increase in temperature will accelerate the denaturation rate of protein. On the other hand, Di Nucci, et al. (2001) also explained that as temperature rises, PEG structure will extend and become highly ordered, which eventually decreased the interaction of protein with PEG. Furthermore, when temperature rises, the surface hydrophobicity increases, resulting in increase of salting out effect of

PEG (Ramyadevi, et al., 2012). Therefore, in this study, his-tagged HBcAg was partitioned into intermediate and bottom phases when the separation temperature was increased. In conclusion, the optimal conditions for phase inversion was mixing with a vortex mixer for 5 min followed by phase separation using centrifugation for 3 min, 2000 xg at 4°C.

## **5.5 Methods scouting for his-tagged HBcAg recovery in IMAP-ATPS**

### **5.5.1 Tie-line length**

Three systems (PEG 2000-IDA-Cu(II)-Na<sub>2</sub>SO<sub>4</sub>, PEG 2000-IDA-Cu(II)-KPB and PEG 4000-IDA-Cu(II)-KPB) with the highest recovery yields, purity, and purification factor were selected and proceeded to study the effect of TLL on the partitioning of his-tagged HBcAg in ATPS. The recovery yields and purity of his-tagged HBcAg in this study increased as TLL increased as shown in Table 4.9. When TLL increased, it indicated that the phase forming components concentration also increased. Therefore, longer TLL improved the salting out power of bottom phase, which enhanced the interaction between his-tagged HBcAg with modified PEG top phase. As a result, the protein recovery in the top phase improved as observed in this study. Similar cases were also reported whereby the length of tie-line was directly proportional to the recovery yields of protein interest (Ooi, et al., 2009; Show, et al., 2012 and Yeh, et al., 2013).

Moreover, increase in TLL will increase the concentration of bottom phase, leading to increase in viscosity in the bottom phase. Therefore, lower

free volume would be available when the viscosity was high and this drove the his-tagged HBcAg to PEG rich top phase and further improved the recovery of his-tagged HBcAg in the top phase (Rito-Palomares and Hernandez, 1998). On the other hand, when TLL increased, the concentration of modified PEG also increased, thus, higher amount of modified PEG is available to interact with his-tagged HBcAg, which resulted in higher recovery yield in the system with longer TLL. Similar outcome was observed in this study for the all three systems tested, whereby TLL was directly proportional to the recovery and purity of his-tagged HBcAg from the top phase. Therefore, the optimal system was recorded with TLL 3 for PEG 2000-IDA-Cu(II)-KPB system as shown in Table 4.9.

### **5.5.2 Phase volume ratio**

PEG 2000-IDA-Cu(II)-KPB system with selected TLL 3 was chosen for phase volume ratio optimization. Phase volume ratio was divided into three ratios (top:bottom), 2.3, 1.0 and 0.4 along the selected TLL. The results demonstrated that phase volume ratio of 0.4 produced the lowest purity, recovery yield and purification factor of his-tagged HBcAg, followed by phase volume ratio of 1.0 and the optimal condition obtained was phase volume ratio of 2.3 (Table 4.10). Phase volume ratio of 2.3 consists of the highest free volume of modified PEG in the top phase, which enhanced the interaction of his-tagged HBcAg with modified PEG. As a result, this promoted the migration of his-tagged HBcAg from other phases into the top phase, which

eventually resulted in increased of recovery yield (Table 4.10) (Sinha, et al., 1996).

On the other hand, the free volume available in top phase for phase volume ratio of 0.4 was limited. Therefore, the free space available to load his-tagged HBcAg into top phase was greatly reduced. Furthermore, the phase volume ratio of 0.4 provided the system with higher bottom phase volume with higher concentration of phase forming salt compared to the other ratios. Due to the limited space in top phase and high salting out power of salt bottom phase, his-tagged HBcAg was driven to precipitate and partitione into the intermediate phase (Table 4.10). Large amount of his-tagged HBcAg was partitioned into the intermediate phase because of the limited interaction of his-tagged HBcAg with modified PEG as well as due to the low concentration of modified PEG available for specific partitioning. As a consequence, low recovery yield and purification factor were obtained in 0.4 phase volume ratio. Similar observation was reported, whereby better partitioning of protein interest to the top phase increased as the phase volume in top phase increased(Huddleston, et al., 1994; Chethana, et al., 2007). Therefore, phase volume ratio of 2.3 was selected for further optimization.

### **5.5.3 Additional of neutral salt**

Neutral salts are frequently used in ATPS to influence the partitioning of target protein into the desired phase (Ferreira et al., 2013). In this study, neutral salt such as NaCl was applied in ATPS to study the effect of this salt on

the partitioning of his-tagged HBcAg in ATPS. NaCl is a very common and non-toxic neutral salt that plays a crucial role in the partitioning of target protein between phases without altering the biological activity of protein of interest (Reh et al., 2007). Few studies have reported that addition of neutral salts into ATPS improved the recovery yield and purification factor of the desired protein (Andrews, et al., 2005, Schmidt, et al., 1996, Ng, et al., 2011). This is because when NaCl concentration increases in ATPS, the partitioning of target protein to the top phase will be improved by changing the partitioning behaviour of the protein of interest. On the contrary, the results obtained from this study did not demonstrate similar trend as shown in Table 4.11. The recovery yield and purification factor of his-tagged HBcAg were inversely proportional to the concentration of NaCl.

There are several reasons that may contribute to this phenomenon. First of all, the addition of NaCl into the system will change the phase compositions of ATPS (Huddleston, et al., 1991). Once the phase composition in the system changed, the phase volume ratio will also change. The results depicted in Table 4.11 clearly showed that the phase volume ratio for top/bottom phase decreased as the NaCl concentrations increased. When neutral salt is added into a system, the binodal curve for the system would shift toward the origin in the phase diagram as the overall salt concentration in the system has increased. Therefore, this would cause the phase volume ratio to decline when higher NaCl concentration was added into a system. As described previously in Section 5.6.2, the phase volume ratio influenced the partitioning of his-tagged HBcAg in ATPS. Due to the decrease in phase volume ratio caused by addition of NaCl,

the purification factor and recovery yield for his-tagged HBcAg were not improved but decreased significantly. Furthermore, increased of NaCl concentration in the system may also increase the viscosity of the system, thus, the partitioning of his-tagged HBcAg to the top phase was affected.

Next, the properties for the target protein may change when neutral salt is added into ATPS. Structurally, his-tagged HBcAg contains a hydrophobic core, which is buried internally with hydrophilic amino acids face externally and interacts with water molecules through hydrogen bonds (Wynne et al., 1999). However, the addition of NaCl at high concentration into the system would improve the hydrophobic interaction with water that caused protein-water interactions to be weakened. Therefore, this could lead to protein precipitation when the attraction of water molecules and salts are increased (Mao et al., 2010; Ratanapongleka, 2012). Precipitation of target protein could also lead to declining amount of soluble his-tagged HBcAg that are able to interact with modified PEG. As observed in the current study, an obvious decrease in recovery yield and purification factor of his-tagged HBcAg was obtained in top phase when 200 mM of NaCl was added into the system. Besides that, based on the Hofmeister series, the chaotropicity of Cl ions is stronger than the phosphate ions. Therefore, a stronger chaotrope tend to destabilize the protein and cause the precipitation of his-tagged HBcAg in this study. This was particularly obvious when higher NaCl concentration was used (Table 4.11).

In addition, phosphate ions are known as water-structure making anions, which avoid the hydrophobic PEG-rich top phase. Whereas Cl ions are water structure breaking anions, which favoured the PEG-rich top phase. Physico-chemical properties of the system are changed by constant competitions between these two ions (Luechau et al., 2009a). Cl ions are distributed unevenly throughout the top and bottom phases when higher NaCl is added into a system. Therefore, this would create electrical potential differences, which could cause the phase composition to change. These are crucial because the partitioning of protein is highly influenced by the electrical interaction and repulsion between the charged protein and charged ATPS (Saravanan, et al., 2008). Besides that, according to Asenjo and Andrew, (2011), PEG rich top phase is positively charged and addition of NaCl would alter the PEG rich top phase charge to negatively charged. Therefore, negatively charged protein would be repelled away from the top phase and resulted in partitioning of the protein to the other phases as observed in this study.

In conclusion, the addition of NaCl into the ATPS did not improve the partitioning of his-tagged HBcAg to the top phase. In contrast, it caused alteration in the system compositions and favoured the partitioning of his-tagged HBcAg to the intermediate and bottom phase. Similar findings were also reported whereby the addition of NaCl into ATPS did not improve the recovery and purity of target protein into the top phase (Capezio, et al., 2005; Abbasiliasi, et al., 2014). Therefore, PEG 2000-IDA-Cu(II)-KPB system, with TLL 3 and phase volume ratio of 2.3 without NaCl addition was selected for further optimizations.

#### 5.5.4 System pH

System pH plays an important role in the partitioning of his-tagged HBcAg to the modified PEG top phase. The selected system pHs used in this study were pH 6, 7 and 8 because HBcAg was reported to be stable in these selected pHs (Nath, et al.,1992). Results from Table 4.12 demonstrated that the purity, purification factor and recovery yield of his-tagged HBcAg increased when the system's pH was increased from 6 to 8. The optimal partitioning condition was observed in the system with pH 8. The target protein and contaminant protein surface properties as well as the ion composition were affected, which eventually resulted in uneven distribution of contaminants between the top and bottom phases (Hatti-Kaul, 2000; Rito-Palomares, 2004). The interaction between his-tagged HBcAg with modified PEG in the top phase was greatly influenced by the net charge on the surface of his-tagged HBcAg and this was clearly determined by the pH used in the system.

The isoelectric point (*pI*) value will influence the net charge of his-tagged HBcAg and it is determined by the surrounding pH value. When pH value is lower than the *pI* value, proteins become positively charged, and when the pH value is higher than *pI* value, proteins become negatively charged. Moreover, when the pH value is similar to the *pI* value, the net charge is balanced (Saravanan, et al., 2008). Proteins are negatively charged at higher pH than at lower pH, and this could cause increase in protein partitioning to the top phase (Ramyadevi et al., 2012). The core protein with *pI* value of 4.5 was

negatively charged from pH 6 to 8 and the amount of negatively charge his-tagged HBcAg increased as the pH value increased (Choi, et al., 2004). As a result, more negatively charged his-tagged HBcAg was partitioned to the top phase due to the positively charged modified PEG. This has led to a sharp increase in the purity, recovery yields and purification factor of his-tagged HBcAg in the top phase as depicted in Table 4.12 due to the increase in interaction between modified PEG and his-tagged HBcAg. Next, the electrostatic interactions between positively charged modified PEG and his-tagged HBcAg could be another contributing factor(Tanuja et al., 1997).

Several studies demonstrated that the amount of negatively charged proteins increased gradually with elevating pH, which led to the increase in the interaction between positively charged PEG and negatively charged protein (Asenjo, et al., 1994; Huddleston, et al., 1991). Similar to this study, a higher recovery yield, purity and purification factor of his-tagged HBcAg were observed when the system pH was elevated from acidic (pH 6) to alkaline (pH 8).

A decreasing trend in for phase volume ratio was observed in this study (Table 4.12). However, this did not significantly (0.1) affect the purity, recovery yield and purification factor of his-tagged HBcAg in phase volume ratio from pH 7 to 8. High recovery of his-tagged HBcAg from the top phase indicated that the free space available to load his-tagged HBcAg into the top phase were still preserved. In addition, it was also observed that the phase

volume ratio at pH 6 (10.25) was the highest compared to pH 7 (2.3) and 8 (2.2). Huge differences in phase volume ratio also caused low recovery of his-tagged HBcAg from system at pH 6. This large volume difference between top and bottom phases resulted an enormous increase of free volume in top phase, which may facilitate the partitioning of both the his-tagged HBcAg and contaminant proteins to the PEG-rich top phase (Patil and Raghavarao, 2007). Therefore, low purity was obtained in the top phase for pH 6 system as shown in this study.

On the other hand, system pH 5 was excluded from this study because this system was unable to achieve a biphasic formation. The binodal curve will be shifted away from the origin when there is a drop in the system pH as reported in Diederich, et al. (2013). Therefore, the phase components needed to form two phase will be greatly increase and this would not be feasible to use in ATPS. Therefore, it was concluded that PEG 2000-IDA-Cu(II)-KPB system, TLL 3 with phase volume ratio of 2.3 without NaCl addition, and pH 8 were selected for further optimizations.

#### **5.5.5 Biomass concentration**

Biomass concentration added into the system will affect the phase volume ratio, phase compositions and influence the partitioning of his-tagged HBcAg into the top phase. In this study, the effect of different final biomass concentration (3, 4, 5, 6 and 7% (w/v)) was investigated on the recovery yield, purification and purity of his-tagged HBcAg. The optimal recovery yield was

achieved when 5% (w/v) biomass concentration was employed (Table 4.13). The purity, purification factor and recovery yield of his-tagged HBcAg started to decline when the biomass concentration was increased above 5%(w/v). Increase in final biomass concentration also indicated the increase of his-tagged HBcAg as well as the contaminant proteins content in the system. Therefore, this could deteriorate an optimized ATPS performance due to presence of cell debris, proteins and other components in unclarified feedstock (Ng, et al., 2011; Paquet, et al., 1994)

Similar observations were also reported by Ng, et al. (2011), whereby increase of crude feedstock concentration could alter the characteristics of an optimized ATPS. When the composition in the phases changed, the phase volume ratio was also altered (Table 4.13). The phase volume ratio has greatly decreased from 2.2 to 1.6 when 5% (w/v) and 7% (w/v) of biomass concentration were used, respectively. A sharp decline in the recovery yields, purity and purification factor were also observed in this study when the biomass concentration was elevated to 7% (w/v). A low phase volume ratio could affect the partitioning of his-tagged HBcAg into the PEG-rich top phase, due to the lower free space available. It will distort the binding of his-tagged HbcAg with modified PEG in the top phase. Therefore, the recovery of his-tagged HBcAg from the top phase by using higher than 5% (w/v) biomass concentrations in the ATPS could lead to low purification factor, purity and recovery yield of his-tagged HBcAg.

Asenjo and Andrews, (2011) also reported that the target protein will be partitioned to intermediate phase as the feedstock concentration exceeded the capability of a particular ATPS. Similar result was observed in this study whereby 5% (w/v) unclarified feedstock was optimal for 5 g ATPS used in this study. Every ATPS has its own maximum capacity for loading, thus, increased in biomass concentration above the maximum capacity resulted in all available free space in the top phase to be occupied, thus forcing the remaining his-tagged HBcAg in the unclarified feedstock to partition into interphase or bottom phase together with other contaminant proteins. As a result, it lost its optimal function and resulted in low recovery yield, purity and purification factors as biomass concentration was increased. Studies carried out by Cho, et al. (2002) and Show, et al. (2012) have also demonstrated that high biomass concentration could deteriorate the performance of ATPS. Therefore, in conclusion, 5% (w/v) unclarified feedstock was selected for the optimum recovery of his-tagged HBcAg in this study.

#### **5.5.6 Optimized conditions for ATPS**

The ATPS composed of PEG 2000-IDA-Cu(II)-KPB system, TLL 3 with a phase volume ratio of 2.3, system pH 8.0, without NaCl addition and loaded with 5% (w/v) unclarified feedstock has successfully recovered 91.3% of his-tagged HBcAg with a purity of 93.6% and a purification factor of 3.0. A band at 21 kDa corresponded to truncated his-tagged HBcAg in PEG-rich top phase was observed in Figure 4.17. The contaminant proteins in the top phase after the optimization have significantly decreased compared to the system

before optimization. In addition, most of the his-tagged HBcAg was partitioned into top phase while his-tagged HBcAg detected in the bottom phase decreased significantly after the optimization. Therefore, ATPS with metal affinity can be considered a feasible method to use in the recovery of his-tagged HBcAg directly from unclarified feedstock in this study.

In a 5g ATPS system in this study, low MW polymer acquired higher performance in his-tagged HBcAg recovery as compared to high MW polymer. This is because the amount of modified PEG 2000 in a 5g ATPS is the highest, followed by PEG 4000 and PEG 6000. Therefore, it contained higher amount of modified PEG available to interact with his-tagged HBcAg in the top phase, which resulted in higher recovery yield in the system with low MW polymer.

The results from this study were compared to the conventional method, whereby the former method has obtained a higher recovery yield with lesser steps of operation. Therefore, it could reduce the overall processing time, hence reduces the cost of operation. The recovery yield of his-tagged HBcAg obtained in this study was 91.3%, which was higher compared to that obtained using sucrose gradient ultracentrifugation. Low recovery yield in sucrose gradient ultracentrifugation may be due to the high concentration of sucrose, which could induce aggregation and deformation of the protein, hence leads to degradation of protein (Rolland, et al., 2001). Apart from that, this method is only suitable for lab scales purification due to its multiple steps of operation to produce clarified protein solution prior to purification. This condition might

cause damage to the protein of interest especially to those proteins that are sensitive to proteolysis (Yap, et al., 2010).

Another method used for his-tagged HBcAg purification was the immobilized metal affinity expanded bed adsorption chromatography (Yap, et al., 2010). Although this method produce a high purity (91%) and purification factor (3.65) of his-tagged HBcAg but the recovery yield (56%) was 55.3% lower than the yield obtained in this study. Besides that, the purity of his-tagged HBcAg obtained using the current method recovered directly from unclarified feedstock was comparable (93.6%) to the purity obtained using sucrose gradient ultracentrifugation method and slightly higher (2.6%) compared to that reported method using immobilized metal affinity expanded bed adsorption method.

Apart from that, a previous study has reported that ATPS can be a feasible method to use to purify HBcAg (Tou, et al., 2014). However, the yield (68%) and purification factor (1.93) were lower compared to that demonstrated in the present study. Therefore, this study has shown that IMAP in ATPS was able to improve the overall performance of ATPS and can be an alternative method to use the purification of HBcAg directly from unclarified bacterial feedstock.

## **5.6 Antigenicity and morphology of purified his-tagged HBcAg**

The antigenicity exhibited by purified his-tagged HBcAg was still preserved after ATPS and was comparable to the his-tagged HBcAg purified using sucrose-gradient ultracentrifugation (Figure 4.18). The results indicated that the core particle was still intact and its antigenicity was also not compromised. The antigenicity of ATPS purified his-tagged HBcAg and sucrose gradient ultracentrifugation purified his-tagged HBcAg could be detected as low as 10 ng in ELISA test. Figures 4.19 and 4.20 showed that the purified his-tagged HBcAg was able to self-assemble into icosahedral capsids and their structure still remained intact with diameters of about 28 to 32 nm.

This is in a good agreement with the observation described by Yap, et al. (2009), whereby the antigenicity of his-tagged HBcAg purified using the immobilised metal affinity chromatography was also not compromised. Moreover, it was also reported that the additional N-terminal tag did not affect the antigenicity and self-assemble capability of the his-tagged HBcAg (Yap, et al., 2009). Similar finding was reported when immobilized metal affinity-expanded bed adsorption chromatography was used to purify his-tagged HBcAg (Yap, et al., 2010). The eluted his-tagged HBcAg produced similar antigenicity and demonstrated the same morphology when viewed under TEM as previously reported by Yap, et al. (2009). The transmission electron micrograph also indicated the diameter for the purified his-tagged HBcAg was approximately 30 nm, which was similar to that observed in the current study.

## CHAPTER 6

### CONCLUSION

In this study, IMAP in ATPS can be a feasible alternative method for his-tagged HBcAg recovery and purification directly from unclarified bacterial feedstock. In order to setup an IMAP in ATPS, a modified PEG (PEG-IDA-metal) that serves as specific ligand for his-tagged HBcAg is required. Although PEG 2000 recorded the highest production of oxirane concentration under the conditions of 2 h activation duration, 1.0% (v/v) BFEE concentration, 0.8% (v/v) epichlorohydrin and 1.2% (v/v) NaOH concentration, all PEG of different molecular weights were subjected into the optimisation of type of metal ions bound to PEG-IDA. Copper ions have shown to exhibit higher binding efficiency to all PEG-IDA compared to nickel ions with approximately 2 times differences in concentration. Therefore, all PEG-IDA-Cu(II) were selected for phase diagram construction with different types of phase forming salts.

In addition, this study has also constructed the binodal curve, tie lines and phase diagram of a total of nine PEG-salts systems involved. The result showed that PEG 6000-IDA-Cu(II)-Na<sub>2</sub>SO<sub>4</sub> system demonstrated the lowest phase forming components needed for biphasic formation among all the nine systems tested. However, this system did not result in a good purity, recovery yield and purification factor for his-tagged HBcAg. On the other hand, PEG

2000-IDA-Cu(II)-KPB system has been shown to generate the highest his-tagged HBcAg recovery yield (91.3%), purity (93.6%) and purification factor (3.0) after a series of optimizations. The optimised conditions were phase inversion for 5 min by using a vortex mixer, phase separation by centrifugation for 3 min at 2000 xg, TLL 3, phase volume ratio of 2.3, system pH 8, without NaCl addition and loaded with 5% (w/v) unclarified feedstock.

Beside, this study has demonstrated that sucrose gradient ultracentrifugation has successfully recovered 12.6% of his-tagged HBcAg with 96.2% in purity and a purification factor of 3.2. The purity and purification obtained were slightly higher than the ones purified using ATPS, but the recovery yield for his-tagged HBcAg purified by ATPS was 78.7% higher compared to the one obtained using sucrose gradient ultracentrifugation. Apart from that, ATPS is a more simple method to use as it only required three units of operations which include preparation of unclarified feedstock, ATPS and dialysis. In contrast, sucrose gradient ultracentrifugation required a total of six units of operations, which involved preparation of unclarified feedstock, centrifugation, ammonium sulphate precipitation, dialysis, sucrose gradient ultracentrifugation, dialysis and concentration of the sample that resulted in product loss up to 87.4%.

Moreover, based on the SDS-PAGE gel image, most of the his-tagged HBcAg was successfully partitioned into the top phase of ATPS and the his-tagged HBcAg detected in the bottom phase was reduced significantly after

optimizations. The antigenicity of ATPS purified his-tagged HBcAg was comparable to the his-tagged HBcAg purified using sucrose gradient ultracentrifugation. Both methods recovered the same size and morphology of icosahedral capsids with an average size of 30 nm in diameter. Therefore, it was concluded that ATPS with metal affinity partitioning can be considered as an effective method for his-tagged HBcAg recovery directly from unclarified bacterial feedstock without losing their native antigenicity and morphology.

The main application of this research is that metal affinity partitioning incorporated in ATPS can be used as alternative pre-clarification step before the final polishing step in the production of vaccine or diagnostic kits for HBV infection either in lab or industrial scale. This method can reduce the time and steps involved in the downstream processing for pharmaceutical products or biologics which eventually reduce the production cost because 70% to 80% of the productions are usually from downstream processing. In future, this method can be extended to partition interest biological components, or used in separation of bio-product and bioconversion in other type of ATPS such as the polymer/polymer ATPS, polymer/low MW alcohol ATPS, and ionic liquid/salt ATPS instead of commonly used polymer/salt ATPS. The comparison between these ATPS can be made based on the purity, purification factor, recovery yields and step of operations.

## REFERENCES

- Abbasiliasi, S. et al., 2014. Primary recovery of bacteriocin-like inhibitory substance derived from *Pediococcus acidilactici* Kp10 by an aqueous two-phase system. *Food Chemistry*, 151, pp. 93-100.
- Ahmad, A. L., Derek, C. J. C., and Zulkali, M. M. D., 2008. Optimization of thaumatin extraction by aqueous two-phase system (ATPS) using response surface methodology (RSM). *Separation and Purification Technology*, 62(3), pp. 702-708.
- Andrews, B.A., Schmidt, A.S. and Asenjo, J.A., 2005. Correlation for the partition behaviour of proteins in aqueous two-phase systems: Effect of surface hydrophobicity and charge. *Biotechnology and Bioengineering*, 90, pp. 380-390.
- Asenjo, J.A., Schmidt, A.S., Hachem, F. and Andrews, B.A., 1994. Model for predicting the partition behaviour of proteins in aqueous two-phase systems. *Journal of Chromatography A*, 668, pp. 47-54.
- Asenjo, J.A. and Andrews, B.A., 2008. Challenges and trends in bioseparations. *Journal of Chemical Technology and Biotechnology*, 83, pp. 117-120.
- Asenjo, J. A., and Andrews, B. A., 2011. Aqueous two-phase systems for protein separation: A perspective. *Journal of Chromatography A*, 1218(49), pp. 8826-8835.
- Asenjo, J.A. and Andrews, B.A., 2012. Aqueous two-phase systems for protein separation and applications. *Journal of Chromatography A*, 1238, pp. 1-10.
- Barbosa. H. S. C., Hine, A. V., Brocchini, S., Slater, N. K. H. and Marcos, J. C., 2010. Dual affinity method for plasmid DNA purification in aqueous two-phase systems. *Journal of Chromatography A*, 1217, pp. 1429-1436.
- Baron, S., 1996. *Medical Microbiology*. 4<sup>th</sup> ed. Galveston, Texas: University of Texas Medical Branch.
- Bernaumat, F., and Bulow, L., 2005. Rapid evaluation of nickel binding properties of His-tagged lactate dehydrogenase using surface Plasmon resonance. *Journal of Chromatography A*, 1(2), pp. 219-224.
- Bernaumat, F., and Bulow, L., 2006. Combined hydrophobic-metal binding fusion tags for applications in aqueous two-phase partitioning. *Protein Expression and Purification*, 46, pp 438-445.
- Birkenmeir, G., Vijayalakshmi, M. A., Stigbrand, T. and Kopperschiager, G., 1991. Immobilized metal ion affinity partitioning, a method combining metal-protein interaction and partitioning of protein in aqueous two-phase systems. *Journal of Chromatography*, 539, pp. 267-277.

- Birnbaum, F. and Nassal, M., 1990. Hepatitis B Virus Nucleocapsid Assembly: Primary Structure Requirements in the Core Protein. *Journal of Virology*, 64(7), pp. 3319-3330.
- Block, T. M., Guo, H. and Guo, J. T., 2008. Molecular virology of hepatitis B virus for clinicians. *Clinical Liver Disease*, 11(4), pp. 685-706.
- Botros, H. G., Nanak, E., Nour, J. A., Birkenmeir, G., and Vijayalakshmi, M. A., 1992. Immobilized metal ion affinity electrophoresis: A study with several model proteins containing histidine. *Journal of Chromatography A*, 1(2), pp. 357-364.
- Brooks, D.E., Sharp, K.A. and Fisher, D., 1985. Theoretical aspects of partitioning. In Walter, H., Brooks, D.E. and Fisher, D. (Eds.), *Partitioning in aqueous two-phase system: Theory, methods, uses and applications to biotechnology*. Orlando, Florida: Academic Press Inc, pp. 11-97.
- Bulgariu, L. and Bulgariu, D., 2008. Extraction of metal ions in aqueous polyethylene glycol- inorganic salt two-phase systems in the presence of inorganic extractants: Correlation between extraction behaviour of and stability constants of extracted species. *Journal of Chromatography A*, 1196-1197, pp. 117-124.
- Capezio, L., Romanini, D., Pico, G.A. and Nerli, B., 2005. Partition of whey milk proteins in aqueous two-phase systems of polyethylene glycol-phosphate as a starting point to isolate proteins expressed in transgenic milk. *Journal of Chromatography B*, 819(1), pp. 25-31.
- Chen, H., Liu, S., Chen, L., Huang, J., and Xiang, S., 2005. Expression of HBcAg mutant with long internal deletion in *Saccharomyces cerevisiae* and observation of its self-assembly particles by atomic force microscopy (AFM). *International Journal of Biological Macromolecules*, 37, pp. 239-248.
- Chen, J., Ding, Z., Pan, H., and Cao, X., 2017. Development of pH-responsive polymer and citrate aqueous two-phase system for extractive bioconversion of cefprozil. *Talanta*, 174, pp. 256-264.
- Chen, M. T., Billaud, J. N., Sallberg, M., Guidotti, L. G., Chisari, F. V., Jones, J., Hughes, J., and Milich, D. R., 2004. *Proceedings the National Academic of Science*, 101(41), pp. 14913-14918.
- Chethana, S., Nayak, C.A. and Raghavarao, K.S.M.S., 2007. Aqueous two phase extraction for purification and concentration of betalains. *Journal of Food Engineering*, 81, pp. 679-687.
- Cho, T.H., Ahn, S.J. and Lee, E.K., 2002. Refolding of protein inclusion bodies directly from *E. coli* feedstock using expanded bed adsorption chromatography. *Bioseparation*, 10, pp. 289-196.
- Choi, K. J., Lim, C. W., Yoon, M. Y., Ahn, B. Y., and Yu, Y. G., 2004. Quantitative analysis of the interaction between the envelope protein

domains and the core protein of human hepatitis B virus. *Biochemical and Biophysical Research Communications*, 319(3), pp. 959-966.

- Clarke, B. E., Newton, S. E., Carroll, A. R., Francis, M. J., Appleyard, G., Syred, A. D., Highfield, P. E., Rowlands, D. J., and Brown, F., 1987. Improved immunogenicity of a peptide epitope after fusion to hepatitis B core protein. *Nature*, 330(6146), pp. 381-384.
- Crowther, R. A., Kiselev, N. A., Bottcher, B., Berriman, J. A., Borisova, G. P., Ose, V., and Pumpen, P., 1994. Three-dimensional structure of hepatitis B virus core particles determined by electron microscopy. *Cell*, 77(6), pp. 943-950.
- Dandri, M. and Petersen, J., 2017, Animal models of HBV infection. *Best Practice & Research Clinical Gastroenterology*, 31(3), pp. 273-279.
- Deng, L. J., Xu, Y., and Huang, J., 2008. Developing a double-antigen sandwich ELISA for effective detection of human hepatitis B core antibody. *Comparative Immunology, Microbiology and Infectious Diseases*, 31(6), pp. 515-526.
- Di Nucci, H., Nerli, B. and Pico, G., 2001. Comparison between the thermodynamic features of alpha1-antitrypsin and human albumin partitioning in aqueous two-phase systems of polyethyleneglycol-dextran. *Biophysical Chemistry*, 89, pp. 219-229.
- Diederich, P., Amrhein, S., Hämmerling, F. and Hubbuch, J., 2013. Evaluation of PEG/phosphate aqueous two-phase systems for the purification of the chicken egg white protein avidin by using high throughput techniques. *Chemical Engineering Science*, 104, pp. 945-956.
- Dongqiang, L., Shanqing, Y., Lehe, M., and Ziqiang, Z., 2000. Preparation of Iminodiacetic Acid-Polyethylene Glycol for Immobilized Metal Ion Affinity Partitioning. *Chinese Journal of Chemical Engineering*, 8(4), pp. 310-314.
- Dordevic, T., and Antov, M., 2017. Ultrasound assisted extraction in aqueous two-phase system for the integrated extraction and separation of antioxidants from wheat chaff. *Separation and Purification Technology*, 182, pp. 52-58.
- Elghanam, M. S., Attia, A. S., Shoeb, H. A., and Hashem, A. E. M., 2012. Expression and purification of hepatitis B surface antigen S from *Escherichia coli*; a new simple method. BMC Res Notes. Published online 2012 Mar 1. doi: 10.1186/1756-0500-5-125.
- Everberg, H., Clough, J., Henderson, P, Jergil, B, Tjerneld, F. and Ramirez, I. B. R., 2006. Isolation of *Escherichia coli* inner membranes by metal affinity two-phase partitioning. *Journal of Chromatography A*, 1118, pp. 244-252.
- Fakhari, M. A., Rahimpour, F. and Taran, M., 2017. Response surface methodology optimization of partitioning of xylanase form *Aspergillus*

- Niger* by metal affinity polymer-salt aqueous two-phase systems. *Journal of Chromatography B*, 1063, pp. 1-10.
- Fan, Y., Lu, Y. M., Yu, B., Tan, C. P., and Cui, B., 2017. Extraction and purification of capsaicin from capsicum oleoresin using an aqueous two-phase system combined with chromatography. *Journal of Chromatography B*, 1063, pp. 11-17.
- Ferreira, L.A. and Teixeira, J.A., 2011. Salt effect on the aqueous two-phase system PEG 8000-sodium sulphate. *Journal of Chemical Engineering Data*, 56, pp. 133-137
- Ferreira, L., Madeira, P.P., Mikheeva, L., Uversky, V.N. and Zaslavsky, B., 2013. Effect of salt additives on protein partition in polyethylene glycol-sodium sulphate aqueous two-phase systems. *Biochimica et Biophysica Acta*, 1834, pp. 2859-2866.
- Gaberc-Porekar, V., and Menart, V., 2001. Perspectives of immobilized-metal affinity chromatography. *Journal of Biochemical and biophysical methods*, 49, pp. 335-360.
- Hatti-Kaul, R., 2000. *Aqueous two-phase system: a general overview: Aqueous two-phase systems: methods and protocols*. Totowa: Humana Press Inc., pp. 1 – 5.
- Hatton, T., Zhou, S., and Standring, D. N., 1992. RNA- and DNA-Binding Activities in Hepatitis B Virus Capsid Protein: a Model for Their Roles in Viral Replication. *Journal of Virology*, 66(9), pp. 5232-5241.
- Herman, S. G. R. K., and Chan, H. L. Y., 2017. Stopping nucleos(t)ide analog treatment in chronic hepatitis B-Who and when?. *Liver Research*, in press.
- Hjorth, R., 1997. Expanded-bed adsorption in industrial bioprocessing: *Recent developments*. *Trends in Biotechnology*, 15(6), pp. 230-235.
- Huang, Z., Santi, L., Lepore, K., Killbourne, J., Arntzen, C. J., and Mason, H. S., 2006. Rapid, high-level production of hepatitis B core antigen in plant leaf and its immunogenicity in mice. Rapid, high-level production of hepatitis B core antigen in plant leaf and its immunogenicity in mice. *Vaccine*, 24(14), pp. 2506-2513.
- Huddleston, J.G., Ottomar, K.W., Ngonnyani, D.M. and Lyddiatt, A., 1991. Influence of system and molecular parameters upon fractionation of intracellular proteins from *Saccharomyces* by aqueous two-phase partition. *Enzyme Microbiology and Biotechnology*, 13, pp. 24-32.
- Huddleston, J.G., Wang, R., Flanagan, J.A., O'Brien, S. and Lyddiatt, A., 1994. Variation of protein partition coefficients with volume ratio in poly(ethylene glycol)-salt aqueous two-phase systems. *Journal of Chromatography A*, 668, pp. 3-11.
- Iqbal, M., Tao, Y., Xie, S., Zhu, Y., Chen, D., Wang, X., Huang, L., Peng, D., Sattar, A., Shabbir, M. A. B., Hussain, H. I., Ahmed, S., and Yuan, Z., 2016. Aqueous two-phase system (ATPS): an overview and advances in

its applications. *Biological Procedure Online*. [online] Available at: <https://doi.org/10.1186/s12575-016-0048-8> [Accessed 19 July 2017].

- Johansson, G., and Andersson, M., 1984. Parameters determining affinity partitioning of yeast enzymes using polymer-bound triazine dye ligands. *Journal of Chromatography*, 303(1), pp. 39-51.
- Johansson, H.O., Lundh, G., Karlstrom, G., and Tjerneld, F., 1996. Effects of ions on partitioning of serum albumin and lysozyme in aqueous two-phase systems containing ethylene oxide/ propylene oxide co-polymers. *Biochemica et Biophysica Acta*, 1290, pp. 289 – 298.
- Johansson, H. O., Feitosa, E., and Junior, A. P., 2011. Phase Diagrams of the Aqueous Two-Phase Systems of Poly(ethylene glycol)/Sodium Polyacrylate/Salts. *Polymers*, 3, pp. 587-601.
- Jozala, A.F., Lopes, A.M., Lencastre Novaes, L.C., Mazzola, P.G., Penna, T.C.V. & Junior, A.P. (2012) Aqueous two-phase micellar system for nisin extraction in the presence of electrolytes. *Food and Bioprocess Technology*, pp. 1-6.
- Karvonen, T., Auranen, K., Kuusi, M., and Leino, T., 2017, Epidemiology of hepatitis B infection in Finland: Implications for immunisation policy. *Vaccine*, 35(3), pp. 412-418.
- Kaul, R. H., ed. 2000. *Aqueous Two-Phase System: Methods and Protocols*. Totowa, New Jersey: Humana Press Inc.
- Kenney, J. M., Bonsdorff, C. H., Nassal, M., and Fuller, S. D., 1995. Evolutionary conservation in the hepatitis B virus core structure: comparison of human and duck cores. *Structure*, 3(10), pp. 1009-1019.
- Kimura, T., Rokuhara, A., Sakamoto, Y., Yagi, S., Tanaka, E., Kiyosawa, and Maki, N., 2002. Sensitive enzyme immunoassay for Hepatitis B virus core-related antigens and their correlation to virus load. *Journal of Clinical Microbiology*, 40(2), pp. 439-445.
- Kimura, T., Rokuhara, A., Matsumoto, A., Yagi, S., Tanaka, E., Kiyosawa, K., and Maki, N., 2003. New Enzyme Immunoassay for Detection of Hepatitis B Virus Core Antigen (HBcAg) and Relation between Levels of HBcAg and HBV DNA. *Journal of Clinical Microbiology*, 41(5), pp. 1901-1906.
- Kumar, A., Galaev, I.Y. and Mattiasson, B., 2007. *Cell separation: Fundamentals, analytical and preparative methods*. Berlin: Springer-Verlag GmbH.
- Li, M., Kim, J.W. and Peeples, T.L., 2002. Amylase partitioning and extractive bioconversion of starch using thermoseparating aqueous two-phase systems. *Journal of Biotechnology*, 93, pp. 15 – 26.
- Laboureau, E., Capiod, J. C., Dessaint, C., Prin, L., and Vijayalakshmi, M. A., 1996. Study of human cord blood lymphocytes by immobilized metal ion affinity partitioning. *Journal of chromatography B*, 680, pp. 189-195.

- Liang, T. J., 2009. Hepatitis B: The virus and Disease. *Hepatology*, 49, pp. s13-s21.
- Liao, Y. C. and Syu, M. J., 2005. Novel immobilized metal ion affinity adsorbent based on cross-linked  $\beta$ -cyclodextrin matrix for repeated adsorption of  $\alpha$ -amylase. *Biochemical Engineering Journal*, 23, pp. 17-24.
- Liao, Y. C. and Syu, M. J., 2009. Effect of poly(ethylene glycol) and salt on the binding of  $\alpha$ -amylase from the fermentation broth of *Bacillus amyloliquefaciens* by  $\text{Cu}^{2+}$ - $\beta$ -CD affinity adsorbent. *Carbohydrate Polymers*, 77, pp. 344-350.
- Lim, S. L., Ooi, C. W., Tan, W. S., Chan, E. S., Ho, K. L., and Tey, B. T., 2017. Biosensing of hepatitis B antigen with poly(acrylic acid) hydrogel immobilized with antigens and antibodies. *Sensor and Actuators B: Chemical*, 252, pp. 409-417.
- Long, S. S., Pickering, L. K., and Prober, C. G., eds. 2012. *Principles and Practice of Pediatric infectious Diseases*. 4<sup>th</sup> ed. Amsterdam, Netherlands: Elsevier.
- Lu, Y., Lu, W., Wang, W., Guo, Q. and Yang, Y., 2013. The optimization of aqueous two-phase extraction of lysozyme from crude hen egg white using response surface methodology. *Journal of Chemical Technology and Biotechnology*, 88, pp. 415-421.
- Luechau, F., Ling, T.C. and Lyddiatt, A., 2009a. Partition of plasmid DNA in polymer-salt aqueous two-phase systems. *Separation and Purification Technology*, 66, pp. 397-404.
- Luechau, F., Ling, T.C. and Lyddiatt, A., 2010. A descriptive model and methods for up-scaled process routes for interfacial partition of bioparticles in aqueous two-phase systems. *Biochemical Engineering Journal*, 50, pp. 122-130.
- Magalhaes, P. O., Lopes, A. M., Mazzola, P. G., Rangel-Yagui, C., Penna, T. C. V., Pessoa, A. & G, P., 2007. Methods of endotoxin removal from biological preparations: a review. *Journal of Pharmaceutical Sciences*, 10, pp. 388-404.
- Mageste, A. B., Lemos, L. R., Ferreira, G. M. D., Silva, M. C. H., Silva, L. H. M., Bonomo, R. C. F. and Minim, L. A., 2009. Aqueous two-phase systems: an efficient, environmentally safe and economically viable method for purification of natural dye carmine. *Journal of Chromatography A*, 1216, pp. 7623-7629.
- Mao, L.N., Rogers, J.K., Westoby, M., Conley, L. and Piercacci, J., 2010. Downstream antibody purification using aqueous two-phase extraction. *Biotechnology Progress*, 26, pp. 1662-1670.
- Merchuk, J.C., Andrews, B.A. and Asenjo, J.A., 1998. Aqueous-two phase systems for proteins separation studies on phase inversion. *Journal of Chromatography B*, 711, pp. 285-293.

- Milich, D. R., Chen, M., Schodel, F., Peterson, D. L., Jones, J. E., and Hughes, J. L., 1997. Role of B cells in antigen presentation of the hepatitis B core. *Immunology*, 94, pp. 14648-14653.
- Milich, D. R., Jones, J. E., Hughes, J. L., Price, J., Raney, A. K., and Mclachlan, A., 1990. *Proceedings of the National Academy of Science*, 88, pp.6599-6603.
- Mondal, K., and Gupta, M. N., 2006. The affinity concept in bioseparation: Evolving paradigms and expanding range of applications. *Biomolecular Engineering*, 23, pp. 59-76.
- Mukhopadhyay, A., 1997. Inclusion bodies and purification of proteins in biologically active forms. *Advanced Biochemical Engineering Biotechnology*, 56, pp. 61-109.
- Nagami, H., Umakoshi, H., Kitaura, T., Thompson III, G. L., Shimanouchi, T. and Kuboi, R., 2014. Development of metal affinity-immobilized liposome chromatography and its basic characteristics. *Biochemical Engineering Journal*, 84, pp 66-73.
- Naito, M. et al., 1997. Simple method for efficient production of hepatitis B virus core antigen in *E. coli*. *Research in Virology*, 148, pp. 299 – 305.
- Nath, N. et al., 1992. Stability of the recombinant hepatitis B core antigen. *Journal of Clinical Microbiology*, 30, pp. 1617-1619.
- Ng, H.S. et al., 2011. Recovery of *Bacillus cereus* cyclodextrin glycosyltransferase and recycling of phase components in an aqueous two-phase system using thermo-separating polymer. *Separation and Purification Technology*, 81, pp. 318-324.
- Ng, M.Y.T. et al., 2006. Heat treatment of unclarified *Escherichia coli* feedstock improved the recovery efficiency of recombinant hepatitis B core antigen. *Journal of Virological Methods*, 137 (1), pp. 134 – 139.
- Nosratabadi, R., Alavian, S. M., Zare-Bidaki, M., Shahrokhi, V. M., and Arababadi, M. K., 2017, Innate immunity related pathogen recognition receptors and chronic hepatitis B infection. *Molecular immunology*, 90, pp. 64-73.
- Oshima, T., Oshima, C. and Baba, Y., 2015. Selective extraction of histidine derivatives by metal affinity with a copper(II)-chelating ligand complex in an aqueous two-phase system. *Journal of Chromatography B*, 990, pp. 73-79.
- Ooi, C.W. et al., 2009. Purification of lipase derived from *Burkholderia pseudomallei* with alcohol/salt-based aqueous two-phase systems. *Biotechnology and Bioprocess Engineering*, 14, pp. 811-818.
- Palenzuela, D., Palenzuela, O., Nunez, L., and Gavilondo, J., 2002. Purification of the recombinant Hepatitis B core antigen, and its Potential Use for the Diagnosis of Hepatitis B Virus infection. *Biotechnologia aplicada*, 19(3).

- Paquet, V., Myint, M., Rogue, C. and Soucaille, P., 1994. Partitioning of pristinamycins in aqueous two-phase systems: A first step toward the development of antibiotic production by extractive fermentation. *Biotechnology and Bioengineering*, 44, pp. 445–451.
- Patil, G. and Raghavarao, K.S.M.S., 2007. Aqueous two phase extraction for purification of C-phycoerythrin. *Biochemical Engineering Journal*, 34, pp. 156-164.
- Pei, Y., Wang, J., Wu, K., Xuan, X., and Lu, X., 2009. Ionic liquid-based aqueous two-phase extraction of selected proteins. *Separation and Purification Technology*, 64, pp. 288-295.
- Pesliakas, H., Zutautas, V., and Baskeviciute, B., 1994. Immobilized metal-ion affinity partitioning of NAD<sup>+</sup> dependent dehydrogenase in poly(ethylene glycol)-dextran two-phase systems. *Journal of Chromatography A*, 678, pp. 25-34.
- Pereira, J. F. B., Vicente, F., Santos-Ebinuma, V. C., Araujo, J. M., Pessoa, A., Freire, M. G. and Coutinho, J. A. P., 2013. Extraction of tetracycline from fermentation broth using aqueous two-phase systems composed of polyethylene glycol and cholinium-based salts. *Process Biochemistry*, 48, pp. 716-722.
- Porath, J., Carlsson, J., Olsson, I., and Belfrage, G., 1975. Metal chelate affinity chromatography, a new approach to protein fractionation. *Nature*, 258, pp 598-599.
- Predki, P. F., 2007. *Functional Protein Microarrays in Drug Discovery*. 1<sup>st</sup> edition, Florida, USA.
- Rabelo, A. P. B., Tambourgi, E. B. and Pessoa, A., 2004. Bromelain partitioning in two-phase aqueous systems containing PEO-PPO-PEO block copolymers. *Journal of Chromatography B*, 807, pp. 61-68.
- Rahimpour, F., Feyzi, F., Maghsoudi, S. and Hatti-kaul, R., 2006. Purification of plasmid DNA with polymersalt aqueous two-phase system: Optimization using response surface methodology. *Biotechnology and Bioengineering*, 95, pp. 627-636.
- Raja, S., Murty, V. R., Thivaharan, V., Rajasekar, V., and Ramesh, V., 2011. Aqueous Two Phase Systems for the Recovery of Biomolecules – A Review. *Science and Technology*, 1(1), pp. 7-16.
- Ramirez, I. B. R., Abedinpour, P. and Jergil, B., 2004. Purification of caveolae by affinity two-phase partitioning using biotinylated antibodies and NeutrAvidin-dextran. *Analytical Biochemistry*, 331, pp. 17-26.
- Ramyadevi, D., Subathira, A. and Saravanan, S., 2012. Phase compositions of aqueous two-phase systems formed by poly(ethylene glycol) and maltodextrin at different temperatures. *International Journal of Chemical Sciences and Application*, 3, pp. 289-292.

- Ratanapongleka, K., 2012. Partitioning behavior of laccase from *Lentinus polychrous* Lev in aqueous two phase systems. *Songklanakarinn Journal of Science Technology*, 34(1), pp. 69.
- Reh, G., Spelzini, D., Tubio, G., Pico, G. and Farrugia, B., 2007. Partition features and renaturation enhancement of chymosin in aqueous two-phase systems. *Journal of Chromatography B*, 860, pp. 98-105.
- Ribeiro, M. Z., Silva, D. P., Vitolo, M., Roberto, I. C. and Pessoa-jr, A., 2007. Partial purification of glucose-6-phosphate dehydrogenase by aqueous two-phase poly ( ethyleneglycol )/ phosphate systems. *Brazilian Journal of Microbiology*, 38, pp. 78-83.
- Rito-Palomares, M. and Hernandez, M., 1998. Influence of system and process parameters on partitioning of cheese whey proteins in aqueous two-phase systems. *Journal of Chromatography B*, 711, pp. 81-90.
- Rito-Palomares, M., 2004. Practical application of aqueous two-phase partition to process development for the recovery of biological products. *Journal of Chromatography B*, 807, pp. 3-11.
- Rokuhara, A., Tanaka, E., Matsumoto, A., Kimura, T., Yamaura, T., Orii, K., Sun, X., Yagi, S., Maki, N., and Kiyosawa, K., 2003. Clinical evaluation of a new enzyme immunoassay for hepatitis B virus core-related antigen; a marker distinct from viral DNA for monitoring lamivudine treatment. *Journal of Viral Hepatitis*, 10(4), pp. 324-330.
- Rolland, D. et al., 2001. Purification of recombinant HBc antigen expressed in *Escherichia coli* and *Pichia pastoris*: comparison of size exclusion chromatography and ultracentrifugation. *Journal of Chromatography B, Biomedical Sciences and Applications*, 753, pp. 51 – 65.
- Rosso, B. U., Lima, C. D. A., Porto, T. S., Nascimento, C. de O., Pessoa Jr, A., Converti, A., Carneiro-daCunha, M. D. G. and Porto, A. L. F., 2012. Partitioning and extraction of collagenase from *Penicillium aurantiogriseum* in poly(ethylene glycol)/phosphate aqueous two-phase system. *Fluid Phase Equilibrium*, 335, pp. 20-25.
- Ruiz, F. R., Benavides, J., Aguilar, O., and Palomares, M. R., 2012. Aqueous two-phase affinity partitioning systems: Current application and trends. *Journal of Chromatography A*, 1244, pp. 1-13.
- Salabat, A., Moghadam, S.T. and Far, M.R., 2010. Liquid-liquid equilibria of aqueous two-phase systems composed of TritonX-100 and sodium citrate or magnesium sulphate salts. *Computer Coupling of Phase Diagrams and Thermochemistry*, 34, pp. 81-83.
- Salamanca, M.H., Merchuk, J.C., Andrews, B.A. and Asenjo, J.A., 1998. On the kinetics of phase separation in aqueous two-phase systems. *Journal of Chromatography B: Biomedical Sciences and Application*, 711, pp. 319-329.

- Sanada, T., Hirata, Y., Naito, Y., Yamamoto, N., Kikkawa, Y., Ishida, Y., Yamasaki, C., Tateno, C., Ochiya, T., and Kohara, M., 2017. Transmission of HBV DNA mediated by ceramide-triggered extracellular vesicles. *Cellular and Molecular Gastroenterology and Hepatology*, 3(2), pp. 272-283.
- Santos, L. H., Carvalho, P. L. G., Rodrigues, G. D., and Mansur, M. B., 2015. Selective removal of calcium from sulphate solutions containing magnesium and nickel using aqueous two phase systems (ATPS). *Hydrometallurgy*, 156, pp. 259-263.
- Santos, J. C., Paula, A. V., Nunes, G. F. M., and deCastro, H. F., 2008. *Pseudomonas fluorescens* lipase immobilization on polysiloxane-polyvinyl alcohol composite chemically modified with epichlorohydrin. *Journal of Molecular Catalysis B: Enzymatic*, 52-53, pp.49-57.
- Saravanan, S., Rao, J.R., Murugesan, T., Nair, B.U. and Ramasami, T., 2007. Partition of tannery wastewater proteins in aqueous two-phase poly(ethylene glycol)-magnesium sulphate systems: effect of molecular weights and pH. *Chemical Engineering Sciences*, 62, pp. 969-978.
- Saravanan, S., Rao, J.R., Nair, B.U. and Ramasami, T., 2008. Aqueous two-phase poly(ethylene glycol)-poly(acrylic acid) system for protein partitioning: Influence of molecular weight, pH and temperature. *Process Biochemistry*, 43, pp. 905-911.
- Schagger, H. Tricine-SDS-PAGE. *Protocol*. [online] Available at: [https://doi:10.1038/nprot.2006.4](https://doi.org/10.1038/nprot.2006.4). [Accessed 20 July 2017].
- Schmidt, A.S., Andrews, B.A. and Asenjo, J.A., 1996. Correlations for the partition behaviour of proteins in aqueous two-phase systems: effect of overall protein concentration. *Biotechnology and Bioengineering*, 50, pp. 617-626.
- Schodel, F., Peterson, D., and Milich, D., 1996. Hepatitis B Virus core and e antigen: immune recognition and use as a vaccine carrier moiety. *Intervirology*, 39(1-2), pp. 104-110.
- Schodel, F., Peterson, D., Zheng, J., Jones, J. E., Hughes, J. L., and Milich, D. R., 1993. Structure of Hepatitis B Virus Core and e-Antigen. *The Journal of Biological Chemistry*, 268(2), pp. 1332-1337.
- Shiri, S., Khezeli, T., Lofti, S. and Shiri, S., 2013. Aqueous two-phase systems: A new approach for the determination of brilliant blue FCF in water and food samples. *Journal of Chemistry*, 2013, pp. 1-6.
- Show, P.L. et al., 2012. Primary recovery of lipase derived from *Burkholderia cenocepacia* strain ST8 and recycling of phase components in an aqueous two-phase system. *Biochemical Engineering Journal*, 116, pp. 226 – 233.
- Silva, D. M. E., and Franco, T. T., 2000. Purification of soybean peroxidase (Glycine max) by metal affinity partitioning in aqueous two-phase systems. *Journal of Chromatography B*, 743(1-2), pp. 287-294.

- Silvério, S.C., Wegrzyn, A., Lladosa, E., Rodríguez, O. and Macedo, E.A., 2012. Effect of aqueous two-phase system constituents in different poly(ethylene glycol)-salt phase diagrams. *Journal of Chemical Engineering Data*, 57, pp. 1203-1208.
- Sinha, R., Singh, S.P., Ahmed, S. and Garg, S.K., 1996. Partitioning of a *Bacillus* alkaline protease in aqueous two-phase systems. *Bioresource Technology*, 55, pp. 163-166.
- Stevens, C. E., Toy, P., Kamili, S., Taylor, P. E., Tong, M. J., Xia, G. L., and Vyas, G. N., 2017, Eradicating hepatitis B virus: The critical role of preventing perinatal transmission. *Biologicals*, in press corrected proof.
- Suffian, I. F. B. M., Garcia-Maya, M., Brown, P., Bui, T., Nishimura, Y., Parlermo, A. R. B. M. J., Ogino, C., Kondo, A., and Al-Jamal, K. T., 2017. Yield optimization of Hepatitis B virus core particles in *E.coli* expression system for drug delivery applications. *Scientific report*, 43160.
- Sun, S. and Li, J., 2017, Humanized chimeric mouse models of hepatitis B virus infection. *International Journal of Infectious Diseases*, 59, pp. 131-136.
- Tan, W.S., Dyson, M.R. and Murray, K., 2003. Hepatitis B virus core antigen: enhancement of its production in *Escherichia coli* and interaction of the core particles with the viral surface antigen. *Journal of Biological Chemistry*, 384, pp. 363 – 371.
- Tan, W.S. et al., 2007. Crystallization and X-ray analysis of the  $T = 4$  particle of hepatitis B capsid protein with an N-terminal extension. *Acta Crystallographica Section F, Structural Biology and Crystallization Communications*, 63 (8), pp. 642 – 647
- Tang, K.F., Abdullah, M.P., Yusoff, K., Tan, W.S., 2007. Interactions of hepatitis B core antigen and peptide inhibitors. *Journal of Medicinal Chemistry*, 50, pp. 5620-5626.
- Tanuja, S., Srinivas, N.D., Raghavarao, K.S.M.S. and Gowthaman, M.K., 1997. Aqueous two-phase extraction for downstream processing of amyloglucosidase. *Process Biochemistry*, 32, pp. 47-54.
- Tarar, M.R., Emery, V.C. and Harrison, T.J., 1996. Expression of a human cytomegalovirus gp58 antigenic domain fused to the hepatitis B virus nucleocapsid protein. *FEMS Immunology & Medical Microbiology*, 16(3-4), pp. 183–192.
- Tou, B. S. Y., Neo, K. E., Tey, B. T., and Ng, M. Y. T., 2014. Effect of phase inversion and separation on hepatitis B core antigen extraction from unclarified bacterial feedstock using aqueous two-phase system. *Separation and Purification Technology*, 130, pp. 45-55.
- Tropp, B.E., 2012. *Molecular Biology: Genes to proteins*, United States: Jones and Barlett Learning, LLC.

- Tubio, G., Nerli, B.B., Pico, G.A., Venancio, A. and Teixeira, J., 2009. Liquid-liquid equilibrium of the Ucon 50-HB5100/sodium citrate aqueous two-phase systems. *Separation and Purification Technology*, 65, pp. 3-8.
- Ulrich, R. et al., 1999. New chimaeric hepatitis B virus core particles carrying hantavirus (serotype Puumala) epitopes: Immunogenicity and protection against virus challenge. *Journal of Biotechnology*, 73(2-3), pp. 141-153.
- Van Suijdam, J.C. and Metz, B., 1981. Influence of engineering variables upon the morphology of filamentous molds. *Biotechnology and Bioengineering*, 23, pp. 111-148.
- Wang, F., Liu, Y. H., Ma, Y., Cui, Z. G., and Shao, L. L., 2016. Application of TMA-PEG to promote C-phycoerythrin extraction from *S. platensis* in the PEG ATPS. *Process Biochemistry*, 52, pp. 283-294.
- Wang, T., Xu, W. J., Wang, S. X., Kou, P., Wang, P., Wang, X. Q., and Fu, Y. J., 2017. Integrated and sustainable separation of chlorogenic acid from blueberry leaves by deep eutectic solvents coupled with aqueous two-phase system. *Food and Bioprocess Technology*, 105, pp. 205-214.
- Whitacre, D. C., Lee, B. O., and Milich, D. R., 2009. Use of hepatitis B virus core proteins as vaccine platforms. *Expert Rev Vaccines*, 8(11), pp. 1565-1573.
- World Health Organisation, 2017. *Hepatitis B*. [Online]. Available at: <http://www.who.int/mediacentre/factsheets/fs204/en/> [Accessed: 10 July 2017].
- Wuenschell, G. E., Wen, E., Todd, R., Shnek, D., and Arnold, F. H., 1991. Chiral copper-chelate complexes alter selectivities in metal affinity protein partitioning. *Journal of chromatography A*, 543, pp. 345-354.
- Wyllie, R., Hyams, J. S., and Kay, M., eds. 2016. *Pediatric Gastrointestinal and Liver Disease*. 5<sup>th</sup> ed. Amsterdam, Netherlands: Elsevier.
- Wynne, S. A., Crowther, R. A., and Leslie, A. G. W., 2014. The Crystal Structure of the Human Hepatitis B Virus Capsid. *Molecular Cell*, 3(6), pp. 771-780.
- Wynne, S. A., Leslie, G. W., Butler, P. J. G., and Crowther, R. A., 1999. Crystallization of hepatitis B virus core protein shells: determination of cryoprotectant conditions and preliminary X-ray characterization. *Acta Crystallographica Section D*, 55, pp. 557-560.
- Yap, W.B., Tey, B.T., Alitheen, N.B.M. and Tan, W.S., 2010. Purification of His-tagged hepatitis B core antigen from unclarified bacterial feedstock using immobilized metal affinity-expanded bed adsorption chromatography. *Journal of Chromatography A*, 1217, pp. 3473-3480.
- Yap, W. B., Tey, B. T., Ng, M. Y. T., Ong, S. T., and Tan, W. S., 2009. N-terminally His-tagged hepatitis B core antigens: Construction, expression, purification and antigenicity. *Journal of Virological Methods*, 160, pp. 125-131.

- Yeh, C.Y. and Lan, J.C.W., 2013. Direct recovery of polyhydroxyalkanoates synthase from recombinant *Escherichia coli* feedstock by using aqueous two-phase systems. *Journal of Taiwan Institute of Chemical Engineers*, <http://dx.doi.org/10.1016/j.jtice.2013.10.020>.
- Yilmaz, M., 2005. Separation and purification of lysozyme by Reactive Green 19 immobilised membrane affinity chromatography. *Food Chemistry*, 89, pp. 11-18.
- Yu, X., Jin, L., Jih, J., Shih, C., and Zhou, Z. H., 2013. 3.5Å cryoEM Structure of Hepatitis B Virus Core Assembled from Full-Length Core Protein. *Public library of science*. [online] Available at: <https://doi.org/10.1371/journal.pone.0069729> [Accessed 12 July 2017]
- Zhang, Z. Q., Lu, W., Wang, Y. B., Wang, Q. C., Zhang, Z. Y., Yang, Z. Q., and Feng, Y. L., 2016. Measurement of the hepatitis B core-related antigen is valuable for predicting the pathological status of liver tissues in chronic hepatitis B patients. *Journal of Virological Methods*, 235, pp. 92-98.
- Zlotnick, A., Cheng, N., Conway, J. F., Booy, F. P., Steven, A. C., Stahl, S. J., and Wingfield, P. T., 1996. Dimorphism of Hepatitis B Virus Capsids is Strongly Influenced by the C-Terminus of the Capsid Protein. *Biochemistry*, 35(23), pp. 7412-7421.

## Appendix A

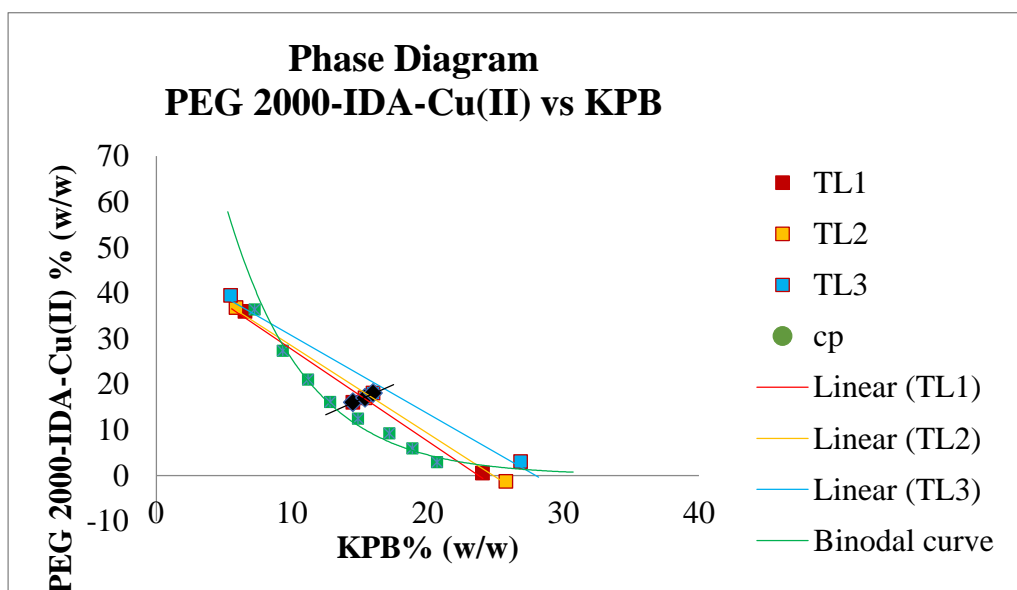
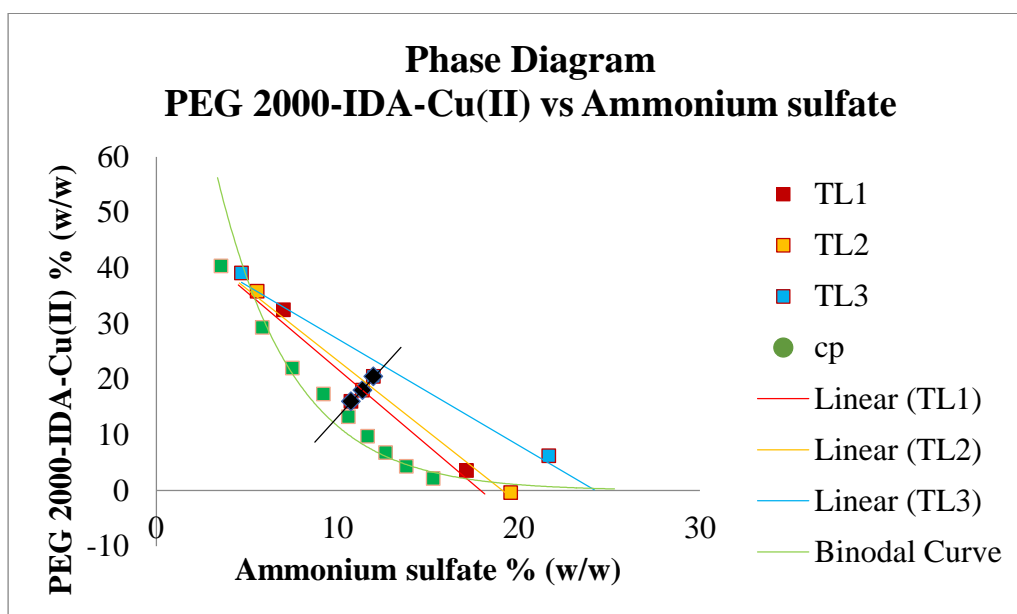
### Conversion chart of Brix value to refractive index

*Sucrose Solution Percent by Weight Concentration (Brix Value) Versus Refractive Index at 20 Celsius and 589nm Wavelength (per ICUMSA)*

	0	0.1	0.2	0.3	0.4	0.5	0.6	0.7	0.8	0.9
0	1.33298	1.33313	1.33327	1.33342	1.33356	1.33370	1.33385	1.33399	1.33413	1.33428
1	1.33442	1.33456	1.33471	1.33485	1.33500	1.33514	1.33529	1.33543	1.33558	1.33572
2	1.33587	1.33601	1.33616	1.33630	1.33645	1.33659	1.33674	1.33688	1.33703	1.33717
3	1.33732	1.33747	1.33761	1.33776	1.33791	1.33805	1.33820	1.33835	1.33849	1.33864
4	1.33878	1.33893	1.33908	1.33923	1.33938	1.33952	1.33967	1.33982	1.33997	1.34012
5	1.34026	1.34041	1.34056	1.34071	1.34086	1.34101	1.34116	1.34131	1.34146	1.34160
6	1.34175	1.34190	1.34205	1.34220	1.34235	1.34250	1.34265	1.34280	1.34295	1.34310
7	1.34325	1.34341	1.34356	1.34371	1.34386	1.34401	1.34416	1.34431	1.34446	1.34461
8	1.34477	1.34492	1.34507	1.34522	1.34537	1.34553	1.34568	1.34583	1.34598	1.34614
9	1.34629	1.34644	1.34660	1.34675	1.34690	1.34706	1.34721	1.34736	1.34752	1.34767
10	1.34783	1.34798	1.34813	1.34828	1.34844	1.34860	1.34875	1.34891	1.34906	1.34922
11	1.34937	1.34953	1.34968	1.34984	1.34999	1.35015	1.35031	1.35046	1.35062	1.35077
12	1.35093	1.35109	1.35124	1.35140	1.35156	1.35172	1.35187	1.35203	1.35219	1.35234
13	1.35250	1.35266	1.35282	1.35298	1.35313	1.35329	1.35345	1.35361	1.35377	1.35393
14	1.35409	1.35424	1.35440	1.35456	1.35472	1.35488	1.35504	1.35520	1.35536	1.35552
15	1.35568	1.35584	1.35600	1.35616	1.35632	1.35648	1.35664	1.35680	1.35697	1.35713
16	1.35729	1.35745	1.35761	1.35777	1.35793	1.35810	1.35826	1.35842	1.35858	1.35875
17	1.35891	1.35907	1.35923	1.35940	1.35956	1.35972	1.35989	1.36005	1.36021	1.36038
18	1.36054	1.36070	1.36087	1.36103	1.36120	1.36136	1.36153	1.36169	1.36186	1.36202
19	1.36219	1.36235	1.36252	1.36268	1.36285	1.36301	1.36318	1.36334	1.36351	1.36368
20	1.36384	1.36401	1.36418	1.36434	1.36451	1.36468	1.36484	1.36501	1.36518	1.36535
21	1.36551	1.36568	1.36585	1.36602	1.36619	1.36635	1.36652	1.36669	1.36686	1.36703
22	1.36720	1.36737	1.36754	1.36771	1.36788	1.36804	1.36821	1.36838	1.36855	1.36872
23	1.36888	1.36907	1.36924	1.36941	1.36958	1.36975	1.36992	1.37009	1.37026	1.37043
24	1.37060	1.37078	1.37095	1.37112	1.37129	1.37147	1.37164	1.37181	1.37198	1.37216
25	1.37233	1.37250	1.37267	1.37285	1.37302	1.37320	1.37337	1.37354	1.37372	1.37389
26	1.37407	1.37424	1.37441	1.37458	1.37476	1.37494	1.37511	1.37529	1.37546	1.37564
27	1.37582	1.37599	1.37617	1.37634	1.37652	1.37670	1.37687	1.37705	1.37723	1.37740
28	1.37758	1.37776	1.37793	1.37811	1.37829	1.37847	1.37865	1.37882	1.37900	1.37918
29	1.37936	1.37954	1.37972	1.37989	1.38007	1.38025	1.38043	1.38061	1.38079	1.38097
30	1.38115	1.38133	1.38151	1.38169	1.38187	1.38205	1.38223	1.38241	1.38259	1.38277
31	1.38296	1.38314	1.38332	1.38350	1.38368	1.38386	1.38405	1.38423	1.38441	1.38459
32	1.38478	1.38496	1.38514	1.38532	1.38551	1.38569	1.38588	1.38606	1.38624	1.38643
33	1.38661	1.38679	1.38698	1.38716	1.38735	1.38753	1.38772	1.38790	1.38809	1.38827
34	1.38846	1.38865	1.38883	1.38902	1.38920	1.38939	1.38958	1.38976	1.38995	1.39014
35	1.39032	1.39051	1.39070	1.39088	1.39107	1.39126	1.39145	1.39164	1.39182	1.39201
36	1.39220	1.39239	1.39258	1.39277	1.39296	1.39315	1.39333	1.39352	1.39371	1.39390
37	1.39409	1.39428	1.39447	1.39466	1.39485	1.39505	1.39524	1.39543	1.39562	1.39581
38	1.39600	1.39619	1.39638	1.39658	1.39677	1.39696	1.39715	1.39734	1.39754	1.39773
39	1.39792	1.39812	1.39831	1.39850	1.39870	1.39889	1.39908	1.39928	1.39947	1.39967
40	1.39986	1.40006	1.40025	1.40044	1.40064	1.40084	1.40103	1.40123	1.40142	1.40162
41	1.40181	1.40201	1.40221	1.40240	1.40260	1.40280	1.40299	1.40319	1.40339	1.40358
42	1.40378	1.40398	1.40418	1.40437	1.40457	1.40477	1.40497	1.40517	1.40537	1.40557
43	1.40576	1.40596	1.40616	1.40636	1.40656	1.40676	1.40696	1.40716	1.40736	1.40756
44	1.40776	1.40796	1.40817	1.40837	1.40857	1.40877	1.40897	1.40917	1.40937	1.40958

## Appendix B

Figures presented phase diagrams of different phase-forming salts with different MW of PEG





Appendix B (continued)

